OAK RIDGE NATIONAL LABORATORY LIBRARIES
3 4456 0548361 5

CENTRAL RESEARCH LIBRARY
DOCUMENT COLLECTION

150

ORNL-3752
Special
No. 4

THE JOINT NATIONAL INSTITUTES OF HEALTH–ATOMIC ENERGY COMMISSION ZONAL CENTRIFUGE DEVELOPMENT PROGRAM SEMIANNUAL REPORT FOR PERIOD JANUARY 1 TO JUNE 30, 1964

OAK RIDGE NATIONAL LABORATORY
operated by
UNION CARBIDE CORPORATION
for the
U.S. ATOMIC ENERGY COMMISSION

CENTRAL RESEARCH LIBRARY
DOCUMENT COLLECTION
LIBRARY LOAN COPY
DO NOT TRANSFER TO ANOTHER PERSON
If you wish someone else to see this document, send in name with document and the library will arrange a loan.

LEGAL NOTICE

This report was prepared as an account of Government sponsored work. Neither the United States, nor the Commission, nor any person acting on behalf of the Commission:

A. Makes any warranty or representation, expressed or implied, with respect to the accuracy, completeness, or usefulness of the information contained in this report, or that the use of any information, apparatus, method, or process disclosed in this report may not infringe privately owned rights; or

B. Assumes any liabilities with respect to the use of, or for damages resulting from the use of any information, apparatus, method, or process disclosed in this report.

As used in the above, "person acting on behalf of the Commission" includes any employee or contractor of the Commission, or employee of such contractor, to the extent that such employee or contractor of the Commission, or employee of such contractor prepares, disseminates, or provides access to, any information pursuant to his employment or contract with the Commission, or his employment with such contractor.

ORNL-3752
Special

Contract No. W-7405-eng-26

BIOLOGY DIVISION

THE JOINT NATIONAL INSTITUTES OF HEALTH–ATOMIC ENERGY COMMISSION ZONAL CENTRIFUGE DEVELOPMENT PROGRAM

SEMIANNUAL REPORT

For Period January 1 to June 30, 1964

N. G. Anderson
Program Coordinator

NOTICE

This document contains information of a preliminary nature and was prepared primarily for internal use. It is subject to revision or correction and, therefore, does not represent a final report. Quotations from or references to this report must not be made in open literature without written permission from the individual authors.

MARCH 1965

OAK RIDGE NATIONAL LABORATORY
Oak Ridge, Tennessee
operated by
UNION CARBIDE CORPORATION
for the
U. S. ATOMIC ENERGY COMMISSION

OAK RIDGE NATIONAL LABORATORY LIBRARIES
3 4456 0548361 5

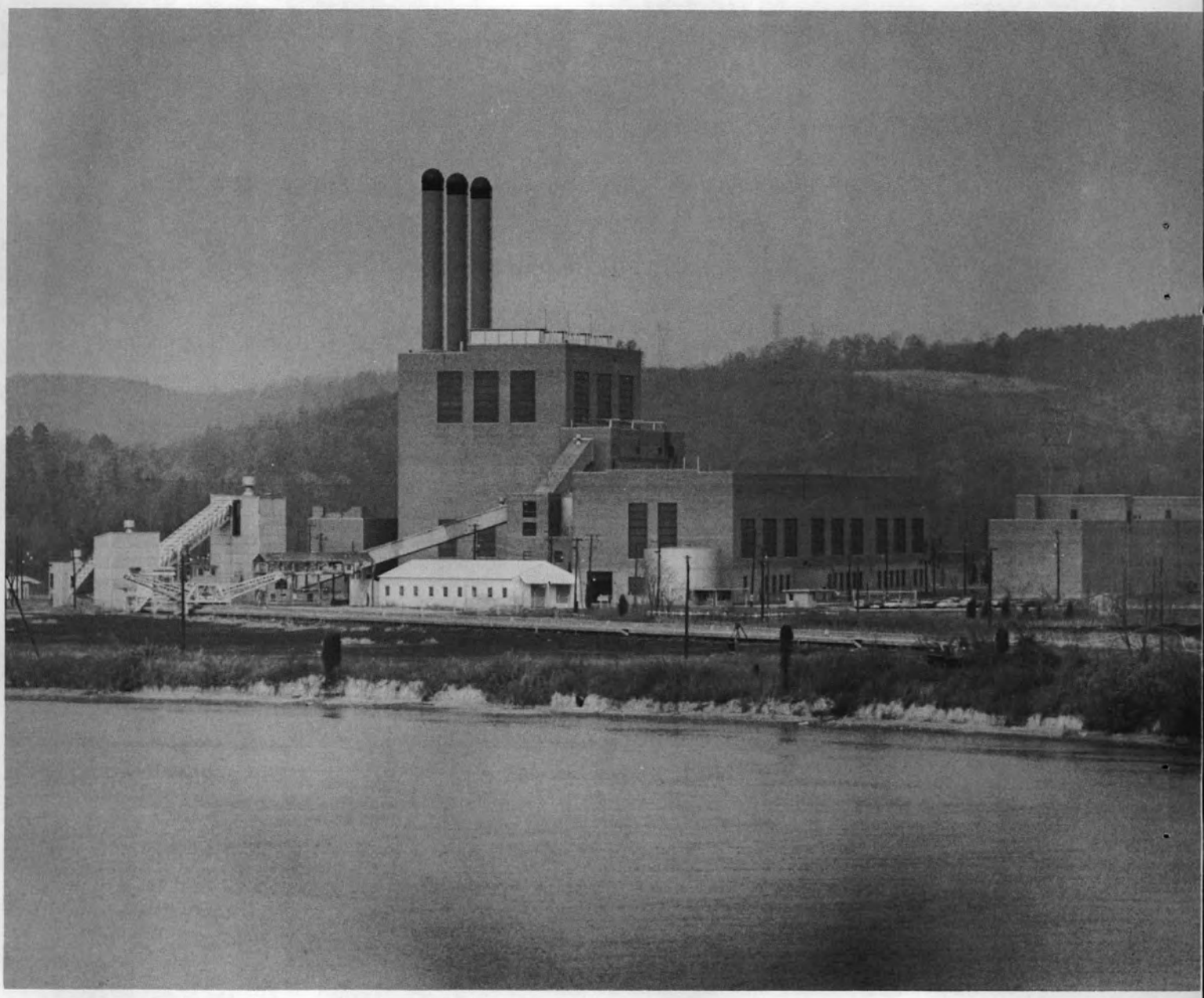

Electrical Power Generating Facilities of Oak Ridge Gaseous Diffusion Plant.

Summary

This report describes work done under the Joint National Institutes of Health–Atomic Energy Commission Zonal Centrifuge Development Program on the application to difficult biophysical separation problems of techniques and instruments developed by the AEC. The objective of this program is to develop separation systems which will allow profiles of subcellular constituents to be constructed which include the maximum number of cell organelles and individual molecular species. Work on zonal centrifuge systems designed to separate particles ranging in size from whole cells to small molecules has progressed with the development of several new rotor systems. The B-IV rotor has been shown to effectively separate quantities of macroglobulin from rat and other animal sera, thereby extending the usefulness of this instrument down to 20S. By application of the two-dimensional S-ρ separation system previously described, a clear spectrum of rat liver glycogen particles has been obtained, and the molecular structure revealed by negative staining is under investigation. Virus-like particles have been recovered from a human breast tumor with the same technique. Further studies on centrifugal fast freezing show that a high percentage of yeast cells survive freezing, but that the lethal damage is done during warming, which must be done rapidly if a high survival rate is to be obtained. Theoretical studies on the particle capacity of gradients in zonal centrifuges are being carried to the point that experimental studies may be designed to examine anomalous sedimentation behavior and band spreading. The low-speed A-IX rotor has been redesigned and strengthened and is now designated A-XII. Scanning systems that would make this rotor an analytical centrifuge have been completed. Continuous-flow rotors in which the sedimenting particles are banded in a gradient during the continuous-flow process (rotor B-VIII) have been built and successfully tested.

A completely enclosed virus separation facility has been designed for large-scale virus separation. In addition to centrifuges, new countercurrent systems for liquid-liquid extractions and the flame ionization detector for nonvolatile samples are under development. A prototype automated system for carbohydrate analysis has been completed and tested with a variety of sugar-containing samples. With an experimental high-pressure capillary column nucleotide analyzer, it has been demonstrated that rapid analysis of very small samples can be performed with micro ion exchange beads, warm columns, a high flow rate, and columns of very small bore.

Contents

SUMMARY iii

I. INTRODUCTION 1

II. BIOMEDICAL APPLICATIONS OF ZONAL CENTRIFUGES DEVELOPED UNDER THIS PROGRAM 3

A. Isolation and Physiochemical Properties of Rat Macroglobulins 3
Preparation of Serum and Zonal Centrifugation 3

B. Isolation of Native Glycogen 5
Preparation of Rat Liver Breis 5

C. Isolation of Particles from Human Tumors 8

D. Effect of the Warming Rate on the Survival of Yeast Cells Frozen Centrifugally 10

III. THEORETICAL STUDIES 13

A. Density Inversion During Centrifugation 13
Formulation 13
Solution 13
Example 14

IV. ROTOR DESIGN 16

A. Stability Studies 16
Theoretical Studies 16
Transient Solution 16
Steady-State Solution 17

B. Rotor Configurations 18
Rotor Shapes 18

C. Metallurgical Studies 18

V. LOW-SPEED ROTORS 19

A. Modifications of Preparative A-Series Rotors 19

B. A Prototype Low-Speed Analytical Rotor 20

C. The A-XII Rotor 20

D. Scanner for A-Series Rotors 26

VI. INTERMEDIATE-SPEED ZONAL ROTORS 29

A. Introduction 29

B. Rotor B-X 29

C. Rotor B-XI 30

D. Rotor B-XII 31

E. Continuous-Flow Centrifugation and Isopycnic Particle Banding 31

VII. INSTRUMENTATION FOR OBTAINING INTEGRAL OF $\omega^2\, dt$ 39

A. Instrument Function Description 39

B. Initial Calibration Procedure 41
Frequency Meter 41
Speed Indicator 42
Integrator 43

C. ω^2 Instrumentation Operation 44
Operational Calibration Checks 44

VIII. CONTAINMENT AND STERILIZATION 45

A. Development of a Contained Laboratory 45

B. Simplified Virus Isolation Systems 46

C. A Leak-Tight, Disposable Plastic Centrifuge Tube 46

IX. ANCILLARY STUDIES 49

A. A Rapid Countercurrent Distribution System 49

B. Carbohydrate Analyzer: Improved System for Color Development 52

C. Capillary Column Chromatography: Preliminary Studies on Nucleotide Separations 55

D. Flame Ionization Analyzer for Determining Carbon in Liquid Streams or Solid Samples 56

I. Introduction

This report is the fourth prepared under the Joint NIH-AEC Zonal Centrifuge Development Program. The central theme remains the exploration of technologies and skills, originally developed for AEC programs, for application to basic biomedical problems. While swords are not easily beaten into scalpels, the possibility of new incisive edges for research tools would appear to justify the effort. The program is being carried out at three locations: the Biology Division laboratories (ORNL) at the Y-12 site, the Technical Division of the Oak Ridge Gaseous Diffusion Plant (ORGDP), and in an area of the ORGDP power generating plant. One floor of a section of this plant has been modified during this report period to house the centrifuge systems described in these reports. The zonal centrifuge program is, therefore, a small, hopefully prophetic attempt at the redirection of part of a vast existing enterprise. A photograph of the electrical power generating facilities of the Oak Ridge Gaseous Diffusion Plant which houses the Joint NIH-AEC Zonal Centrifuge Development Program is included as a frontispiece.

The development of zonal centrifuges is by no means complete; however, this report marks a turning point in their development. First, a program aimed at adapting the centrifuge systems thus far developed to the large-scale isolation of virus particles and viral subunits has been undertaken in collaboration with the Board for Vaccine Development of the National Institute of Allergy and Infectious Diseases. Second, drawings of the B-IV, B-V, B-VIII, A-IX, and A-XII rotors and cores have been released to industry through the AEC Division of Technical Information Extension at Oak Ridge. Specifications and drawings of new developments will continue to be released as rapidly as possible. Third, a seminar attended by 73 representatives from industry and from research laboratories across the country was held on April 30–May 1, 1964, under the auspices of the ORNL Office of Industrial Cooperation. Plans for a training course in zonal centrifuge operation are under way and will be held in Oak Ridge, September 16–18, 1964. Last, arrangements have been made to publish some of the results of this program as a supplement to the *Journal of the National Cancer Institute*. As detailed results appear in the open literature, the necessity for extensive reports for limited distribution is minimized. Future reports in this series will, therefore, be in summary form.

Since the problem of bringing zonal centrifuges into general use has been at least partially solved, the direction of future efforts must now be considered. If the past history of biophysical tools is indicative of the future history of new ones, then we should aim at once for simplification of components and operating technique. With this in mind, the B-X and B-XI rotors described in this report have been developed. These eliminate the high-speed upper bearing, and still allow operation at speeds sufficiently high to separate ribosomal subunits. Work on the development of other rotors designed for specific purposes will continue, together with studies on the containment of both centrifuges and ancillary virological research systems. For the present, the chief biological problem is the identification of the many fractions which can now be isolated. This work will progress slowly, as collaborative studies with interested investigators are arranged.

As is indicated by the contents of this and previous reports, several techniques in addition to those concerned with centrifugation are being explored. These include: the wire-fed flame ionization analyzer, the carbohydrate analyzer, the high-pressure nucleotide analyzer, digital chromatographic data reduction, countercurrent

distribution, ultrafast freezing, and new methods for achieving electrophoretic separations. While these involve interesting and valuable new separation and analytical systems, it may be asked how these relate to the problem of cancer in man.

As previously reported, methods for isolating and identifying virus-like particles in plasma and in tissue breis have been developed and shown to be effective. The problem of demonstrating that these particles are both infectious and oncogenic is outside the present scope of this program. The isolation of viral antigens which have been shown to be present in many animal tumors, often in a nonparticulate form, offers an additional challenge to separation methods. If some human neoplasms are ultimately shown to be the end result of virus infection, then the problem of preparing suitable vaccines must be considered. Live-virus vaccines will be extremely difficult to develop and, indeed, may not be considered in view of the difficulty of demonstrating that human oncogenicity has been eliminated. Killed virus preparations may suffer from the same hazard. The possibility of isolating the effective antigens from virus-infected cells in a high state of purity must, therefore, be given close attention. This will involve better protein fractionation methods, together with improved analytical systems for the subunits of which the antigens may be composed.

II. Biomedical Applications of Zonal Centrifuges Developed Under This Program

A. ISOLATION AND PHYSICOCHEMICAL PROPERTIES OF RAT MACROGLOBULINS

W. D. Fisher R. E. Canning

As experimental studies with the B-IV zonal ultracentrifuge have progressed, particles of smaller dimensions have been separated. In experiments with ribosomal subunits, particles having sedimentation coefficients as low as 30S were distinguished. To explore the lower limits of the separations which might be achieved with this system, the possibility of isolating plasma macroglobulins has been examined.

Of the various gamma globulins of plasma possessing antigenic activity, the so-called 7S gamma globulins have been extensively studied with respect to structure and biological activity; the 19S gamma globulins are more difficult to isolate in quantity and have been less extensively studied.[1] Since good analytical separations of 19S antibodies have been obtained in sucrose density gradients with swinging bucket rotors,[2] an attempt was made to isolate rat macroglobulin in the B-IV zonal centrifuge described by Anderson and coworkers.[3] This paper reports the isolation and physicochemical properties of an apparently homogeneous rat macroglobulin.

Preparation of Serum and Zonal Centrifugation

A globulin fraction from pooled rat serum was obtained by two precipitations with 40% ammonium sulfate followed by exhaustive dialysis against tap water. The resulting fraction was made up in 0.2 μ Miller-Golder buffer (pH = 7.5) to one-fifth the original plasma volume. This material was then separated with a 1-liter sucrose gradient (10–15% in 0.2 μ Miller-Golder buffer) using 400 ml of overlay. Centrifugation was to $350{,}000 \times 10^6$ $\omega^2 t$ (approximately 6 hr at 40,000 rpm).

Sedimentation measurements were made with a Spinco model E analytical ultracentrifuge with 12-mm cells.

Electrophoretic and diffusion measurements were performed with a Spinco model H unit using 11-ml cells.

Immunoelectrophoresis was done as described by Grabar and Williams.[4]

Carbohydrate was measured by the anthrone method.

The separation of rat macroglobulin by the B-IV rotor is shown in Fig. II-A-1. The starting sample represents 60 ml of rat plasma; the yield was 250 mg of macroglobulin. After concentration by pressure dialysis the leading peak was ultracentrifugally and immunoelectrophoretically homogeneous (Figs. II-A-2 and II-A-3). The physical-chemical properties of the material are listed in Table I. The carbohydrate content of the macroglobulin is 10%. Treatment with 0.1 *M* mercaptoethanol dissociated the macroglobulin into subunits of approximately 8S.

The data reported show that the B-IV zonal centrifuge can be used to prepare a homogeneous rat macroglobulin in preparative quantities. This extends the demonstrated usefulness of the zonal centrifuge into the size range of Sephadex separations. In conjunction with protein chromatographic

[1] R. R. Porter, *Brit. Med. Bull.* 19, 197 (1963).

[2] G. M. Edelman, H. G. Kunkel, and E. C. Franklin, *J. Exptl. Med.* 108, 105 (1958).

[3] N. G. Anderson *et al.*, *Life Sci.* 3, 667–71 (1964).

[4] P. Grabar and C. A. Williams, *Biochim. Biophys. Acta* 10, 193 (1953).

methods, zonal centrifugation should be a useful tool in studying the immunological relationship of the various antibodies in plasma, especially the 20S antibodies, which by previous methods are the more difficult to isolate. The isolation of other macroglobulins (chicken, mouse, and fish) by zonal centrifugation is in progress.

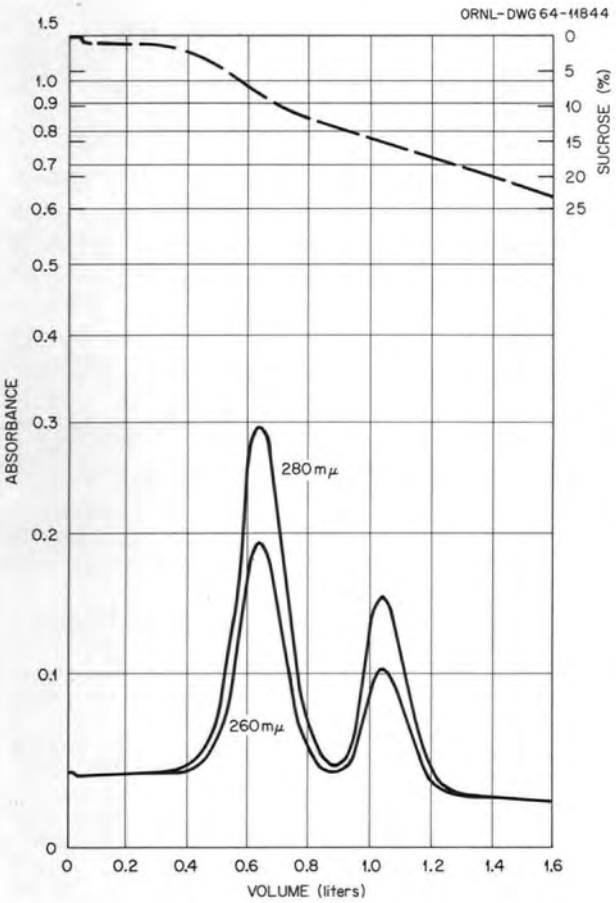

Fig. II-A-1. Separation of Rat Macroglobulin in B-IV Zonal Centrifuge. Upper curve, sucrose concentration; lower curves, absorbancy (0.2-cm light path).

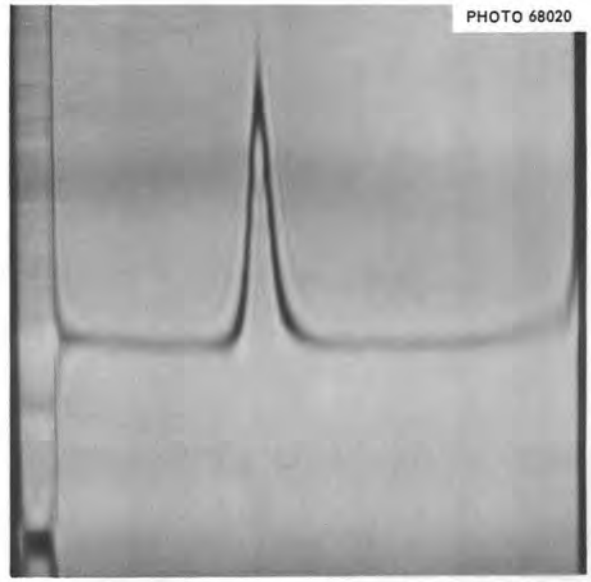

Fig. II-A-2. Ultracentrifuge Pattern for Rat Macroglobulin in 0.2 μ Miller-Golder Buffer After 20 Min at Speed (59,780 RPM).

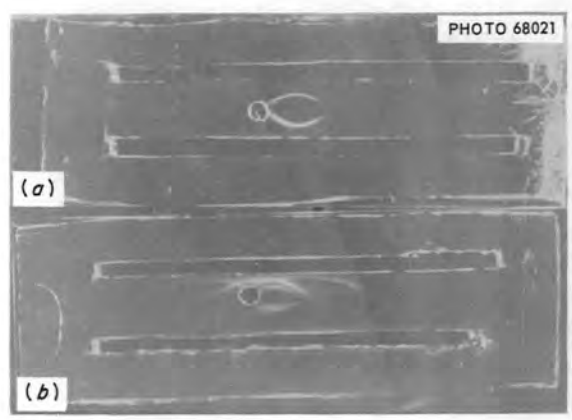

Fig. II-A-3. Immunoelectrophoretic Patterns of (*a*) Macroglobulin and (*b*) Rat Serum. In both cases the upper trough contains rabbit-anti-whole-rat serum and the bottom trough rabbit-anti-rat macroglobulin.

Table I. Physicochemical Properties of Rat Macroglobulin

Sedimentation constant, $S_{20,w}$	20.0S
Diffusion constant, $D_{20,w}$	2.22×10^{-7} cm^2/sec
Calculated particle specific volume, $\overline{V}$	0.744 ml/g
Molecular weight (s, D, $\overline{V}$)	859,400
Electrophoretic mobility at pH 6.2 phosphate buffer, $\mu = 0.1$	-4.22×10^{-5} cm^2 v^{-1} sec^{-1}
Isoelectric point	pH 4.38

B. ISOLATION OF NATIVE GLYCOGEN

N. G. Anderson W. W. Harris
A. A. Barber

The subcellular components of tissues may be separated to give a two-dimensional pattern by using rate zonal centrifugation followed by isopycnic zonal centrifugation as previously described.[5] Experimentally, a number of bands are observed with both normal and malignant tissues, which must now be characterized in much greater detail. In this study we are interested in the band tentatively identified as glycogen in orienting experiments. In previous studies it has been shown that homogeneous virus particles sedimented as narrow, discrete zones in the presence of the components of a tissue brei, suggesting that the wide zones observed with microsomes, for example, are actually due to particle polydispersity. Glycogen is an excellent material for examining this point, since the available evidence suggests that it exists in tissues in a wide range of sizes, and, in addition, it has not been observed to behave as an osmometer.

While glycogen is the major energy and carbohydrate reserve of many human tissues, a number of problems concerning both its structure and mechanism of synthesis remain to be solved. The majority of physical studies have been carried out on material isolated by either cold 5–10% aqueous trichloroacetic acid extraction or by extraction with 30% KOH at 100°C as described by Pflüger.[6] With both methods the glycogen is precipitated from solution by ethanol. The sedimentation coefficients for material obtained by this procedure range from 20S to 300S (refs. 7–12) with some material as high as 2000S.[13] In all instances it is polydisperse. In freshly prepared liver homogenates, Lazarow showed that glycogen behaves as a much larger particle, with a sedimentation coefficient closer to several thousand for the major portion of the particles.[14,15] Electron micrographs of glycogen in tissue sections bear out Lazarow's conclusions.[16–21] The native structure of glycogen cannot be satisfactorily determined from sections, however, and it has not been possible to determine whether glycogen exists as a beaded chain structure, as a rosette, or as a tight cluster of subunits. Electron microscopy of the isolated particles using negative staining is therefore desirable to elucidate the tertiary structure of native glycogen.

Preparation of Rat Liver Breis

Sprague-Dawley rats were stunned and exsanguinated, and the liver from each was rapidly removed and weighed in a tared beaker of cold 8% sucrose. The volume was adjusted to give a 10% (w/v) brei, and the liver was homogenized in a cold coaxial hand homogenizer. After being strained through cheesecloth, 20 ml of the cold brei was introduced into a B-IV zonal centrifuge rotor operating at 5°C and at a speed of 3000 rpm. A 200-ml overlay of pH 7.5, $\mu = 0.1$ Miller-Golder buffer was used to move the sample layer free of the core. The rotor was then accelerated to 20,000 rpm for 15 min. After deceleration to 5000 rpm, the rotor was unloaded as previously described.[5] The ultraviolet absorbance diagram and the computer S^* plot are shown in Fig. II-B-1.

---

[5] *Joint NIH-AEC Zonal Centrifuge Development Program Semiann. Rept. July 1–Dec. 31, 1963*, ORNL-3656.

[6] E. F. W. Pflüger, *Das Glycogen*, p. 530, Bonn, 1905.

[7] W. J. Polglase, D. M. Brown, and E. L. Smith, *J. Biol. Chem.* **199**, 105–12 (1952).

[8] D. J. Bell *et al.*, *Biochem. J.* **42**, 405–8 (1948).

[9] W. A. J. Bryce *et al.*, *J. Chem. Soc.* 711–15 (1958).

[10] W. A. J. Bryce *et al.*, *J. Chem. Soc.* 3845–51 (1958).

[11] F. Meyer and J. P. Zalta, *Compt. Rend.* **247**, 357–59 (1958).

[12] A. Calderbank *et al.*, *Biochem. J.* **74**, 223–29 (1960).

[13] S. A. Orrell, Jr., and E. Bueding, *J. Am. Chem. Soc.* **80**, 3800 (1958).

[14] A. Lazarow, *Anat. Record* **84**, 31–50 (1942).

[15] A. Lazarow, *Arch. Biochem. Biophys.* **7**, 337–43 (1945).

[16] J. P. Revel, L. Napolitano, and D. W. Fawcett, *J. Biophys. Biochem. Cytol.* **8**, 575–89 (1960).

[17] H. E. Karrer and J. Cox, *J. Ultrastruct. Res.* **4**, 191–212 (1960).

[18] M. H. Himes and A. W. Pollister, *J. Histochem. Cytochem.* **10**, 175–85 (1962).

[19] R. Laguens and N. Bianchi, *Exptl. Mol. Pathol.* **2**, 534–40 (1963).

[20] H. Sheldon, M. Silverberg, and I. Kerner, *J. Cell. Biol.* **13**, 468–73 (1962).

[21] H. Themann, *Naturwissenschaften* **47**, 155 (1960).

The fractions between the starting layer and the mitochondrial layer were then banded, using CsCl in No. 30 rotor tubes. A band at a density of approximately 1.62 was observed extending from tube 7 past tube 31. Material recovered from these bands was examined in the electron microscope, with phosphotungstate being used as a negative stain. The results are shown in Fig. II-B-2. The sedimentation coefficients for the fractions shown are indicated in Fig. II-B-1. If the hydrodynamic volume of the particles is calculated from the density and sedimentation data, a value for the radius of the particles is obtained which is less than one-half that observed in cuts 12–31. This is in agreement with the actual observations, which indicate that the particles are not solid

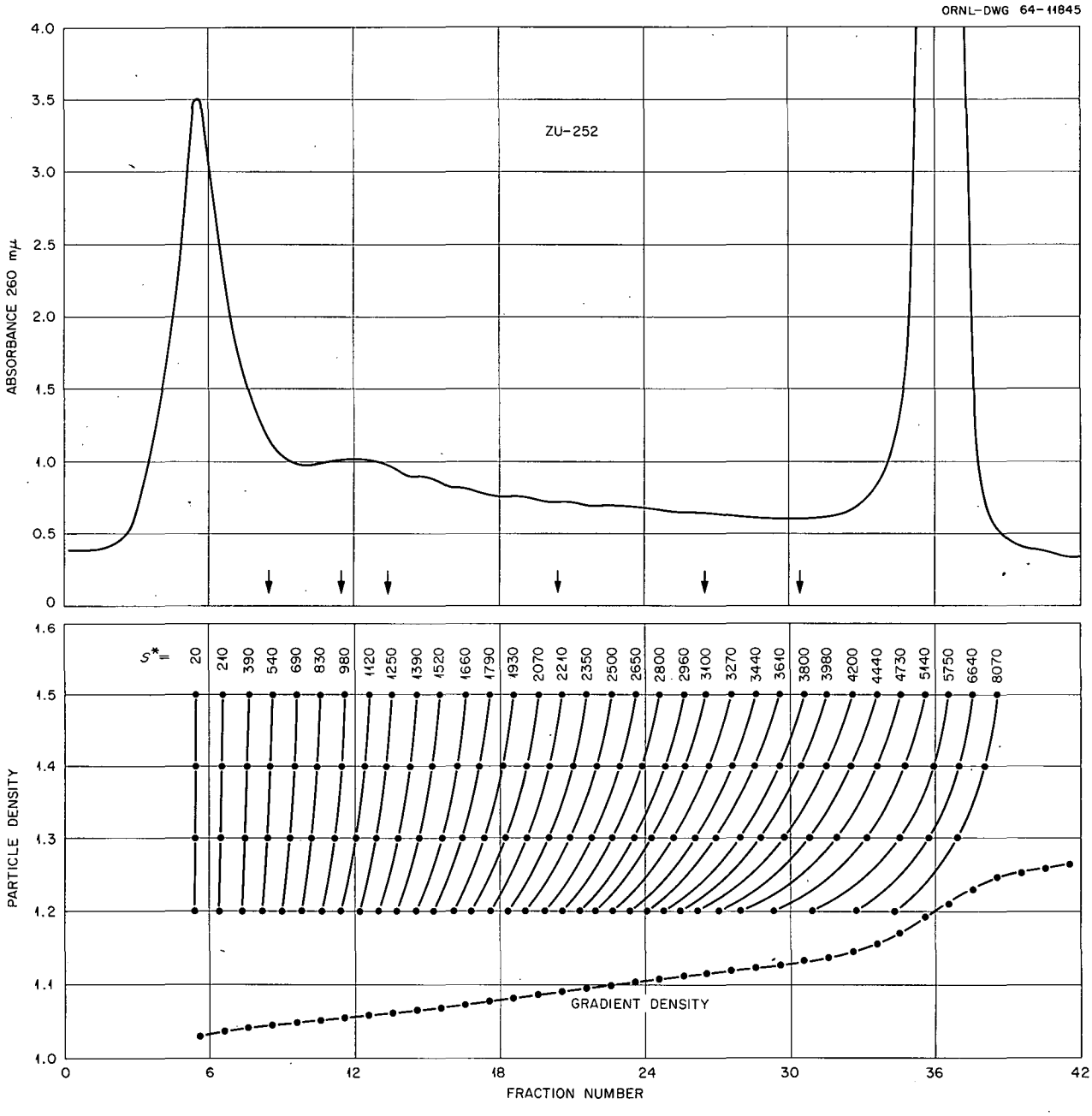

Fig. II-B-1. Rate Zonal Separation of Rat Liver Brei in B-IV Zonal Centrifuge. Details described in text.

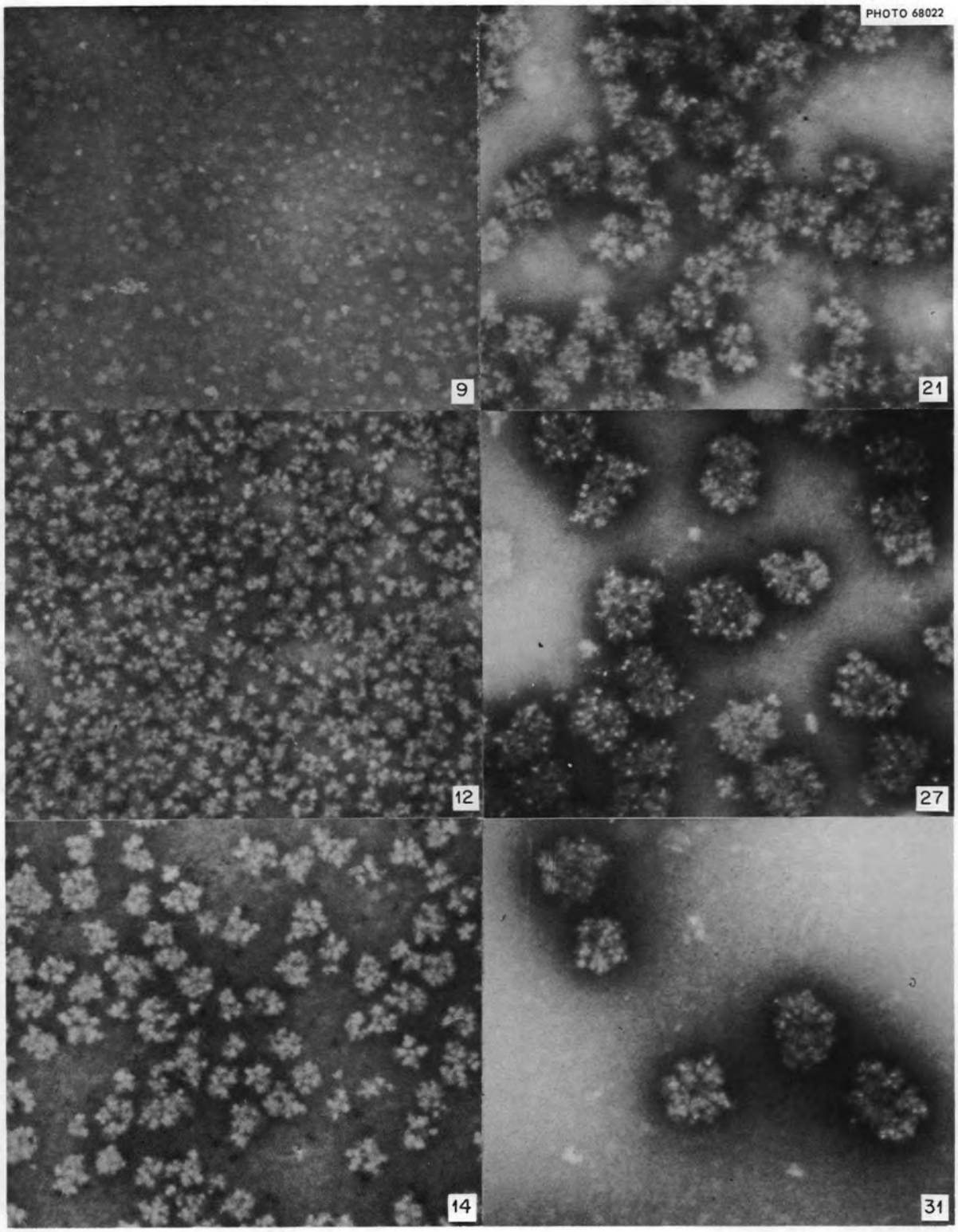

Fig. II-B-2. Electron Micrographs of Glycogen Isolated by Banding Fractions 9, 12, 14, 21, 27, and 31 in Fig. II-B-1 in CsCl. 72,000×.

but are composed of an aggregate of substructures held together in a popcorn-ball configuration. The fine structure of these particles is now being intensively studied.

C. ISOLATION OF PARTICLES FROM HUMAN TUMORS

N. G. Anderson W. W. Harris

During this report period the usefulness of the S-ρ method for the isolation of virus-like particles from human tumors has been examined by using a few tissue samples. Four human leukemic spleens and two breast tumors have been studied. The results demonstrate that (1) virus-like particles can be found in human cancer tissue, (2) comparable studies on normal tissue must be performed, and (3) a thorough analysis of all the bands isolated is desirable to provide reference points. An example of the latter is the work on the glycogen band presented in the previous section.

The most promising results were obtained with a 49-g primary human breast tumor frozen immediately after surgical removal and kept at −60°C until ready for use. A 10% homogenate of the tumor was prepared in 0.05 *M* pH 6.7 sodium

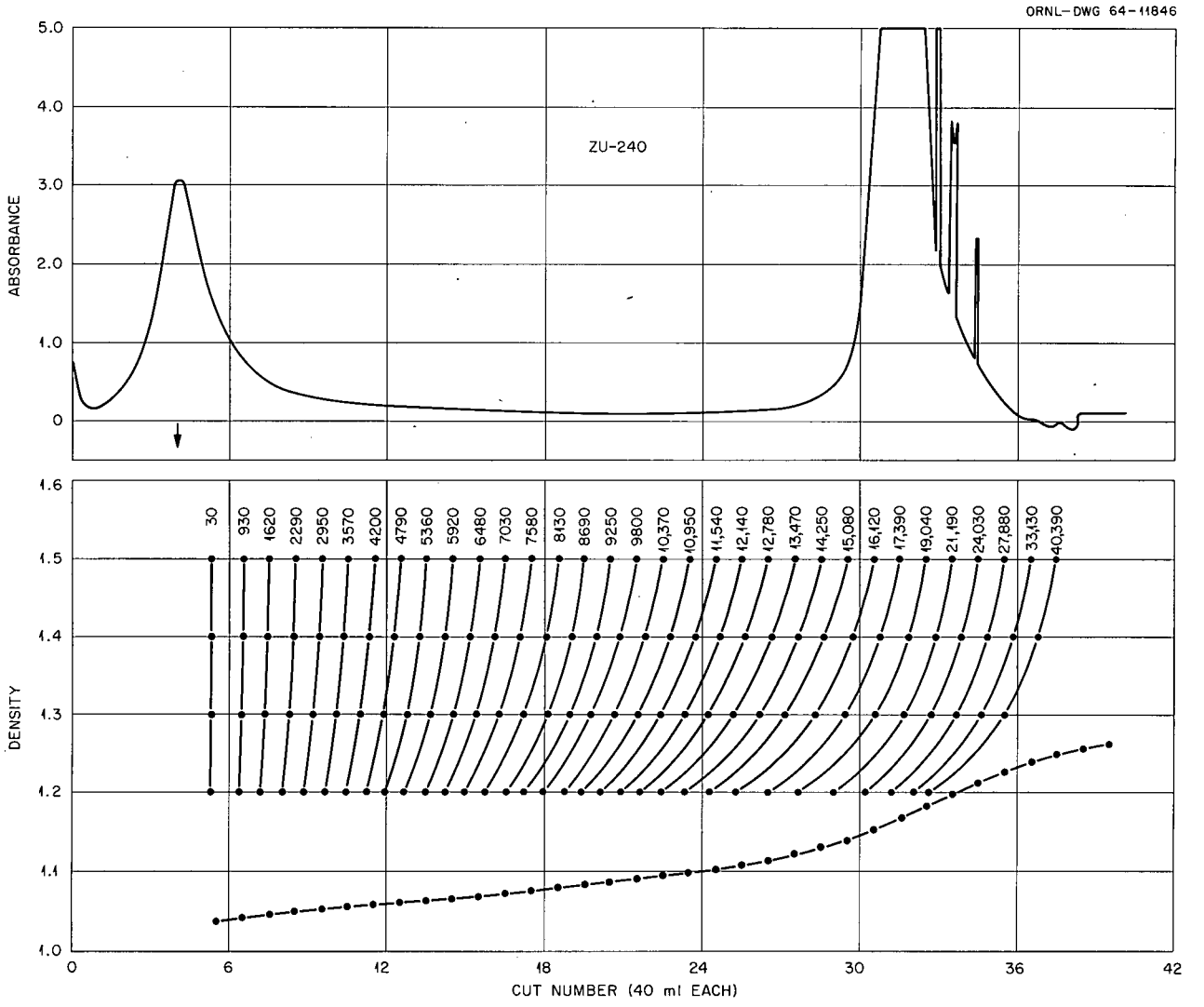

Fig. II-C-1. B-IV Zonal Centrifuge Run Diagram for Human Breast Tumor.

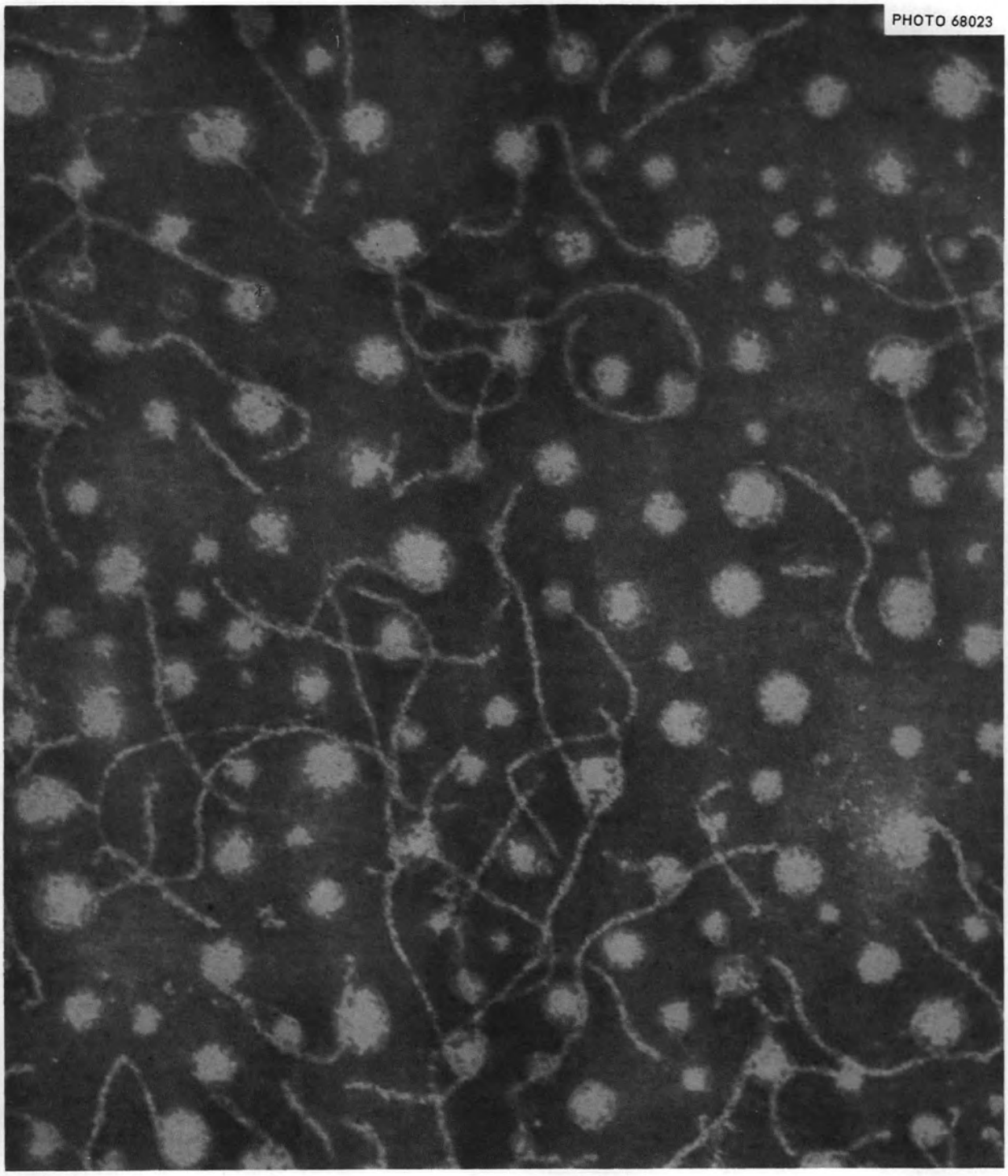

Fig. II-C-2. Virus-Like Particles Observed in Fraction Obtained by Rate Zonal Centrifugation and Isopycnic Banding of Human Breast Tumor. Obtained in cut No. 4 from run shown in Fig. II-C-1. 80,000×.

citrate. The larger tissue fragments were removed by slow-speed centrifugation, after which particles ranging in size from mitochondria to small viruses were sedimented in the Spinco No. 30 angle-head rotor for 30 min at 24,000 rpm. The pellets were resuspended to a final volume of 28 ml and used as the starting sample in the B-IV zonal ultracentrifuge. The centrifuge was run until $\int \omega^2 \, dt = 1236 \times 10^7$. The recovered zonal centrifuge fractions were layered over 9 g of dry CsCl in No. 30 rotor tubes and centrifuged overnight at 24,000 rpm. The run diagram and computer plot are shown in Fig. II-C-1.

Under these conditions the virus-like particles would not be spread through more than a few tubes. Cuts 4–9 were examined in the electron microscope. The particles shown in Fig. II-C-2 were banded from cut 4, whose position is indicated in Fig. II-C-1. The particles averaged 125 μ in diameter, with a central denser portion having a diameter of approximately 100 μ. The strands also seen in the micrograph would occupy about 20% of the core if they originated from this source. The similarity between these particles and the particles which are associated with mammary tumors in mice is of more than passing interest.

With these and subsequent studies, techniques for examining tumors for virus particles have advanced to the point where a continuing search program may be considered.

D. EFFECT OF THE WARMING RATE ON THE SURVIVAL OF YEAST CELLS FROZEN CENTRIFUGALLY

J. G. Green Peter Mazur

The survival of yeast cells frozen at cooling rates of 1°C/min or above appears to depend largely on whether or not ice forms within the cells. Low cooling rates (~1°/min) favor high survivals because they cause the cells to dehydrate and, as a consequence, prevent intracellular crystallization. With higher cooling rates (>50°/min), the cells do not have sufficient time to dehydrate, and so they freeze internally.[22–24]

However, another phenomenon appears in rapidly cooled cells: their survival becomes dependent on the rate of warming and thawing, with rapid warming yielding the higher survivals.[22] Crystal size is known to decrease with increasing cooling velocities, and it has been hypothesized[22] that rapid cooling produces smaller crystals within yeast cells and that these small crystals, because of their higher surface free energy, grow to damaging size during slow warming but not during rapid warming. The technique of centrifugal freezing described previously[25,26] provides a means of testing this hypothesis, since it permits reproducible, extremely rapid freezing of cell suspensions. Therefore, it has been applied to determine the effects of varied warming rates on the subsequent survival of rapidly frozen unicellular yeast (*Saccharomyces cerevisiae*).

The yeast was cultured in liquid media,[22] isolated by centrifugation, washed three times with sterile distilled water, and resuspended in sterile water to a final concentration of about 2×10^8 cells/ml. In previous experimentation, the cell suspension was injected from a hypodermic needle into the spinning rotor containing liquid nitrogen; however, in the present study, 4 ml of the cell suspension was introduced into the rotor as an aerosol from a glass atomizer designed to give minimal evaporation of water from the cells during delivery and to produce small droplets. The freezing of the suspended cells was conducted in a rotor spinning at 3600 rpm in an International PR-2 centrifuge, since earlier unreported studies yielded best cell survival from this treatment. The frozen suspension, still in liquid nitrogen, was transferred to a chilled, insulated cup to expedite transfer to the containers used in warming.

Two series of warming experiments were performed. In the first series, the frozen cells in a small amount of liquid nitrogen were poured into a beaker containing 1 liter of 0.08 *M* potassium phosphate plating diluent at temperatures of 5, 15, 25, 35, 45, and 55°C. To facilitate dispersion of the suspension during warming, the solution was stirred by a propeller agitator at a speed which caused sporadic vortex breakup.

---

[22] P. Mazur, *Biophys. J.* 1, 247 (1961).

[23] P. Mazur, *Biophys. J.* 3, 323 (1963).

[24] P. Mazur, *J. Gen. Physiol.* 47, 347 (1963).

[25] N. G. Anderson and J. G. Green, *Biol. Div. Semiann. Progr. Rept. Aug. 15, 1962*, ORNL-3352, p. 115.

[26] N. G. Anderson, J. G. Green, and P. Mazur, *Joint NIH-AEC Centrifuge Development Program Semiann. Rept. July 1–Dec. 31, 1962*, ORNL-3415, p. 60.

Since the rate of warming of the cell suspensions could not be measured in these experiments, a second series of experiments was performed utilizing the following techniques.

1. The cell suspension was warmed to room temperature within the rotor.
2. The frozen suspension in liquid nitrogen was transferred to shell vials chilled to −196°C, and warmed to room temperature in air.
3. The frozen suspension, free of liquid nitrogen, was ladled into shell vials chilled to −10°C. In one trial the cells were warmed to room temperature in air, but in subsequent trials the vials were fixed to a copper block with silicone grease to increase the rate of warming.
4. The frozen suspension in liquid nitrogen was poured into plastic centrifuge tubes chilled to −196°C which were dipped into a 35°C water bath upon evaporation of the liquid nitrogen.
5. The frozen suspension in a small amount of liquid nitrogen was poured into a liter of plating diluent at 35°C.

The warming rates of the suspensions in trials 1 through 4 were monitored in duplicate by fine thermocouples placed in the frozen suspension, and the thermocouple output was recorded continuously by a Leeds and Northrup Speedomax G recorder with dual chart-speed attachment. The warming rate for trial 5 could not be measured directly, and estimated values are given.

Viability of the untreated control and treated suspensions was assessed by hemacytometer counting and suitable plating techniques.[22]

Although droplet size of suspensions from a hypodermic needle decreases and becomes more uniform with increasing rotor speed, droplet size from aerosol delivery appears to be relatively independent of rotor speed and may be minimally affected by shearing effects at the liquid-nitrogen–air interface of the spinning rotor. In all trials, the frozen droplets obtained from aerosol delivery were noticeably smaller than particles obtained from delivery through a hypodermic needle.

The results of the first series of experiments are shown in Fig. II-D-1. The increase in survival with increasing bath temperature to 35°C can be attributed to the increased rate of warming, but the decrease in survival at higher temperatures may be caused by damage to the cells resulting from exposure to the higher temperature and may

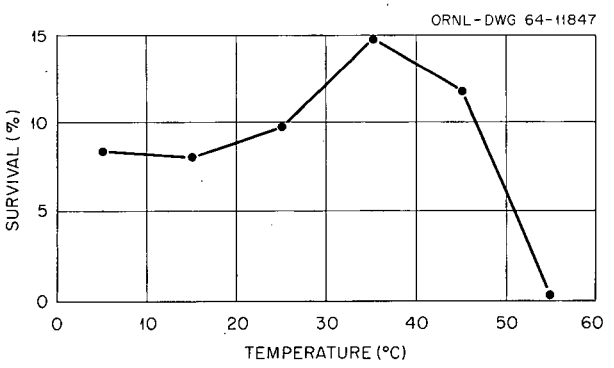

Fig. II-D-1. Survival of Centrifugally Frozen Yeast Cells Warmed in 1-liter Phosphate Diluent Baths at Different Temperatures.

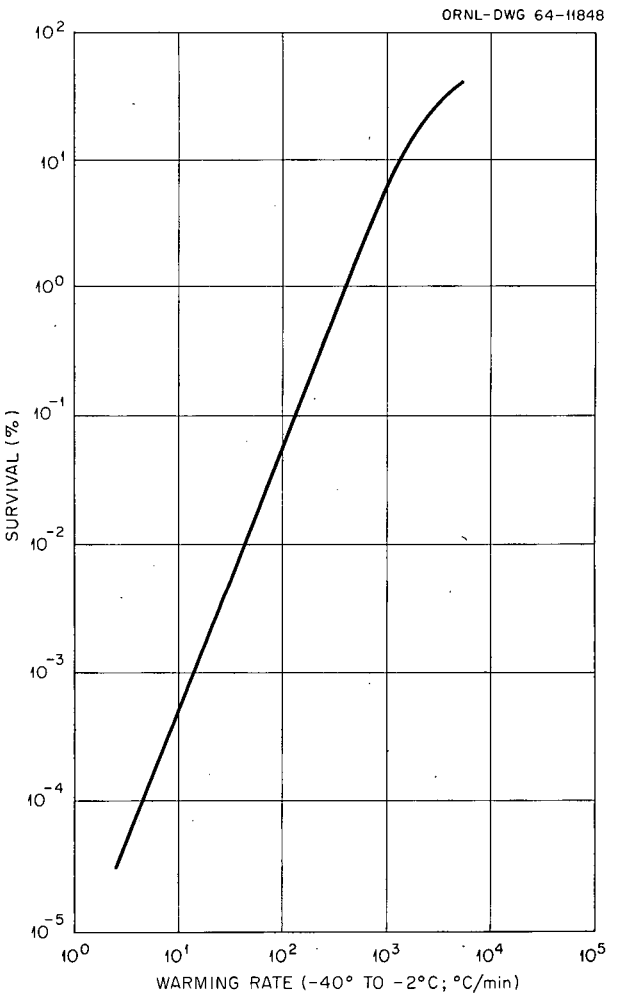

Fig. II-D-2. Effect of Warming Rate on Centrifugally Frozen Yeast Cells.

be only indirectly or not at all related to the freezing treatment. The fact that no difference in survival appears in the 5 and 15°C treatments is probably related to the coalescence of the warming droplets into larger ice particles at the two temperatures.

The results of the second series of experiments, depicted in Fig. II-D-2, confirm the fact that the survival of rapidly frozen cells is directly related to the warming rate. They strengthen the hypothesis that the survival of the cells is related to changes in crystal size and structure during the critical warming period. Since the exact freezing rate is not known, its effect cannot be independently assessed in this study.

Further study to measure the actual cooling rate of the suspension droplets and the warming rate in stirred solutions is in progress. In addition, effort to increase the warming rate appears warranted.

III. Theoretical Studies

A. DENSITY INVERSION DURING CENTRIFUGATION

Stephen Prager[1]

Formulation

We consider a centrifuge filled with a solvent whose density ρ_0 increases with increasing distance r from the axis. (These density variations are, of course, produced by a concentration gradient of a suitable solute A which, following Svensson,[2] we consider as part of the solvent.) Into this system we introduce a macromolecular species B of volume $\overline{V}$ per molecule and density $\rho_s > \rho_0$; let the initial concentration distribution of B be $c_0(r)$, in molecules per unit volume. The migration of B particles in the centrifugal field causes their concentration to depend upon time as well as position, so that after a time t the new concentration distribution will be $c(r, t)$. These concentration changes in turn affect the distribution of density in the centrifuge and give rise to the possibility that the total density ρ of solvent plus B may in some regions actually decrease with increasing r, creating a hydrostatically unstable situation. It is with the occurrence of such instabilities, produced in an initially stable system by the sedimentation of B, that we shall concern ourselves.

To render the problem a little more tractable, we make the following assumptions: (1) There is no diffusion, either of B or of the solute A which produces the density gradient, during the time of a run. (2) The volume fraction $\overline{V}c$ of B is everywhere and at all times small compared to unity, so that we can ignore the displacement of solvent by migrating B particles. With these two assumptions, the solvent density $\rho_0(r)$ becomes time independent, which greatly simplifies the calculations.

The time dependence of the concentration distribution $c(r, t)$ is governed by the continuity equation

$$\frac{\partial c}{\partial t} = -\frac{1}{r}\frac{\partial}{\partial r}(rvc) , \tag{1}$$

where v, the migration velocity of B, is, in the absence of diffusion, given by

$$v = \frac{\omega^2 \overline{V}}{F(r)}[\rho_s - \rho_0(r)]r , \tag{2}$$

ω being the angular velocity, in radians per unit time, at which the centrifuge is spinning, and F the friction coefficient for the B species. Although we shall later assume that F is constant, it must in general be considered a function of r because of the variation in the solvent viscosity with changing concentration of A.

Combination of (1) and (2) leads to the partial differential equation

$$\frac{\partial c}{\partial t} = -\frac{\omega^2}{r}\frac{\partial}{\partial r}\left\{\frac{\overline{V}r^2[\rho_s - \rho_0(r)]c}{F(r)}\right\} , \tag{3}$$

to be solved subject to the initial condition

$$c(r, 0) = c_0(r) . \tag{4}$$

Solution

Equation (3) may be solved by the method of characteristics. We multiply both sides of (3) by

[1]University of Minnesota. Research performed under subcontract number *729* for the Oak Ridge Gaseous Diffusion Plant, operated by Union Carbide Corporation under contract with the U.S. Atomic Energy Commission.

[2]H. Svensson, L. Hagdahl, and K. -D. Lerner, *Sci. Tools* 4, 1 (1957).

$\bar{V}r^2(\rho_s - \rho_0)/F$ and define a new concentration variable

$$\zeta \equiv \bar{V}r^2(\rho_s - \rho_0)c/F \tag{5}$$

to obtain

$$\frac{\partial\zeta}{\partial t} = -\frac{\omega^2\bar{V}r[\rho_s - \rho_0(r)]}{F(r)}\frac{\partial\zeta}{\partial r}. \tag{6}$$

Division by $\partial\zeta/\partial r$ now gives

$$\left(\frac{\partial r}{\partial t}\right)_\zeta = \frac{\omega^2\bar{V}r[\rho_s - \rho_0(r)]}{F(r)}, \tag{7}$$

from which the contours of constant ζ in the (r, t) plane may be calculated by integration:

$$\omega^2 t = \int_{r_0(\zeta)}^{r} \frac{F(r)\,dr}{\bar{V}r[\rho_s - \rho_0(r)]}, \tag{8}$$

where $r_0(\zeta)$ satisfies the relation

$$\zeta = \bar{V}r_0^2\,[\rho_s - \rho_0(r_0)]\,c_0(r_0)/F(r_0)\,. \tag{9}$$

Equation (8) is, in implicit form, the desired solution of (3).

Example

Let us consider the particular case of a density gradient of the form

$$\rho_0(r) = \rho_s - \frac{k}{r^n}, \tag{10}$$

where k and n are positive constants, and let us further assume that the friction coefficient F is independent of r. Substitution of (10) into (8) then gives

$$\omega^2 t = \frac{F}{\bar{V}nk}[r^n - r_0^n(\zeta)]\,. \tag{11}$$

To obtain $r_0(\zeta)$, we must specify $c_0(r)$, and for this purpose we suppose that at $t = 0$ a band extending from $r = r_1$ to $r = r_2 > r_1$ is loaded with B to maximum capacity, so that the total density is initially given by

$$\rho(r, 0) = \begin{cases} \rho_0(r) & (r < r_1)\,, \\ \rho_0(r_2) & (r_1 < r < r_2)\,, \\ \rho_0(r) & (r < r_2)\,. \end{cases} \tag{12}$$

Clearly, any further loading of B into the band would produce a density inversion.[2]

The density ρ is related to the concentration c by the equation

$$\rho = \rho_0 + c\bar{V}(\rho_s - \rho_0)\,. \tag{13}$$

Combining (13) with (5), we have

$$\rho = \rho_0 + \frac{F\zeta}{r^2}\,. \tag{14}$$

The initial position dependence of ζ is, therefore,

$$\zeta(r, 0) = \begin{cases} 0 & (r < r_1)\,, \\ \dfrac{kr^2}{F}\left(\dfrac{1}{r^n} - \dfrac{1}{r_2^n}\right) & (r_1 < r < r_2)\,, \\ 0 & (r > r_2)\,. \end{cases} \tag{15}$$

The function $r_0(\zeta)$ is obtained by inversion of (15), and $\zeta(r, t)$ then follows from (11):

$$\zeta(r, t) = \begin{cases} 0 & [(r^n - \tau)^{1/n} < r_1]\,, \\ \dfrac{k(r^n - \tau)^{2/n}}{F}\left(\dfrac{1}{r^n - \tau} - \dfrac{1}{r_2^n}\right) & [r_1 < (r^n - \tau)^{1/n} < r_2]\,, \\ 0 & [(r^n - \tau)^{1/n} > r_2]\,, \end{cases} \tag{16}$$

where $\tau \equiv \omega^2\bar{V}nkt/F$. At time t, the band containing the B species thus extends from $r = (r_1^n + \tau)^{1/n}$ to $r = (r_2^n + \tau)^{1/n}$, and within it the density varies according to the relation

$$\rho = \left(\rho_s - \frac{k}{r^n}\right) + \frac{k(r^n - \tau)^{2/n}}{r^2}\left(\frac{1}{r^n - \tau} - \frac{1}{r_2^n}\right)$$
$$[(r_1^n + \tau)^{1/n} < r < (r_2^n + \tau)^{1/n}]\,. \tag{17}$$

A simple criterion for whether or not density inversion takes place within the band results

from a comparison of ρ at the band's leading and trailing edges; the inequality

$$\rho\,[(r_1^n + \tau)^{1/n}, \tau] < \rho\,[(r_2^n + \tau)^{1/n}, \tau] \qquad (18)$$

is certainly a necessary requirement if an inversion is to be avoided.

Substitution of (17) into (18) leads, after simplification, to the stability condition

$$\left(1 + \frac{\tau}{r_1^n}\right)^{(2/n)-1} > \left(1 + \frac{\tau}{r_2^n}\right). \qquad (19)$$

For $n \leqq 1$, the inequality (19) will always be satisfied, since $r_1 < r_2$, while for $n \geqq 2$, the exponent $(2/n) - 1$ is negative, so that (19) is always violated. We expect, therefore, that the sedimentation of B will stabilize the initial band in the former case and destabilize it in the latter. The intermediate situation, $1 < n < 2$, is more complicated. For the initial stability to be maintained, it is first of all necessary that (19) be satisfied for small τ, for which the left-hand side of the inequality may be expanded, to give, after simplification,

$$\frac{r_1}{r_2} < \left(\frac{2}{n} - 1\right)^{1/n}. \qquad (20)$$

However, even if (20) is obeyed, the band will ultimately become unstable if allowed to sediment long enough. The critical time τ^* for the onset of instability may be obtained by finding the nonzero solution of the equation

$$\left(1 + \frac{\tau^*}{r_1^n}\right)^{(2/n)-1} = \left(1 + \frac{\tau^*}{r_2^n}\right). \qquad (21)$$

This work is being continued to allow the development of three general types of gradients. The first is the optimal gradient for fractionating a continuous spectrum of particles. The greatest particle-supporting capacity will be required at the level of the starting zone. As the particles become spread through the gradient, the required supporting capacity at all levels will decrease. Minimal capacity is required near the bottom of the gradient. The second type represents the opposite extreme case, where only particles of one species are present. The optimal gradient in this instance is one in which the capacity is everywhere the same (when the total number of particles is considered). The difference in density between the particles and the suspending medium decreases as the particles sediment into denser portions of the gradient. At the same time, the particle concentration decreases due to radial dilution. Both of these effects require that convex gradients (gradients whose slope decreases with increasing radius) be employed. The third general class of gradient is one designed for the separation of a given particulate mixture. As an example, sucrose gradients can be devised which allow nuclei and mitochondria to be banded isopycnically, while microsomes, and even polysomes, are separated on a rate basis. Theoretical studies must go hand in hand with their experimental verification using biological materials.

IV. Rotor Design

A. STABILITY STUDIES

H. P. Barringer

Theoretical Studies

Four coupled linear differential equations in complex variables which predict the motions of a rigid rotor can be used for high-speed centrifuge rotor analysis.[1] The complete solution of these equations involves a transient and a steady-state condition which is too tedious for hand solution; therefore, the equations have been programmed on the IBM 7090 computer as two separate cases for the transient solution and the steady-state solution. Figure IV-A-1 shows the model used for the rotor and the equations which have been developed.

Transient Solution

The transient solution is obtained when the right-hand sides of the equations in Fig. IV-A-1*b* are set to zero and the solution form is assumed. The computer input requires distance A, distance B, weight of the rotor W, gravitational constant g, transverse moment of inertia I_1, polar moment of inertia I_3, spin frequency of the rotor ω, damping constant C_1, damping constant C_2, weight of the sprung mass W_1, weight of the sprung mass W_2, shaft spring constant K_1, shaft spring constant K_2, spring constant K_{1s}, spring constant K_{2s}, fractional amount of the weight supported by the top bearing γ, and certain command information for the computer. The computer uses the data and equations to calculate roots of an eighth-order polynominal in s with complex roots ($s = \mu + i\nu$), where the roots are the natural modes of oscillation. More specifically, $-\nu/\mu$ is a measure of the rotor's instability (the larger the value, the greater the instability), $-1/\mu$ is the decay constant in sec-

ORNL-DWG 64-11849

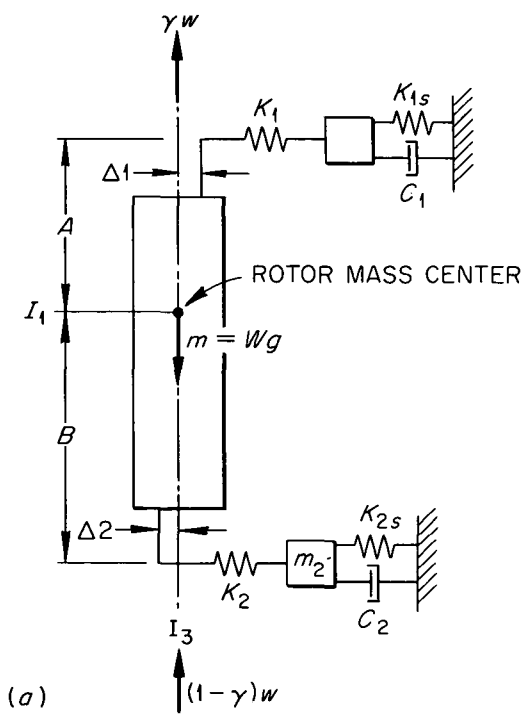

(*a*)

$$m\ddot{z} + K_1(Z - z_1 + aw) + K_2(Z - z_2 - bw) = Q_Z$$
$$m_1\ddot{z}_1 + C_1\dot{z}_1 - K_1(Z - z_1 + aw) + K_{1s}z_1 = Q_{Z1}$$
$$m_2\ddot{z}_2 + C_2\dot{z}_2 - K_2(Z - z_2 - bw) + K_{2s}z_2 = Q_{Z2}$$
$$I_1\ddot{w} - iI_3\omega\dot{w} + K_1a(Z - z_1 + aw) - K_2b(Z - z_2 - bw) + Mg[\gamma a - (1-\gamma)b]w = Q_w$$

(*b*)

Fig. IV-A-1. (*a*) Schematic Model of a Rigid Rotor; (*b*) Equations of Motion of a Rigid Rotor.

[1] R. E. Kelley, *Rigid Rotor Dynamics*, University of Virginia (EP-3912-315-63U), 1963, p. 16.

onds, $\nu/2\pi$ is the mode frequency in cycles per second, and $[(-1/\mu)\ (\nu/2\pi)]$ is the number of cycles for the mode to decay.

When the roots, s, are obtained, relative amplitudes of motion for the rotor ends, damper masses, etc., can be computed when the rotor mass center is displaced one unit. Calculations are required at different rotor spin frequencies, since gyroscopic forces can severely alter the anticipated results based on zero spin frequencies. One typical study of the B-IV rotor is shown in Fig. IV-A-2, where the criterion $-\nu/\mu$ is plotted as contour lines on the spin frequency and damping constant plane. These data show the value of optimum damping constant and areas where rotor instability may be severe. Only root 3 is shown in Fig. IV-A-2, since this is the most erratic root for this particular rotor configuration, and the other seven roots have much lower values of $-\nu/\mu$ in the plotted range of damping constants (polynomial s will have four roots which are positive, i.e., where the whirl frequency is in the direction of the rotor spin frequency, and four roots which are negative, i.e., where the whirl frequency is opposite to the direction of the rotor spin frequency). Root 3 is a positive whirl frequency.

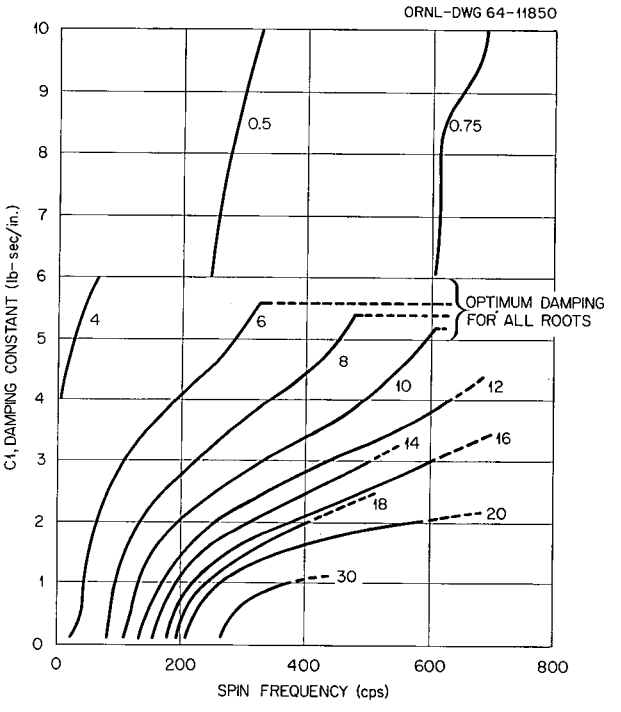

Fig. IV-A-2. Topographical Map of Instability Criterion ($-\nu/\mu$). Damping constant vs spin frequency for B-IV rotor. The numbered curves denote various amplitudes.

Steady-State Solution

The steady-state solution gives the rotor motion which would occur after the transient motions have decayed (the decay time for some transient motions can be in the range of fractions of a second to fractions of days, depending on the situation). This motion is excited by forcing functions attributed to displacement of the rotor shafts from the mass center. The computer input uses the information given in the transient case plus the displacements $\Delta 1$ and $\Delta 2$ of the shafts and the angle α between the shaft displacements; and the computer output gives motions of the rotor ends, damper masses, etc., at various spin frequencies. The data associated with the transient solution are shown in Fig. IV-A-3 for the

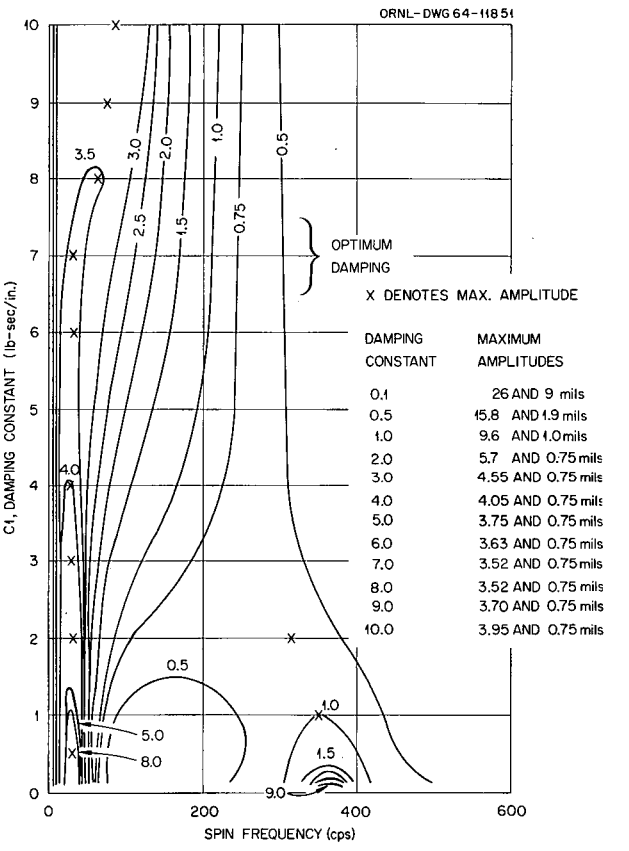

Fig. IV-A-3. Topographical Map of Rotor Runout (RT). Spin frequency vs damping constant for B-IV rotor.

steady-state solution, where the amplitude of the top of the rotor is plotted as contours on the spin frequency and damping constant plane. These data show where the optimum damping constant occurs and the consequence of a damping constant that is too low.

Information from Figs. IV-A-2 and IV-A-3 indicates that the optimum damping is not equivalent and requires a design compromise for proper operation of the rotor. Thus, the optimum transient solution gives $C_1 \approx 5.5$ lb sec in.$^{-1}$, while the steady-state solution gives $C_1 \approx 7.0$ lb sec in.$^{-1}$, and the computed damping constant for the B-IV damper gives $C_1 \approx 3.0^+$ lb sec in.$^{-1}$ when shear of the oil and squeeze film effects are considered.[2]

B. ROTOR CONFIGURATIONS

H. P. Barringer

Rotor Shapes

There are four general rotor configurations for use in centrifuges: (case 1) short length, large diameter, as with angle-head rotors; (case 2) short length, elongated in the radial direction, as with analytical rotors; (case 3) long lengths, small diameter, as with long bowl centrifuges; and (case 4) length about equal to diameter, as with a sphere. Cases 1 and 2 give stable configurations, case 3 gives a configuration of increasing difficulty, while case 4 is difficult to stabilize, since it seeks to tumble.

The above cases can be chosen by the ratio of their mass moments of inertia:

cases 1 and 2, $I_{spin}/I_{transverse} > 1$;
case 3, $I_{spin}/I_{transverse} < 1$; and
case 4, $I_{spin}/I_{transverse} \approx 1$.

There are practical limits on most shapes for case 1, where $I_{spin}/I_{transverse}$ cannot exceed 2, and for case 4, where the value is approximately 1. However, cases 2 and 3 can vary over wide intervals. For a rule of thumb, $1.1 < I_{spin}/I_{transverse} < 0.2$; a greater distance from the minimum values gives a more stable rotor.

The practical significance of these ratios is that for cases 1 and 2 only one support shaft is required, while cases 3 and 4 require shafts on each end of the rotor to maintain stability.

The combination of a mathematical model programmed for a high-speed computer, and test stands and facilities for the experimental determination of the physical parameters of experimental rotors, will allow us in the future to develop new experimental rotors with a greater probability of successful performance.

C. METALLURGICAL STUDIES

K. T. Ziehlke W. S. Dritt

Stress corrosion problems associated with 7075-T6 aluminum in concentrated cesium chloride have not been observed with beta titanium or 18% nickel Maraging steel. Test procedures previously described[3] have been used on polished beta titanium (160,000 psi bending stress level), Kanigen-plated 18% nickel Maraging steel (230,000 psi bending stress level), and low-phosphorus electroless plated 18% nickel Maraging steel (230,000 psi bending stress level) specimens. The samples at stress levels of 95% of the estimated yield strengths have accumulated over 1500 hr test time without failure.

Soon after the stress corrosion tests were begun, one Kanigen-plated test coupon developed small cracks in the plating and was removed to prevent contamination of the cesium chloride bath. The cracks were a result of the high stress level and low ductility of the Kanigen plating.

New rotor materials, platings, and coatings will be developed during the course of this program. The interaction of these with gradient and suspending media will continue to be examined metallurgically.

[2] O. Pinkus and B. Sternlicht, *Theory of Hydrodynamic Lubrication*, p. 220, McGraw-Hill, New York, 1961.

[3] W. S. Dritt and K. T. Ziehlke, *Joint NIH-AEC Zonal Centrifuge Development Program Semiann. Rept. Jan. 1–June 30, 1963*, ORNL-3502, pp. 27–28.

V. Low-Speed Rotors

N. Cho

A. MODIFICATIONS OF PREPARATIVE A-SERIES ROTORS

For a number of purposes, including the attempted isolation of chromosomes from synchronized tissue cultures, low-speed rotors having a smaller capacity are required. The simplest means for achieving this end is to devise a core which fills most of the internal rotor space with solid material. The A-XIII core (Fig. V-A-1) decreases the internal volume of the rotor from 1350 to 350 ml. To allow the separation to be scanned with a photoelectric cell (see below), the solid sectors of the core were painted a dead black.

In the initial design, a solid Lucite plate with two segments removed was used as a means of reducing the internal volume. During testing, the liquid gradient and the sample were found to leak into the clearance between the core plate and the end caps, resulting in an appreciable loss in resolution. An O-ring seal was adapted to seal off the space between the end caps and the solid core sectors.

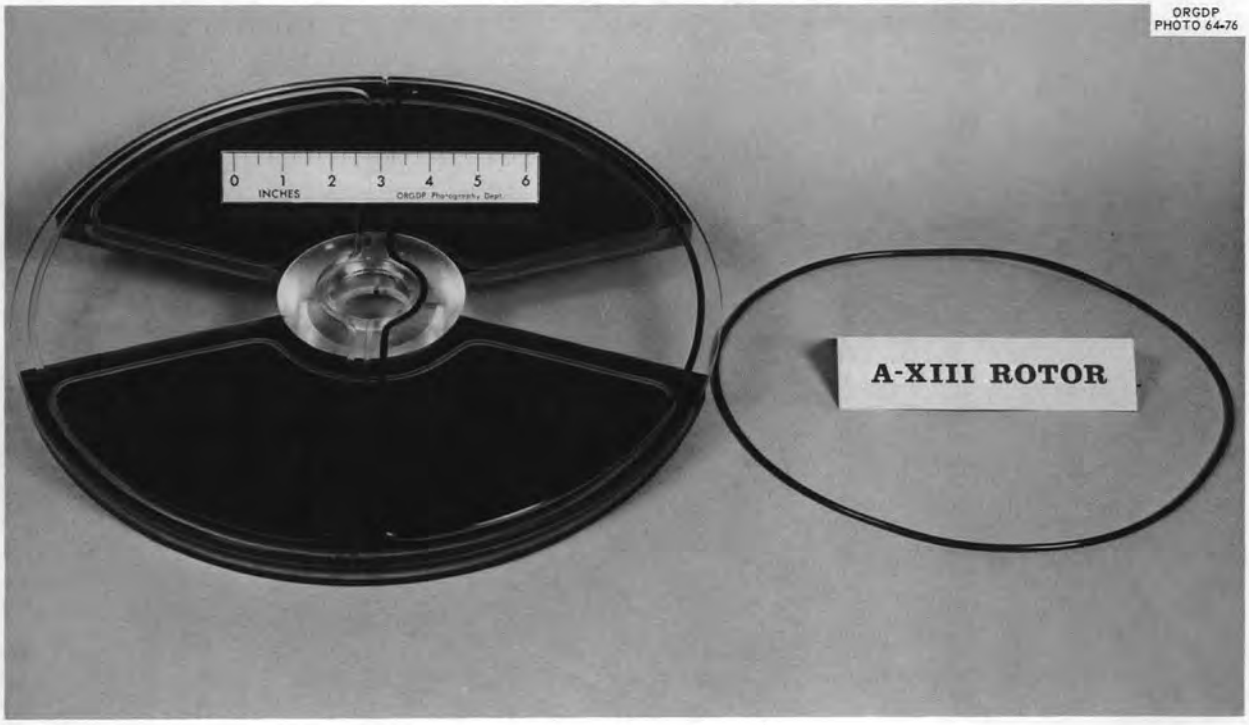

Fig. V-A-1. Core A-XIII for Use with Rotor A-IX or A-XII.

B. A PROTOTYPE LOW-SPEED ANALYTICAL ROTOR

For experimental studies concerned with gradient stability and capacity, a prototype low-speed analytical rotor (A-XI) has been constructed (Fig. V-B-1). Two 20-ml cells having depths and radii identical with the A-IX and A-XII rotors are mounted on a circular steel plate. The fluid line seal is identical with that previously described.[1] The rotor is designed for 6000-rpm operation with the International model PR-2 centrifuge, and has been tested with a scanner to 4100 rpm.

[1] *Joint NIH-AEC Zonal Centrifuge Development Program Semiann. Rept. July 1–Dec. 31, 1963,* ORNL-3656, pp. 43–44.

C. THE A-XII ROTOR

A failure in the acrylic end cap of an A-IX rotor along the outer periphery was experienced after several months of successful use. The failure, shown in Fig. V-C-1, occurred at low speed (1000 rpm) with a 17 to 55% sucrose gradient in the rotor. A complete stress analysis including the effects of thermal stress was made, and was checked in a series of studies on plastic models. It was concluded that the failure was due to stresses on the end cap caused by uneven clamping pressure. A torque wrench has now been specified as an assembly tool to ensure even clamping of the rotor end plates. The remaining A-IX rotors have remained in routine service without further incident.

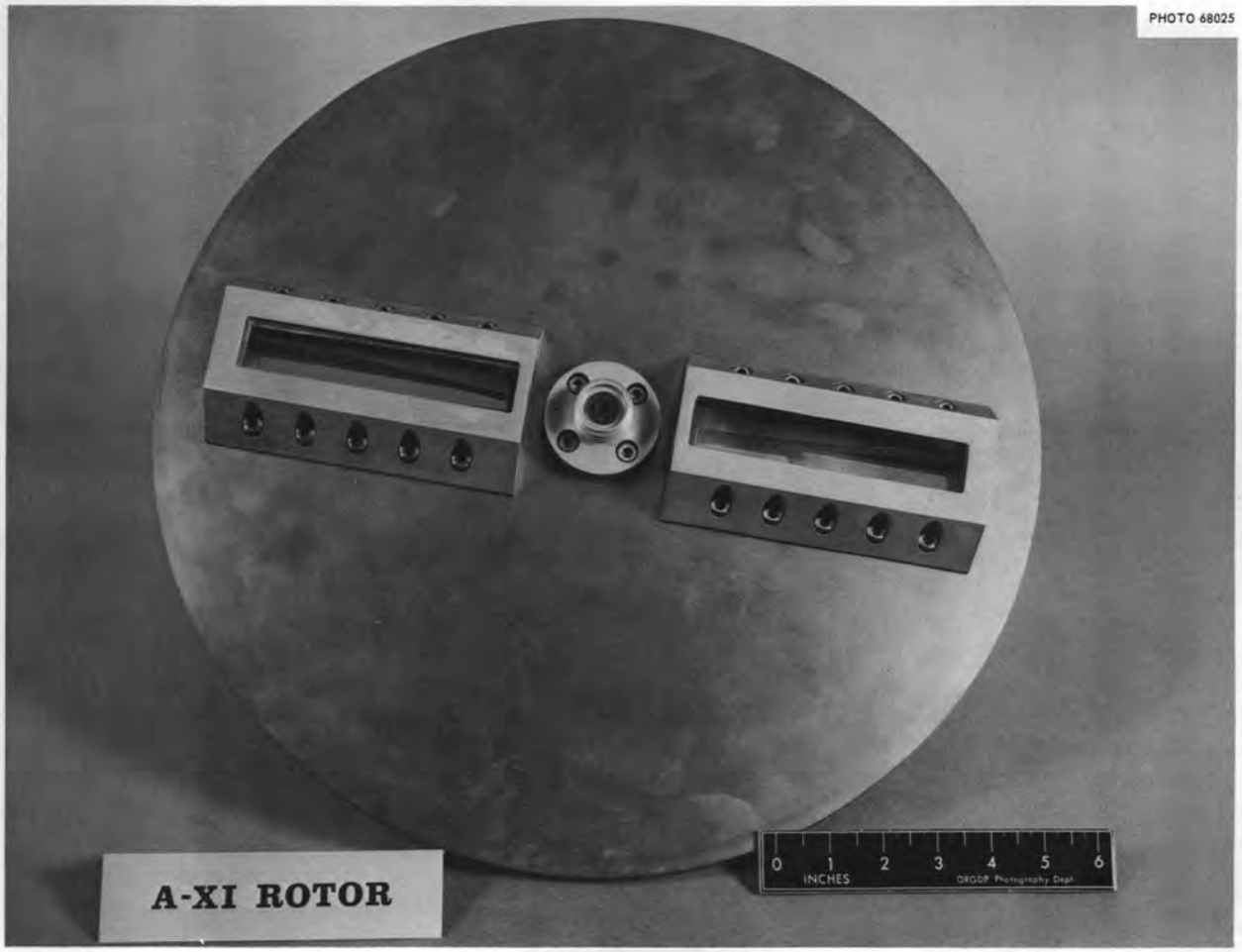

Fig. V-B-1. Prototype of Low-Speed Analytical Rotor.

To ensure, as far as possible, that further failures do not occur, the rotor has been redesigned as the A-XII rotor. In the A-XII rotor the thickness of the acrylic resin in the area where failure occurred has been increased. A combination of a gasket and a metal-to-metal stop has been added to distribute and control the clamping pressure.

Experiments were also performed to determine the effect of changing the number of septa. The banding performance obtained with ragweed pollen was examined using two, four, and eight septa. The results with four and eight were indistinguishable, whereas considerable loss in resolution was observed with two septa. The number of septa has, therefore, been reduced to four in the A-XII rotor. Drawings of this rotor are shown in Figs. V-C-2, V-C-3, V-C-4, and V-C-5.

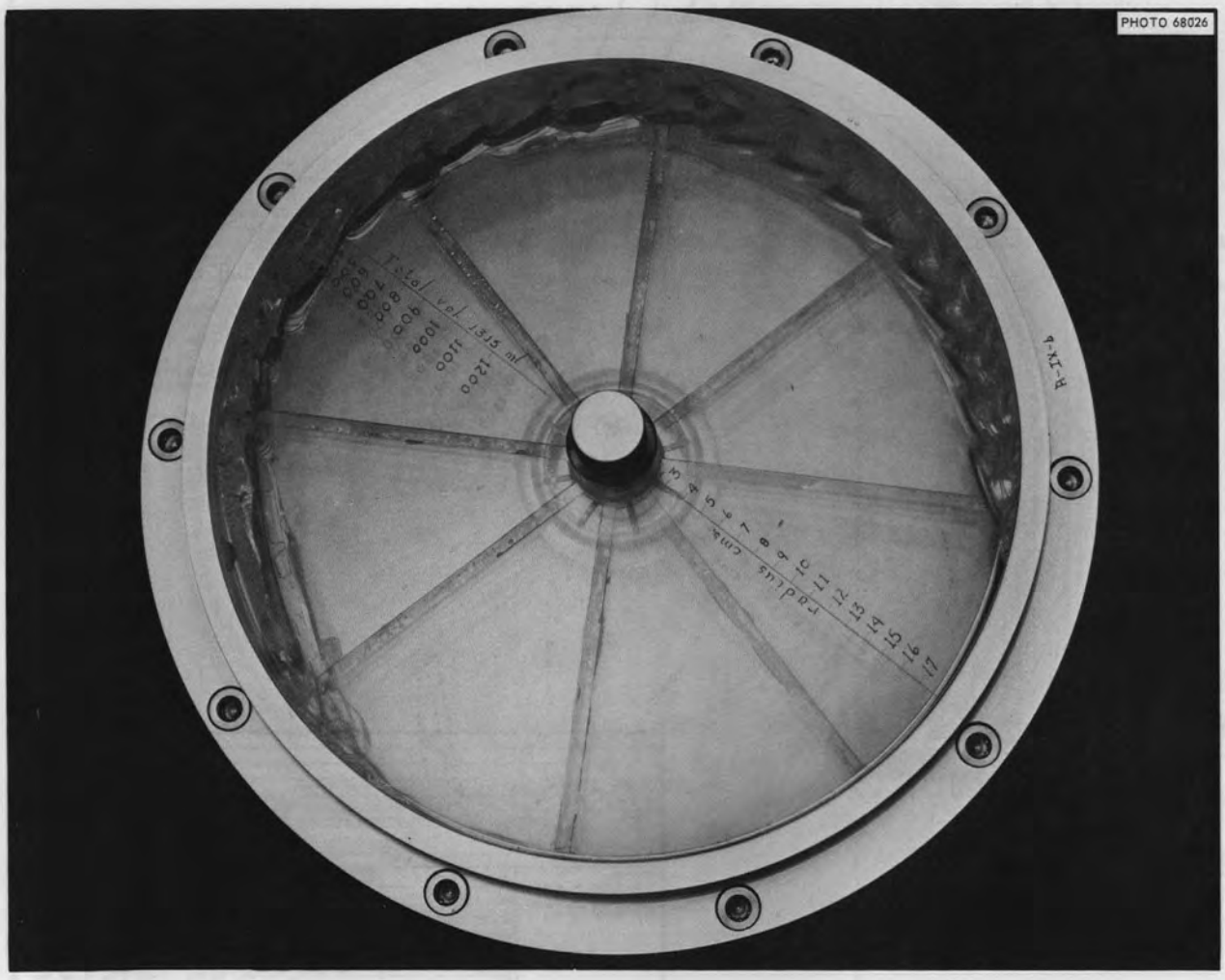

Fig. V-C-1. Failure of A-IX Zonal Rotor.

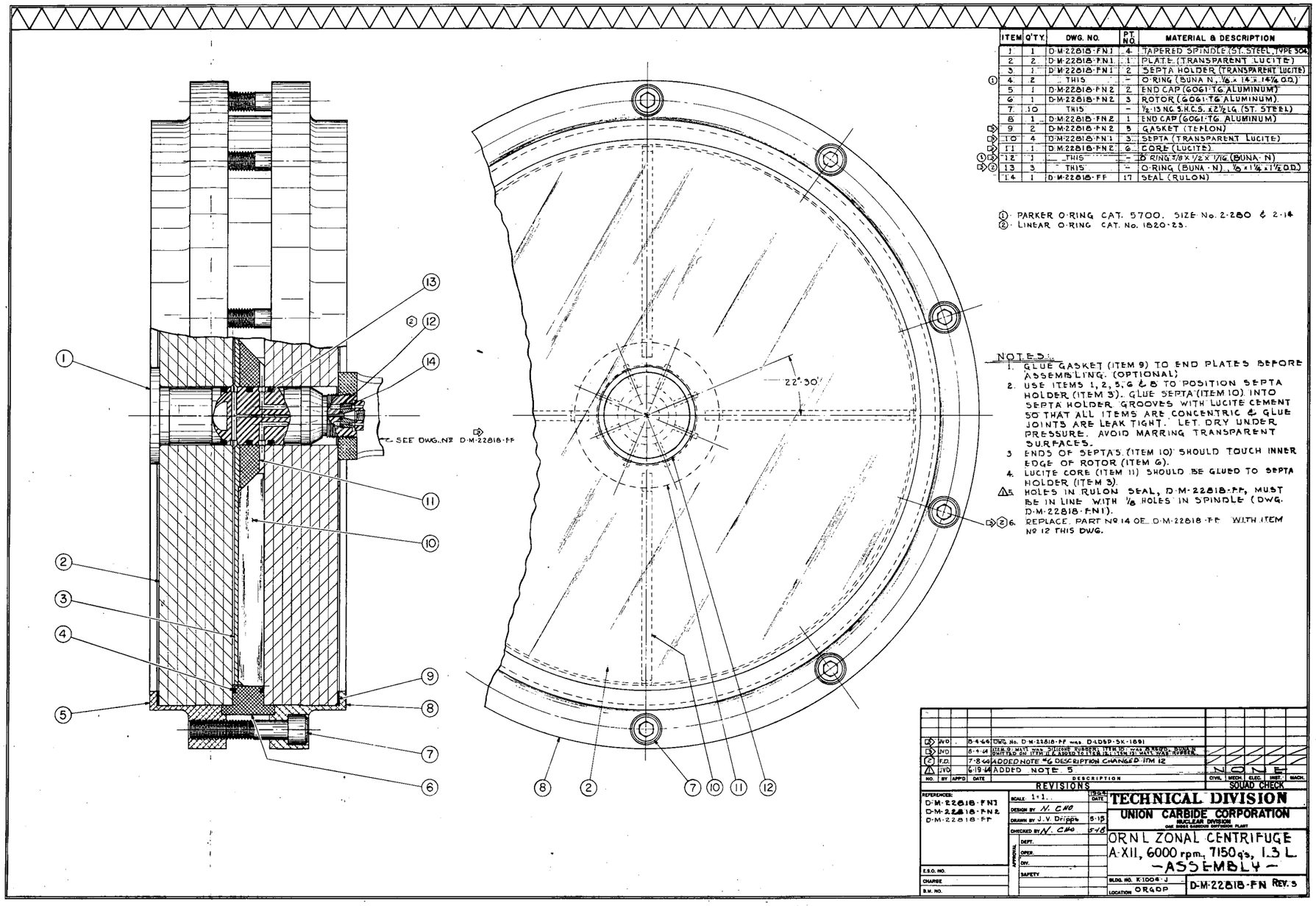

Fig. V-C-2. Drawing of A-XII Zonal Rotor.

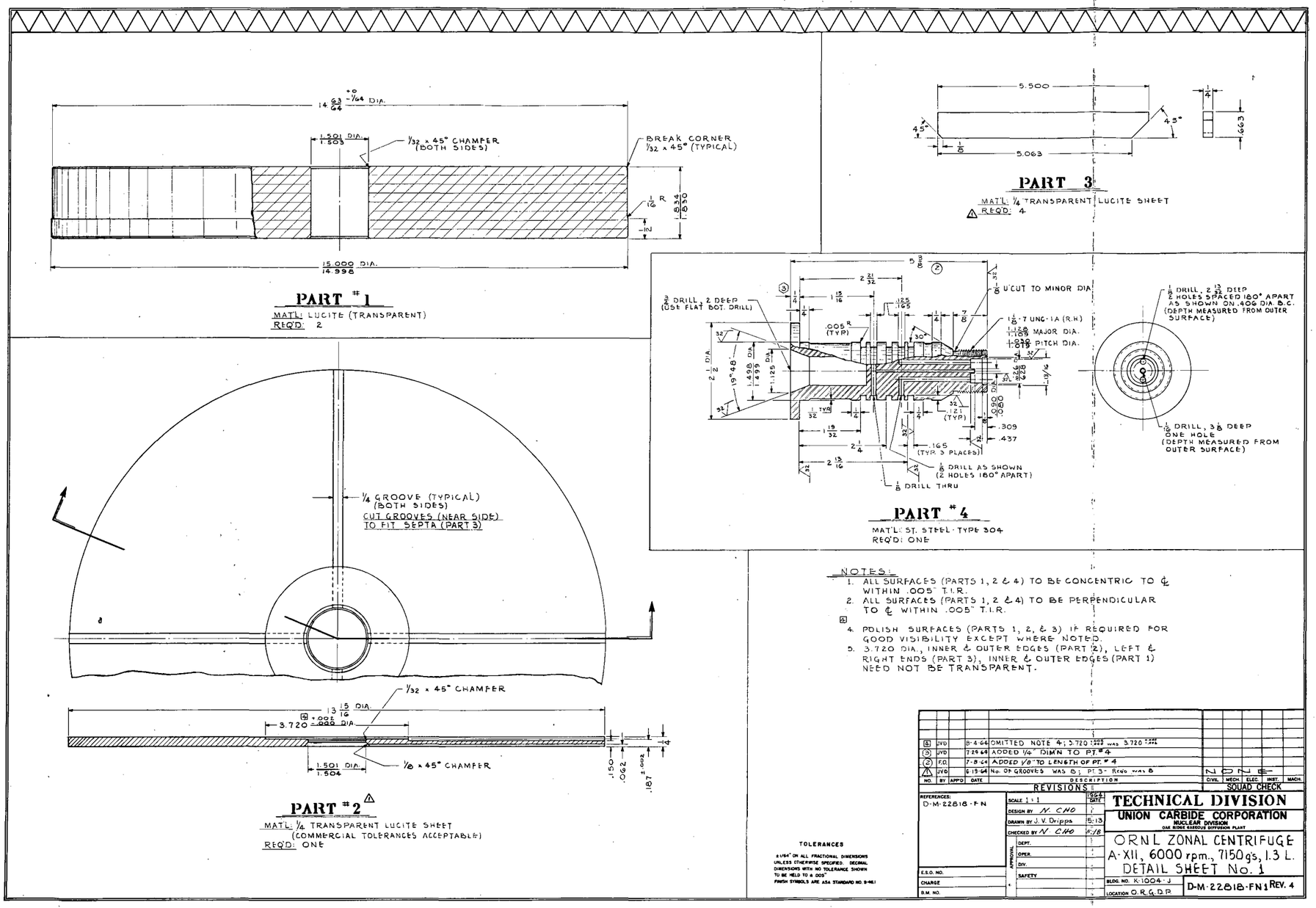

Fig. V-C-3. Drawing of Parts of A-XII Zonal Rotor.

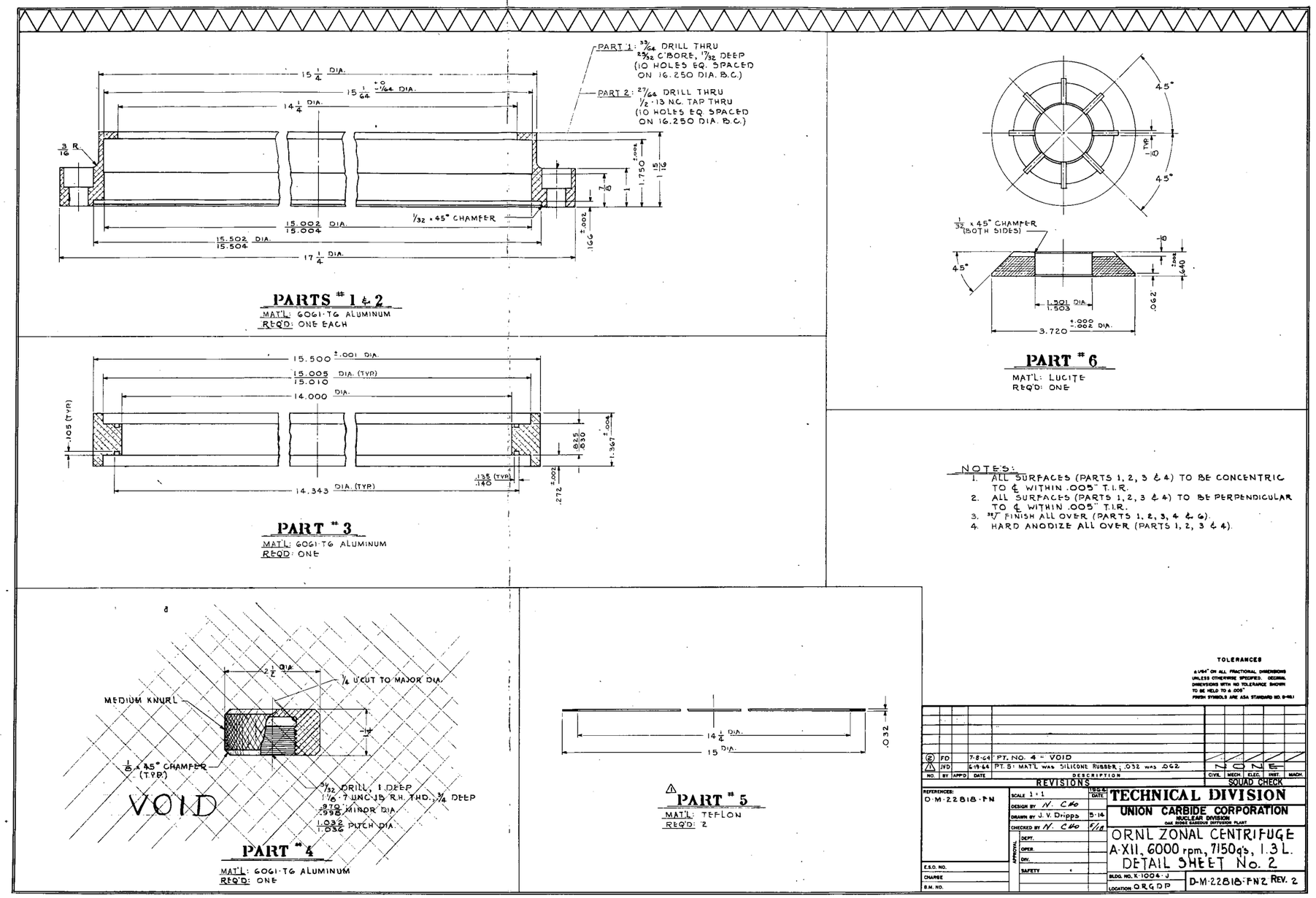

Fig. V-C-4. Drawing of Parts of A-XII Zonal Rotor.

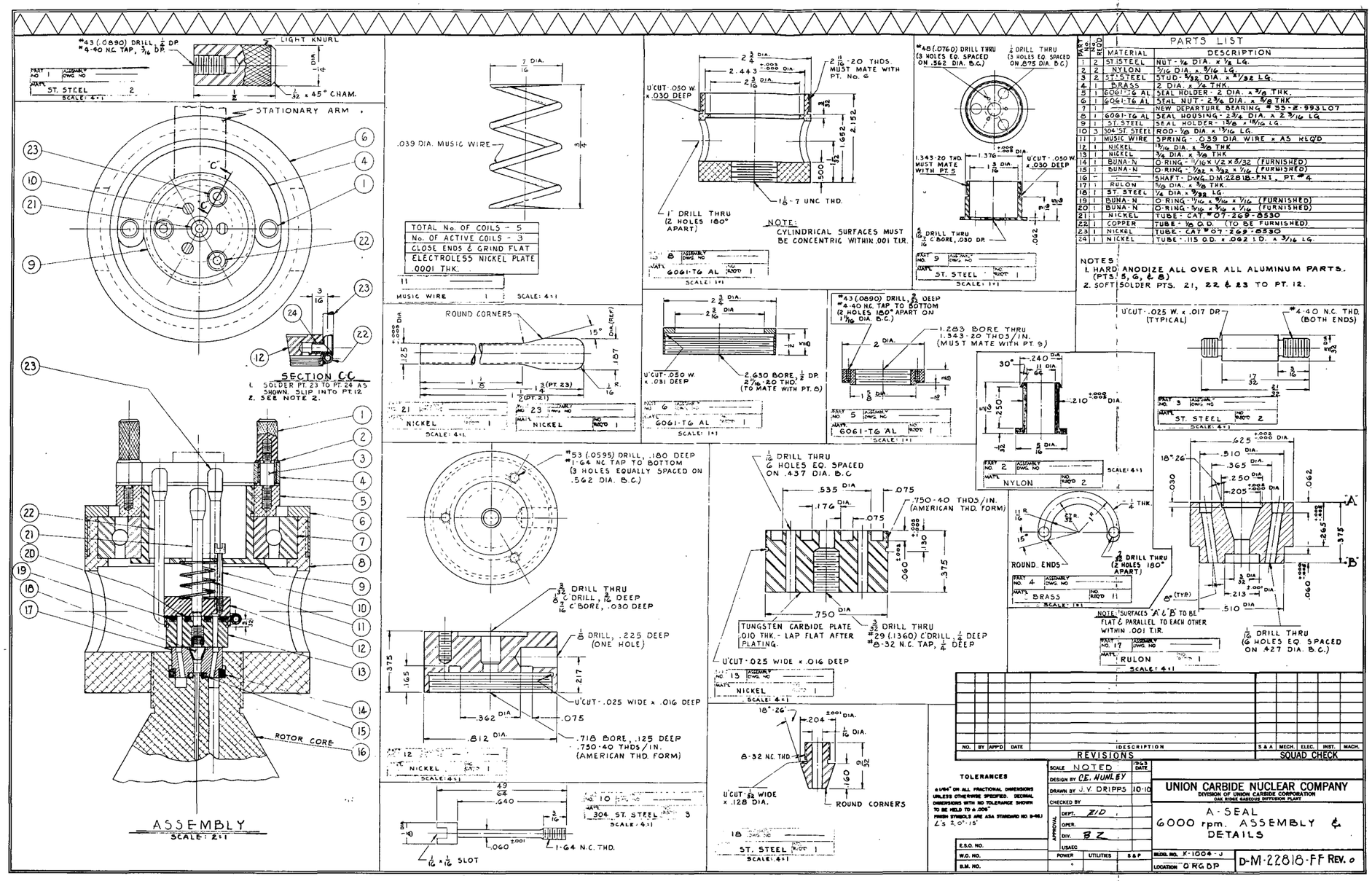

Fig. V-C-5. Drawing of Parts of A-XII Zonal Rotor.

D. SCANNER FOR A-SERIES ROTORS

The A-XII rotor is capable of yielding precise data on the sedimentation rates of large particles if measurements can be made during the course of centrifugation. The simplest way of doing this is with a simple photoelectric scanner, as shown in Fig. V-D-1.

The scanner uses a standard 6-v lamp as a light source and a cadmium selenide photocell as a detector to measure transmitted light. Most of the decrease in transmission of a particle zone is due to scattered light. The photocell is therefore arranged to scan the rotor with a very narrow pencil of light. The output of the photocell is fed to the *Y* axis of an *X-Y* recorder. The position

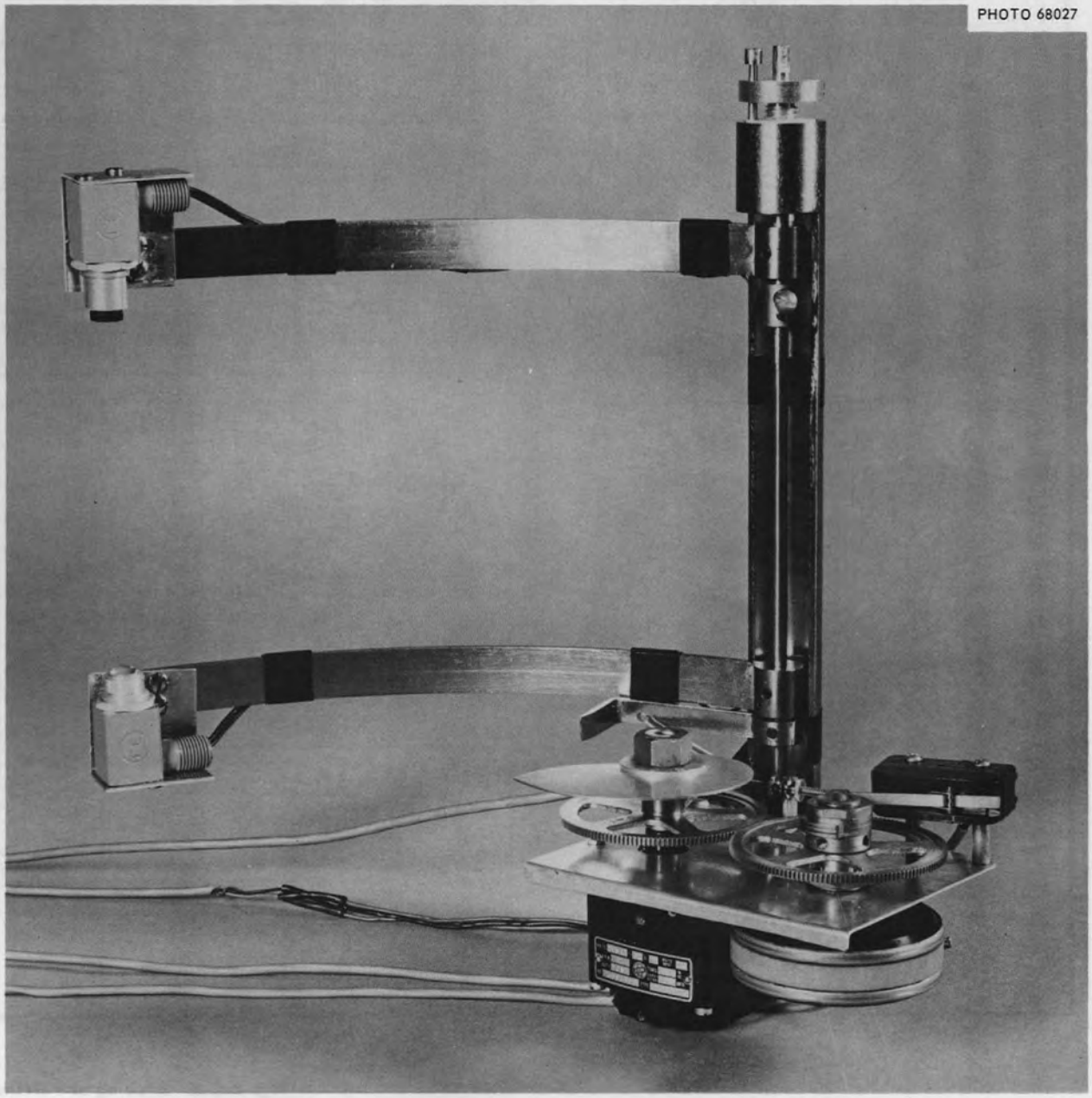

Fig. V-D-1. Photoelectric Scanner for A-Series Rotor.

of the photocell on the rotor radius with respect to the rotor axis is measured by a potentiometer which controls the voltage to the X axis. While the scanner swings through an arc as it traverses the cell, the position-measuring potentiometer is driven through a cam system in such a way as to give a voltage output which is proportional to the true radius. The X-Y recording is thus linear with rotor radius. Scans are repeated at preset intervals, but the recorder pen does not record on the return cycle of the scanner. Normally, the X axis of the recorder is set to give a plot in which the radius is enlarged by a factor of 3 for clarity. The location of sedimenting bands or zones can thus be precisely determined.

The optimum interval between repetitive scans varies markedly with particle sedimentation rate and with rotor speed. A timer is incorporated in the scanner to provide a preselected scanning interval of 1, 5, 10, 15, 20, or 25 min per cycle. After the completion of ten scans, the scanner is automatically shut off. The system may be used with the A-IX, A-X, A-XI, A-XII, and A-XIII rotors. With the A-X, A-XI, and A-XII rotors the mechanical lag of the X-Y recorder and the relatively high rotor speed help eliminate any tendency toward

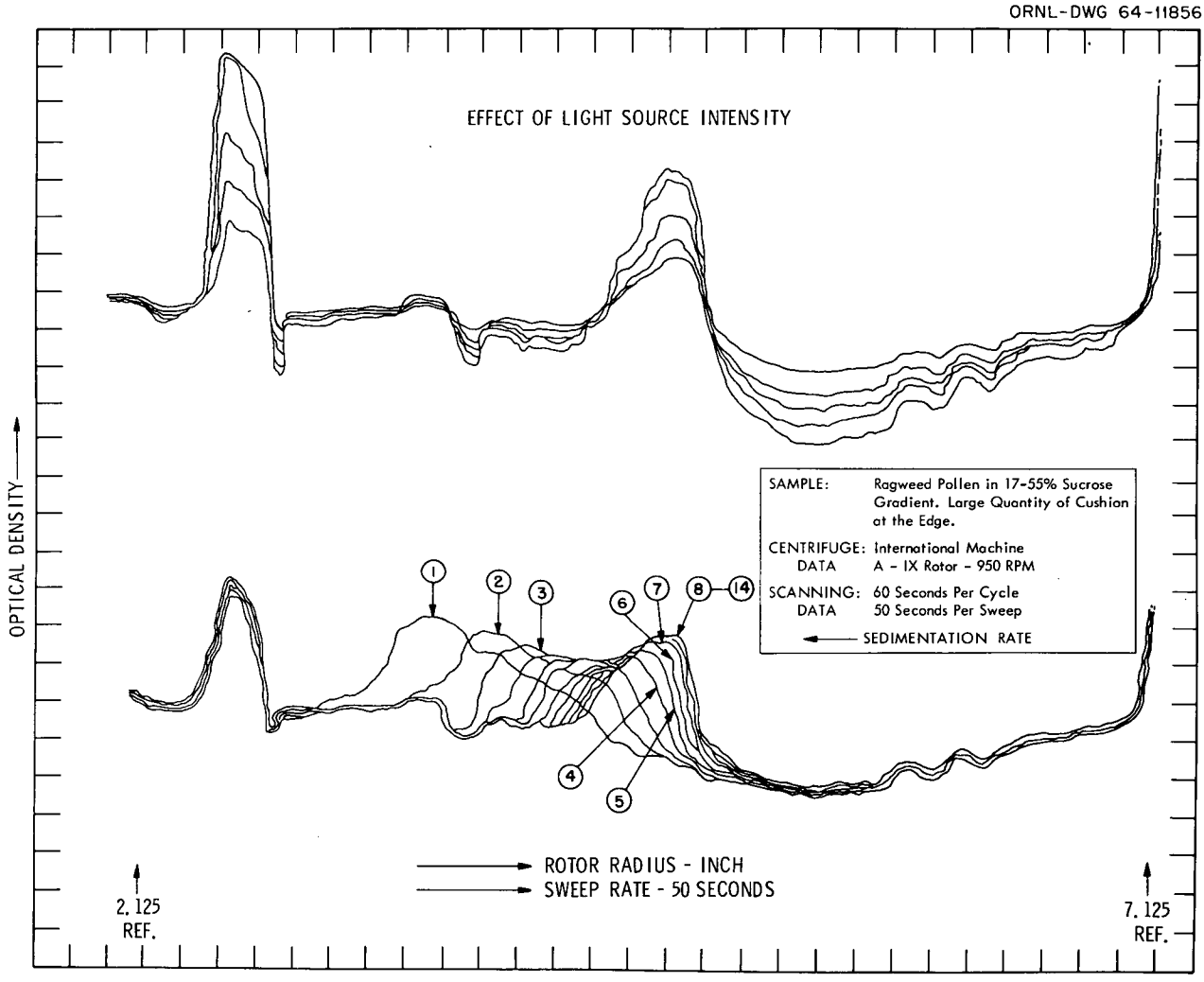

Fig. V-D-2. Scan of Particles Sedimented in A-XII Rotor Using Photoelectric Scanning Device.

pulsing generated by the interruption of light by the solid sector areas of the rotor. An example of a scan made with this instrument is shown in Fig. V-D-2. Variations of the scanner under consideration include versions which measure either backward- or forward-scattered light.

For improved visual observation of sedimenting bands, a uniform light source below the rotor is required. A source consisting of three concentric fluorescent lamps with suitable reflectors and diffusers which fits in the International PR-2 centrifuge is shown in Fig. V-D-3.

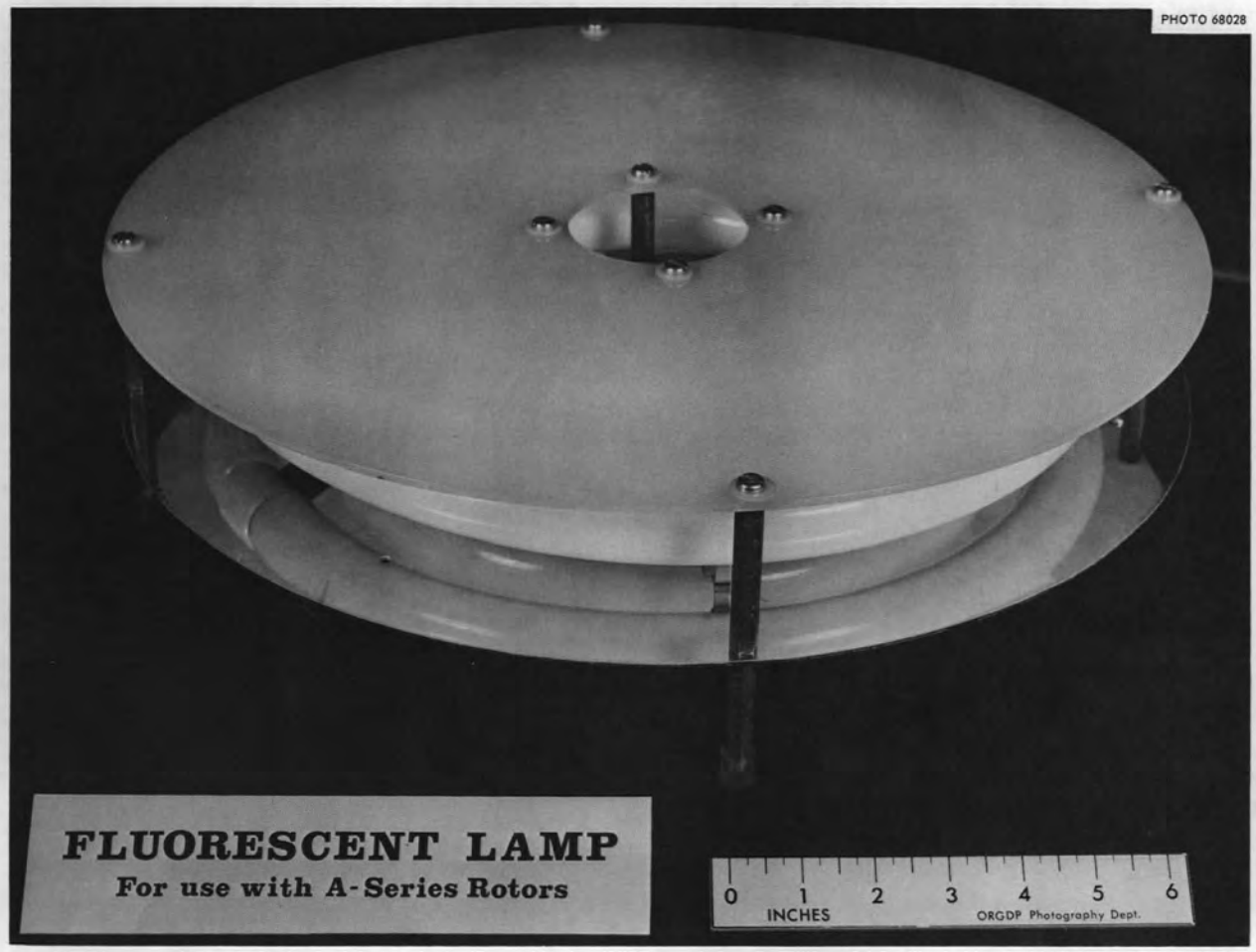

Fig. V-D-3. Fluorescent Light Source for Use with A-Series Rotors.

VI. Intermediate-Speed Zonal Rotors

A. INTRODUCTION

H. P. Barringer

Several intermediate-speed rotors are available for zonal centrifugation as a batch operation, for total sedimentation on a continuous-flow basis, or for total sedimentation with isopycnic banding accomplished within the same rotor. These rotors are complex systems when all associated parts are assembled, and continuous supervision is required for proper operation.

During this report period we have been interested in developing simpler rotors for continuous-flow centrifugation and in providing a simple zonal rotor for batch centrifugation. The new, simple batch-type zonal rotors described here will probably find wide acceptance, since they can be used on existing laboratory equipment.

B. ROTOR B-X

H. P. Barringer

Batch-type use of the B-IV rotor has comprised more than 50% of the total operation of all zonal centrifuges thus far. When the B-IV is used, an upper bearing, high-speed seal, seal coolant, and seal oil supply must be operating for successful centrifugation This extra equipment is eliminated in the B-X rotor.

The B-X rotor has an $I_{spin}/I_{transverse} = 1.35$ ratio which is similar to the ratio of an angle-head rotor, so that a top bearing for the rotor is not required. The rotor chamber contains 685 ml of fluid and is designed, when constructed of Maraging steel, to spin at 40,000 rpm (119,000g at $R_{max} = 2.625$ in.) with cesium chloride having a density of 1.7.

Fig. VI-B-1. Aluminum Model of B-X Intermediate-Speed Removable-Seal Zonal Rotor.

An aluminum model of the B-X rotor (Fig. VI-B-1) has been fabricated to check the rotor concept prior to construction of the rotor from 18% nickel Maraging steel. Satisfactory test results have been obtained with sucrose gradients at 30,000 rpm in the model L Spinco centrifuge.

For batch centrifugation, such as rate zonal separations, the rotor is installed in the model L Spinco centrifuge and rotated at 2000 rpm. The removable seal, similar to the A-series rotor seal, is slipped onto the rotor while it is spinning, and gradient material and samples are pumped into the rotor, using the same operating sequence employed with the B-IV rotor. The sliding contact seal is then removed, and a leak-tight cap is slipped onto the top end of the rotor to prevent leakage of the rotor fluids during high-speed centrifugation. When the rotor is thus sealed, the chamber is evacuated, and the rotor is operated at full speed as with a standard angle-head rotor.

Unloading of the rotor while it is spinning is accomplished in a similar manner as described above, by removing the sealing cap and attaching the contact seal during rotation at 2000 rpm.

C. ROTOR B-XI

H. P. Barringer

The B-XI rotor, shown in Fig. VI-C-1, is a larger version of the B-X rotor described above. An aluminum model of the B-XI has been tested successfully to 24,000 rpm. The Maraging steel version is designed to spin at 30,000 rpm (89,500*g* at R_{max} = 3.50 in.) while containing 1725 ml of cesium chloride. At full design speed this rotor will store 590,000 ft-lb of energy.

An A-type seal has been modified for the B-X and B-XI type rotors described elsewhere in this report. The seal slips onto the spinning rotor core and is accelerated to speed by friction. The seal is then held in position by two flexible arms which attach to the rotor cooling-chamber wall. The operation of the seal is the same as for the A type described in the previous report.[1]

[1]C. E. Nunley, *Joint NIH-AEC Zonal Centrifuge Development Program Semiann. Rept. July 1–Dec. 31, 1963*, ORNL-3656, pp. 43–44.

Fig. VI-C-1. Aluminum Model of B-XI Intermediate-Speed Removable-Seal Zonal Rotor.

D. ROTOR B-XII

H. P. Barringer

Rotor B-XII is similar to B-IV except in the materials of construction. Maraging steel used in the B-XII permits speeds of 50,000 rpm with cesium chloride, and the rotor can be steam sterilized.

Spin tests to 35,000 rpm have showed good rotor stability, and high-speed testing will continue as time permits.

E. CONTINUOUS-FLOW CENTRIFUGATION AND ISOPYCNIC PARTICLE BANDING

J. W. Amburgey, Jr. G. B. Cline
N. G. Anderson

The B-V was the first centrifuge system designed and built specifically for concentrating virus particles from large volumes of fluid by continuous-flow centrifugation.[2-4] Some test particles successfully isolated in this rotor system include adenovirus 2, echovirus 28, and T-3 bacteriophage. These particles were deposited on the rotor wall during centrifugation, a collecting technique which has been found to inactivate certain viruses. This system is therefore limited, for most applications, to the isolation of those particles not affected by the impact of pelleting. To overcome this limitation a more versatile continuous-flow centrifuge system (B-VIII) has been developed. This system permits sedimentation of the particles into a density gradient formed peripherally to a central tapered core. The particles are banded isopycnically in the density gradient imprisoned in the rotor as the sample fluid flows between the core and the gradient.

The problem is to introduce a gradient into a spinning rotor, maintain it in a stable configuration close to the rotor wall during the course of the run, arrange to flow a large volume of virus-containing material over the centripetal surface of the gradient, and then to recover the gradient as a sequence of fractions of increasing density containing the banded fractions at the end of the run. This must all be done through the two fluid lines attached to the rotor.

This new technique incorporates, into a single operation, the two steps of particle trapping in the rotor and particle banding in a density gradient. The B-VIII centrifuge is, therefore, specifically designed for the isolation of labile viruses such as the respiratory syncytial virus. Sketches of the core are shown in Figs. VI-E-1 and VI-E-2. The B-VIII core is designed to operate in the same rotor shell used with the B-V.

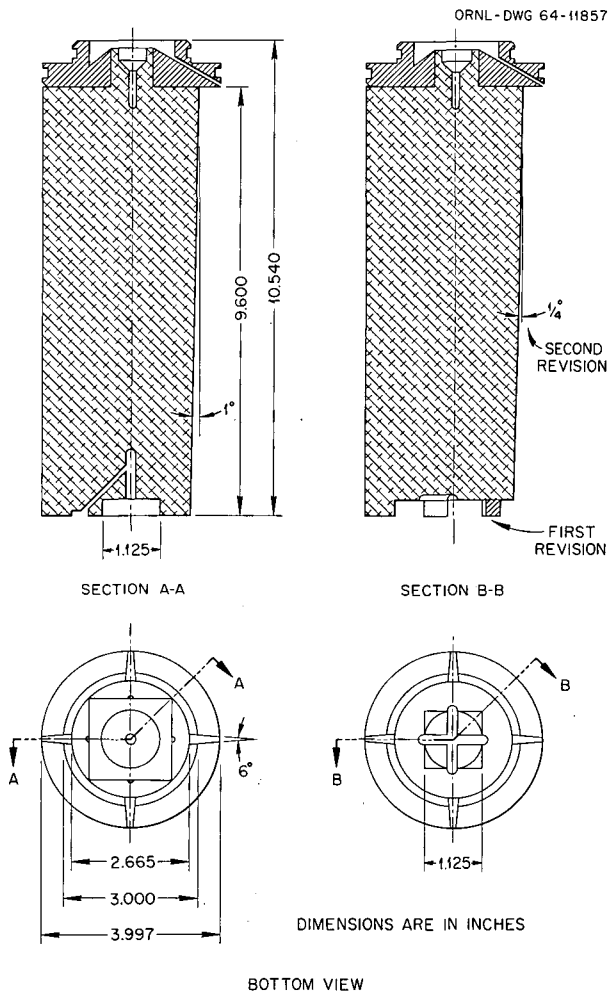

Fig. VI-E-1. Drawings of B-VIII Core for Continuous Flow Centrifugation Combined with Isopycnic Banding.

[2]N. G. Anderson, *Nature* **199**, 1166–68 (1963).

[3]N. G. Anderson, *Joint NIH-AEC Zonal Centrifuge Development Program Semiann. Rept. Dec. 31, 1962*, ORNL-3415.

[4]N. G. Anderson, *Joint NIH-AEC Zonal Centrifuge Development Program Semiann. Rept. Oct. 11, 1963*, ORNL-3502.

ORNL-DWG 64-11858

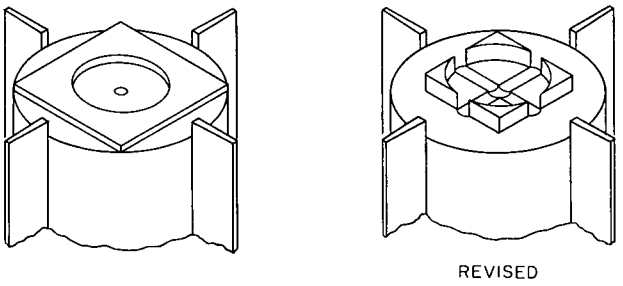

Fig. VI-E-2. Original and Revised Configuration of Bottom of B-VIII Core.

A total of four separation runs have been completed employing the B-VIII rotor system and the principle of isopycnic particle banding during continuous-flow centrifugation. Cesium chloride, cesium tartrate, and potassium citrate gradient solutions were used in making these separation runs. The gradients were loaded at speeds ranging from 0 to 8000 rpm. No operational difficulties were encountered during gradient loading. Density gradients were established by diffusion of the denser fluid, entering the rotor at the periphery, into the inboard volume of water remaining in the rotor. The lighter fluid was displaced toward the center of the rotor and out through the effluent flow line. Figure VI-E-3 shows the density as a function of the rotor radius for some of the typical gradients recovered.

Following centrifugation of the sample media for each of the runs, the gradient containing the banded particles was unloaded through a uv monitoring spectrophotometer to determine the location of the banded particles. Adeno 2, respiratory syncytial, and Moloney viruses were used as test particles and were found to be banded isopycnically in a discrete zone after centrifugation of 2 to 5 liters of culture media. Electron microscopic examination of adenovirus samples from these zones showed the particles to be intact and free of contamination. Run summaries are included in Table 1.

The flow lines were submerged in water while accelerating to operating speed following the gradient loading for the first separation run. At 28,000 rpm a pressure in excess of 15 psig was required to start the sample flow through the rotor, and pressures up to 15 psig were needed to maintain the flow. The maximum loading pressure for the seal, used with this rotor system, is between 15 and 25 psig. Pressures in this range cause the seal faces to separate, resulting in cross-leakage of the two flow streams and coolant water. During the next three separation tests it became apparent that the high inlet pressures were related to the diffusion of gradient material into the rotor volume contained in the core taper. A continuous water flow maintained during acceleration for these tests minimized the startup pressure by keeping the diffusing gradient material flushed out of the taper volume. Figure VI-E-4 shows the inlet pressure as a function of speed for the four separation runs. A series of experimental tests were conducted to define and possibly suggest a solution to the problem of high inlet pressures.

With the assistance of A. S. Berman, an attempt was made to roughly calculate the pressure required to force a fluid through the rotor at a given speed and density gradient. To simplify the calculation the flow path through the rotor was compared to a manometer with a fluid of different density in each of the legs, as illustrated in Fig. VI-E-5. The densities of the sample fluid and effluent stream were determined from refractive index measurements; however, these measurements

ORNL-DWG 64-11859

RUN NO.	KIND	GRADIENT VOL USED	DENSITY	ROTOR SPEEDS (rpm) LOADING	OPERATING	EFFLUENT VOL (TOTAL)
ZU-216 ▲	CsCl	500 ml	1.62	0	38,000	~3.5 liters
ZU-222 ○	*	300 ml	1.51	8000	36,000	~4.0 liters
ZU-220 △	**	250 ml	1.54	8000	30,000	~4.5 liters
ZU-219 ●	CsCl	300 ml	1.62	750	28,000	~8.0 liters

* Cs (TARTRATE)
** K (CITRATE)

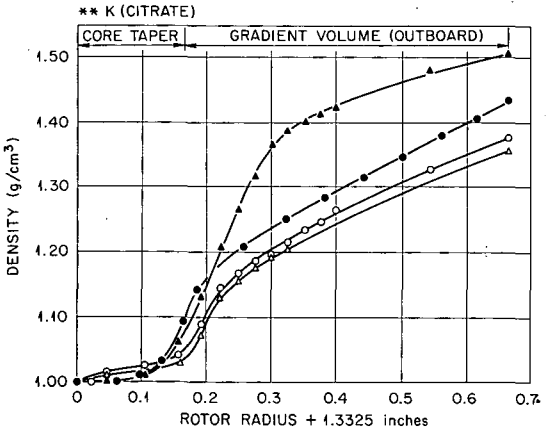

Fig. VI-E-3. Gradient Density as a Function of Rotor Radius for Typical Gradients Used in B-VIII Rotor.

Table 1. B-VIII Separation Runs

Run No.	Top Operating Speed (rpm)	Gradient		Test Particle	Sample Volume (liters)	Gradient Unloading Speed (rpm)	Average Flow (liters/hr)
		Material	Loading Speed (rpm)				
ZU-216	28,000	Cesium chloride	Statically	Adeno 2	3	8000	1.7
ZU-219	36,000	Cesium chloride	2000	Respiratory syncytial	5	8000	1.5
ZU-220	30,000	Potassium citrate	8000	Moloney	3	8000	2.0
ZU-222	30,000	Cesium tartrate	8000	Moloney	2	8000	1.9

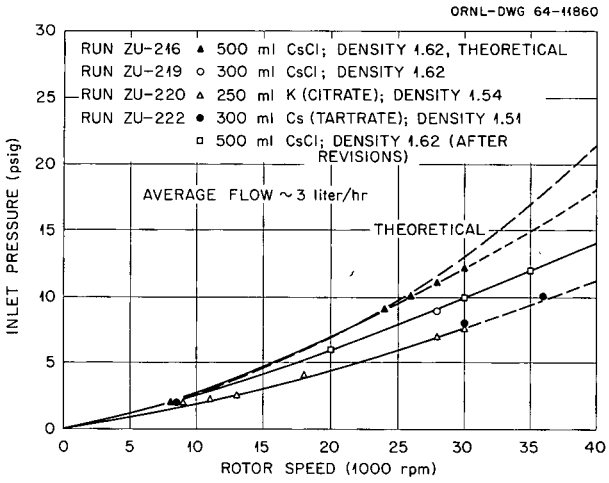

Fig. VI-E-4. Inlet Pressure as a Function of Speed with the B-VIII Rotor.

were not considered accurate for the density range (1.00 to 1.05 g/cm^3) and gradient materials used. Further studies would have been required for accurate density measurements; but they were not considered necessary for these calculations, since only a close approximation was desired. Diffusion coefficients were also ignored. The pressure differential was calculated from the equation

$$(P_0 - P_s)\text{atm} = 0.873 \times 10^{-8}\,(\text{rpm})^2 \times$$

$$[D_2^2(\bar{\rho}_{2s} - \bar{\rho}_{21}) + D_1^2(\bar{\rho}_{21} - \bar{\rho}_{10}) - D_s^2(\bar{\rho}_{2s})]\,,$$

where

D_1 = diameter at small end of core taper,
D_2 = diameter at large end of core taper,
D_s = smallest diameter at which effluent leaves the rotating system,
P_0 = pressure at the axis,
P_s = pressure at D_s,
$\bar{\rho}_{2s}$ = average density between D_s and D_2 at the top (measured),
$\bar{\rho}_{21}$ = average density between D_1 and D_2 at the bottom (estimated),
$\bar{\rho}_{10}$ = average density between axis and D_1 at the bottom (measured).

Figure VI-E-4 includes the theoretical curve for the steepest cesium chloride gradient used. It should be noted that the theoretical and measured pressures are in close agreement.

In considering possible design changes, alteration of the rotor seal assembly showed the greatest promise but was ruled out as being impractical for the present, since it would require changes in associated components of the rotor system. The two most practical design changes evident from the previous data were to open up the bottom of the core and to reduce the core taper. It was argued that removing a portion of the core at the bottom end would increase mixing of denser gradient fluid in this area and result in a density increase of the fluid in the bottom leg of the manometer flow path, and that reducing the taper of the core would decrease the density gradient of the fluid throughout the flow path because of

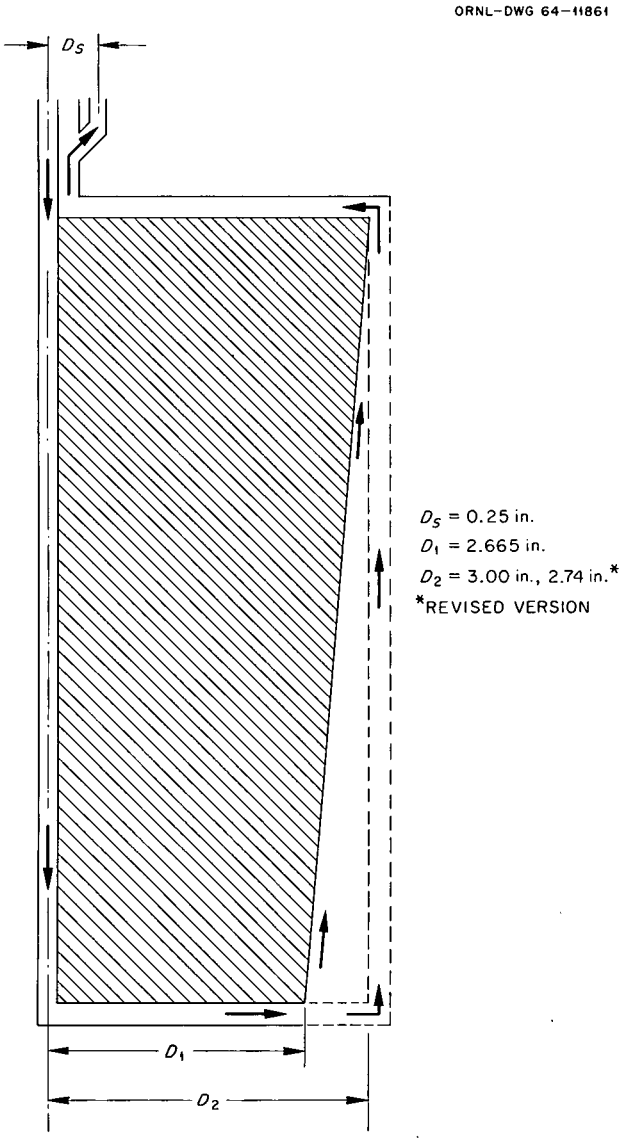

Fig. VI-E-5. Flow Path Diagram for the B-VIII Rotor System.

the smaller fluid volume contained in the taper. Figures VI-E-1 and VI-E-2 show these design changes and the sequence in which they were made.

The test results following the first revision indicated that while an increase in the mixing effect in the bottom of the rotor occurred, the density of the fluid was increased in the entire flow path, resulting in an increase in the inlet pressures.

In the second design change the core taper was reduced from 1° to ¼° by machining from the large end of the core taper; consequently, the core diameter at this end was reduced from 3 in. to 2.74 in. The inlet pressures were reduced by approximately 35% when compared with the results following the first revision. Theoretically, the smaller core diameter accounted for approximately 15% of this pressure decrease, and the reduction of the fluid density in the flow path was responsible for the remaining pressure reduction. Figure VI-E-6 shows the inlet pressure as a function of speed for both revisions and the original design.

In preparation for each of the experimental tests conducted, the rotor and flow lines were filled completely with water, making sure that all the air was removed. During the test, air could collect in the rotor system from two sources: by introduction with the inlet flow stream, and from gas actually contained in the sample fluid and separated out during centrifugation. A small tube was installed in the top of the seal which extended

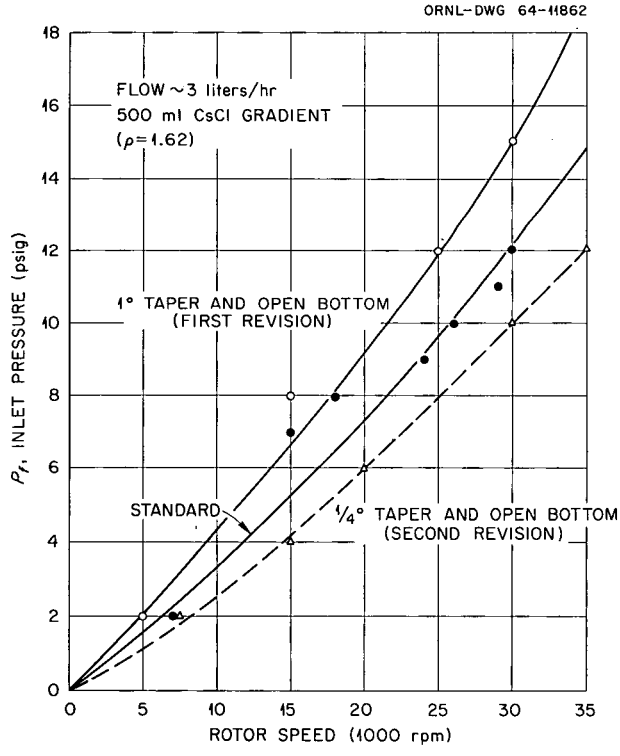

Fig. VI-E-6. Inlet Pressure as a Function of Speed for Original and Revised B-VIII Systems.

down through the center or inlet flow channel to a position just below the seal faces. This tube removed the air entering or collecting in this area of the center flow channel, along with a small amount of the sample fluid. The sample fluid removed with the air was returned to the sample reservoir. A schematic of the fluid lines is included in Fig. VI-E-7, and the operating sequences are shown in Fig. VI-E-8.

With the revised core and certain operating precautions, virus particles can be isolated satisfactorily by continuous-flow centrifugation in the B-VIII centrifuge system. The high inlet pressure encountered during centrifugation is an inherent feature which has been minimized through operational experience and minor design changes. A B-IX core is being designed that incorporates suggestions based on experimental data obtained with the B-VIII rotor system.

The key points to be considered in the design and operation of a B-VIII type rotor system are:

1. Design
   a) The taper of the core should be made as small as possible without sacrificing resolution.
   b) The flow channels through the core should be small but large enough to carry the maximum flow handled by the seal.
   c) The opening in the bottom of the core should be barely large enough to carry the flow.
   d) A small tube extending down the center channel of the seal to slightly below the seal faces is required to permit the expelling of gas which collects in this area.
   e) The core diameter should be kept as small as possible.
2. Operation
   a) Maintain a liquid flow at all times after loading the gradient.
   b) Operate with a minimum density gradient and at the minimum speed required to isolate the particles desired.
   c) Remove the air from the sample fluid before centrifugation.
   d) Periodically remove gas from the effluent flow channel by pinching off the line and releasing promptly.
   e) Use a gradient material with a minimum diffusion rate when a choice of materials is offered.

ORNL-DWG 64-11863

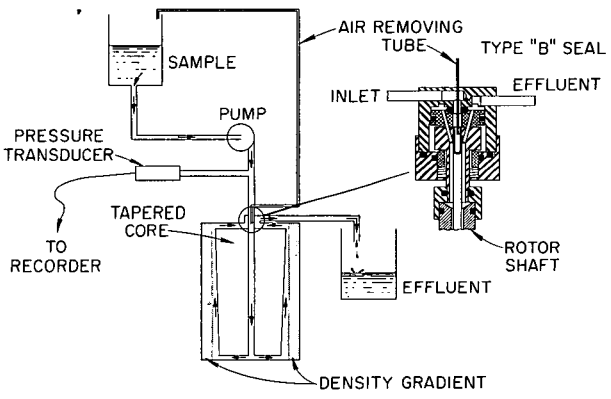

Fig. VI-E-7. Schematic Diagram of B-VIII Rotor System and Seal.

G-64-154

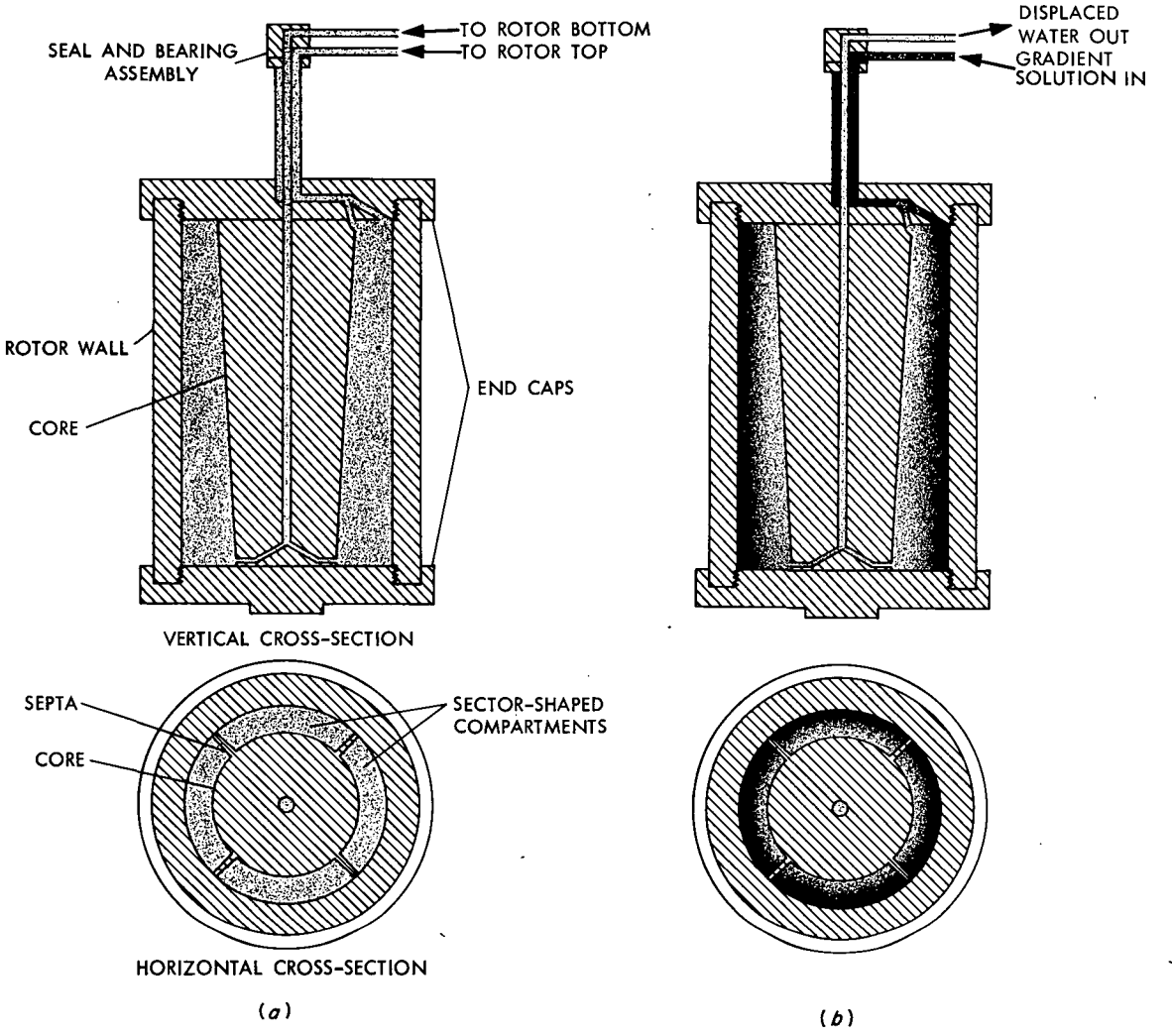

Fig. VI-E-8. Operating Sequence of B-VIII Continuous-Flow–Isopycnic-Banding Rotor. (*a*) B-VIII rotor in vertical and horizontal cross-section. The rotor is accelerated to *ca.* 3000 rpm filled with water. (*b*) The gradient-forming solution is pumped into the rotor through the fluid line leading to the top of the rotor chamber, displacing out part of the water originally present through the bottom rotor line. (*c*) During acceleration and after reaching operating speed, fluid which contains particles is continuously pumped through the rotor. The direction of flow is in through the line leading to the bottom of the core and out through the upper core line. Note that particles contained in the fluid stream continuously sediment out into the imprisoned gradient and band there. (*d*) After completion of the continuous-flow portion of the operation, the rotor is decelerated to unloading speed (3000 to 5000 rpm) and a dense fluid pumped in through the upper core line to displace the gradient out of the rotor. The taper of the core is sufficient to constrict the bands into the lower exit line. (*e*) Completion of recovery of the gradient with separated particle zones. The gradient flows through an ultraviolet light absorption monitor and into fraction collector tubes.

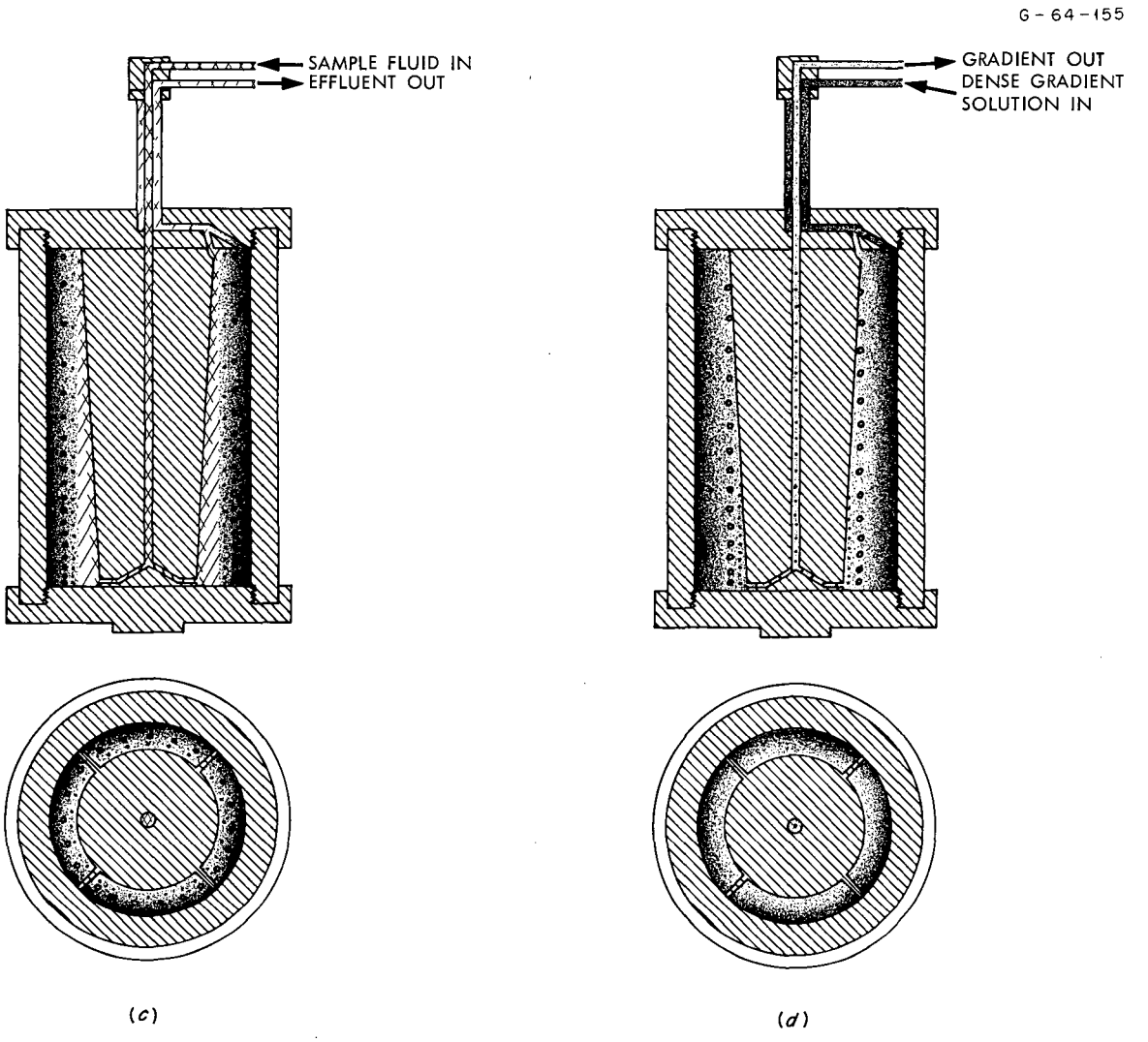

Fig. VI-E-8 (continued).

G-64-156

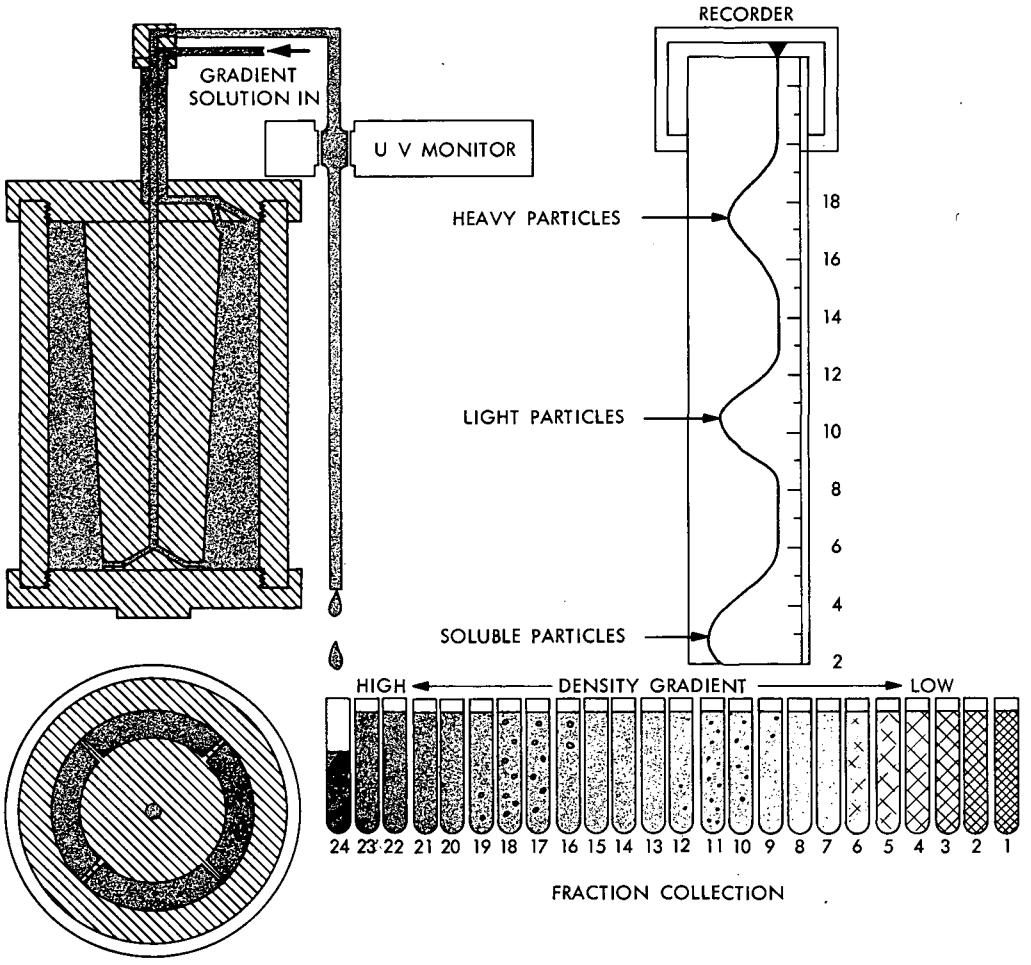

(e)

Fig. VI-E-8 (continued).

VII. Instrumentation for Obtaining Integral of $\omega^2\ dt$

M. J. Bartkus

A system has been developed under this program to provide a numerical value of the integral

$$\int_{t=t_0}^{t=t_1} (\omega^2\ dt)$$

expressed in units of radians squared per second multiplied by 10^6. The system consists of a proximity sensor, amplifier, frequency-to-direct-current converter, a potentiometric indicator with a special squaring circuit, an integrating circuit, a frequency test panel, and associated power supplies. A description of the individual units will be followed by a description of the initial and operational calibration procedure for the system.

A. INSTRUMENT FUNCTION DESCRIPTION

A proximity probe, distance detector, and power supply are used to provide an output frequency in cycles per second, equal to 0.6 of the rotor speed in revolutions per second. This output frequency is routed through a frequency test panel, which will be described later, to a frequency meter. The probe is a pancake-shaped inductive load, Bently model H2-084-3, connected to a distance detector, model 152, which has a carrier frequency of approximately 2 Mc/sec. An electrically conductive surface, in close proximity to the coil, for example, less than 0.025 in. spacing, acts as a shorted turn and reduces the amplitude of the carrier frequency in the coil. A small shift in frequency also occurs. A demodulating circuit in the detector removes the carrier frequency and provides an output related to the distance between the conducting surface and the probe. When the distance varies periodically, the detector generates an alternating voltage. A 15-v negative supply, Bently model E15, energizes the detector circuit.

The detector ac output voltage is converted in a frequency meter to a negative going dc output proportional to the average input frequency. A Hewlett-Packard model 500 BR frequency meter is used to perform the conversion. Each cycle of the ac voltage is amplified and then converted to a square wave by a Schmitt trigger circuit. Diode clipping and an integrating circuit convert the square wave into a sharp negative pulse, which triggers a one-shot cathode coupled multivibrator. The meter and output are part of the plate circuit of the multivibrator. An auxiliary phantastron circuit regulates the ON time of the one-shot circuit and hence the duration of the current pulse flowing through the meter and output circuit. Large capacitors in the output circuit filter or average the current pulses to produce a dc output. The repetition rate or frequency of input signal thus determines the average value of the output. The design value of load resistance is 1400 ± 100 ohms. Maximum accuracy error of ±2% and linearity error of ±0.1% are specified.

The frequency meter output current produces an upscale deflection on the speed indicator proportional to rotor speed. A full-scale deflection is equivalent to a rotor speed of 60,000 rpm. A special squaring circuit, which has been developed, utilizes a slave slide-wire on the indicator to provide a dc output proportional to the square of the rotor velocity.

The speed indicator is a null balancing electronic indicator, Leeds and Northrup Speedomax H, with an input full-scale sensitivity of 10 mv. The difference between the input voltage and a bucking voltage, supplied by the main slide-wire, is sensed by a high-gain chopper-type amplifier. The amplifier provides power to a motor which moves a

slide-wire contact. An unbalance of 5 to 10 μv normally will result in motor action to reduce the differential voltage. The rated accuracy of the Speedomax H is 0.3% of the scale span maximum error.

An analysis of the circuit presented in Fig. VII-A-1 demonstrates that the output voltage is proportional to the square of the input voltage. Utilizing Ohm's law the following may be written:

$$E_1 = i(R_2 + R_3) , \tag{1}$$

$$E_2 = iR_2 = V_{sw} \cdot P , \tag{2}$$

where

E = volts,
i = amperes,
R = ohms,
V_{sw} = indicator full-scale sensitivity (volts),
P = percent of full scale.

The last part of the second equation results from the null-seeking servo, which moves the main slide-wire contact until the bucking voltage is equal to the input voltage. Therefore (2) can be rewritten:

$$P = \frac{iR_2}{-V_{sw}} . \tag{3}$$

Since the output slave slide-wire is mechanically coupled to the main slide-wire,

$$E_0 = iR_3P . \tag{4}$$

ORNL-DWG 64-11865

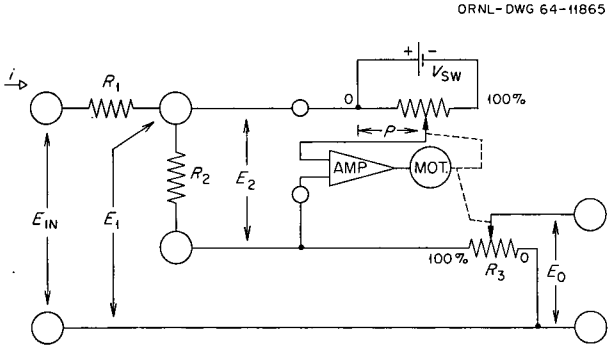

Fig. VII-A-1. Voltage Squaring Circuit.

Substituting (3) into (4),

$$E_0 = iR_3\left(i\,\frac{R_2}{-V_{sw}}\right) = i^2\left(\frac{R_3R_2}{-V_{sw}}\right) . \tag{5}$$

Since R_2, R_3, and $-V_{sw}$ are fixed parameters,

$$E_0 = i^2K , \tag{6}$$

where

$$K = \left(\frac{R_3R_2}{-V_{sw}}\right) .$$

Equation (1) can be rewritten as

$$i = E_1\left(\frac{1}{R_2 + R_3}\right) . \tag{7}$$

Substituting this in (6), we obtain

$$E_0 = E_1^2\left[\left(\frac{1}{R_2 + R_3}\right)^2 K\right] . \tag{8}$$

Defining E_1 in terms of E_{in},

$$E_1 = E_{in}\left(\frac{R_2 + R_3}{R_1 + R_2 + R_3}\right) , \tag{9}$$

and substituting in (7) ,

$$E_0 = E_{in}^2 \times \left[\left(\frac{R_2 + R_3}{R_1 + R_2 + R_3}\right)^2\left(\frac{1}{R_2 + R_3}\right)^2 \cdot K\right] . \tag{10}$$

Since the bracketed terms are constant, we arrive at the proof that the output voltage is proportional to the square of the input voltage. In the final circuit, R_1 (500 ohms) serves to provide required load for the frequency meter; R_2 (16.66 ohms) develops 10 mv indicator full scale when the frequency meter output of 0.6 ma flows through the circuit; R_3 is a standard 1000-ohm slave slide-wire.

The squaring circuit error resulting from loading by the Speedomax input is less than 1 part in 10^6. However, input impedance of the Lectrocount integrator is between 20,000 and 30,000 ohms.

This produces an error in the squaring circuit output of approximately 5%. The error decreases linearly with input voltage E_{in} to 10% of E_{in}(max) when the error becomes almost zero.

The squaring circuit output is electronically integrated with respect to time and converted to a numerical value which is proportional to

$$\int_{t=t_0}^{t=t_1} (\omega^2\, dt)$$

in multiples of 10^6. The integration time is controlled by a switch on the electronic integrator front panel and switch contacts in the test panel.

A Royson Lectrocount II performs the electronic integration. In it, the difference between an input voltage and a feedback voltage is impressed on a high-gain chopper-type amplifier. The amplifier drives a discriminator and filter circuit. The filtered signal establishes the feedback voltage and controls the repetition rate of a pulse generator. A mercury wetted contact relay, driven by the pulse generator, actuates an electromechanical count register. Zero and span adjustments are provided in the integrator circuit. The output of the integrator is a linear function of its input with less than 1% error.

A test panel, previously mentioned, is used to calibrate the ω^2 integrating system and to verify the calibration at intervals. A regulated 28-v dc supply provides power for three plug-in oscillators. The oscillators, 60, 300, and 540 cps, enable calibration at 10, 50, and 90% of speed indicator full scale. The switch, used to select the desired test frequency, also provides power to a preset timer which controls the integrating interval during the tests. The test switch also is used to select the output of the rotor speed detector and simultaneously to enable the front panel switch on the integrator, which controls the integrating interval, to be actuated. The Delta F solid-state oscillators have an accuracy error of 0.15%. The timing error of the ATC Atcotrol timer is claimed to be less than 0.5%.

The overall error of the system can be as high as 4.2%, but reasonable calibration reduces the error to less than 1.0%.

B. INITIAL CALIBRATION PROCEDURE

The ω^2 integration instrumentation should be initially calibrated by technically qualified personnel. Test panel timer adjustment, frequency meter adjustment, electronic indicator slave slidewire adjustment, and integrator adjustment are required.

Note: Before calibration is attempted, the instruments should be powered for 30 min.

Timer: The timer on the test panel must be adjusted to obtain a 101.5-sec timing interval.

The procedure is to connect an EPUT timer, such as the Berkley model 7360, to the test panel connector labeled "Integrator Shunt" through necessary circuitry. The timer provides a circuit closure during the timed period to start and stop the EPUT unit. After the timer adjustment is complete and lock installed on the timer face, the adjustment should be verified by observing the time interval of five test periods. Similarly, by using the timer and the EPUT unit as a counter, the accuracy of the three test oscillators should be verified.

Upon completion of the test panel calibration the proper cable plugs should be installed in the connectors on the test chassis rear.

Frequency Meter

Two self-checks are available on the Hewlett-Packard model 500BR frequency meter. With the output plug removed, the RANGE switch is placed in "CAL" position and the "CAL" control, located below the panel meter, is adjusted to obtain a full-scale reading on the meter. Next, the "RANGE" switch is rotated to the 100-cps position and the "SENSITIVITY" control rotated counterclockwise to the 60-cps position. Note the panel meter indication (6 ± 0.1). Replace the output plug in the jack on the chassis rear and adjust the "REC" control until the meter indicates the previously noted reading. The Speedomax speed indicator pointer should be at full scale (60,000 rpm).

Placing the "RANGE" switch in the 1-kc position and the "SENSITIVITY" control midway between the end positions, the test panel can be used to verify both the frequency meter and the Speedomax indicator calibration. The following table indicates target values for the B-IV system:

Test Panel (% full scale)	Frequency Meter (1-kc scale)	Speedomax rpm	Integrator Counts (101.5 sec)
		×10,000	
0	0	0	1–4
10	0.6	6	40
50	3.0	30	1000
90	5.4	54	3225

Speed Indicator

The Speedomax H speed indicator normally requires no adjustment. However, the zero speed indication should be checked. When the Speedomax input is shorted, the pointer should coincide with the scale zero. If a significant error (> 0.2%) is noted, adjustment of the measuring slide-wire position is required. This slide-wire is located on the rear of the pointer drive assembly, which may be swung out of the indicator cabinet. Removal of the shield, loosening two screws holding the measuring slide-wire molding, and then carefully rotating the measuring slide-wire molding until the pointer coincides with the scale zero are necessary. Upon firmly tightening the screws, the zero position should be verified.

The procedure for establishing the zero position of the slave slide-wire is more complex and is dependent upon the calibration of the Royson Lectrocount II integrator. The first step is to check the calibration of the integrator. With all cables properly connected and the Speedomax input unshorted, place the test switch in 90% full-scale position and the integrator counter switch ON. Reset the counter to zero and after waiting 5 to 10 sec, press the test panel START switch. The total count should be noted. Next, place the test switch in the zero speed position. Reset the counter to zero, wait 5 to 10 sec, press the test START button, and note the total count following the timed interval. At least one count must be indicated. If no counts are obtained in the zero speed position, an adjustment must be made to the integrator ZERO control. This will be described later.

Assuming a zero count of 1 or more was noted, the difference between the two counts is the span of the integrator. The difference is then multiplied by 2.78 to obtain a span count to be used in the following procedure. For example, 90% count of 2310 minus a zero count of 10 yields a difference of 2300 counts, which when multiplied by 2.78 yields a new span of 6400 counts. The output plug is next removed from the frequency meter. The Speedomax input is shorted by placing a jumper, on the terminal board at the rear of the recorder, between terminals 15 and 17. Two wires connected to terminal 20 are removed from the terminal and jumpered to 17. This isolates the slave slide-wire and completely grounds the Speedomax indicator input. A $1\frac{1}{2}$-v battery is then placed across the slave slide-wire by connecting the positive battery post to recorder terminal 20 and the negative post to terminal 19. Pushing the test START button will initiate a zero frequency test. A total count of 6 more than the original zero speed test indicates that the slave slide-wire is within 0.1% of its true zero position and requires no adjustment. For example, if a count of 4 is obtained in this test and a count of 1 obtained originally, the increase in count is 3, which is 0.05% zero offset and is tolerable. The offset is based on percent of Royson integrator span previously calculated. However, if there was no increase in background, an adjustment is indicated, because the slave slide-wire may be operating below the zero resistance point. A count difference of more than 7 counts also indicates need for an adjustment.

The slave slide-wire is held in position on the main shaft connecting the measuring slide-wire to the pointer. A large hexagon nut, loosened by use of a special wrench supplied with the Speedomax, permits rotation of the slave. After adjustment of the slave slide-wire, a zero speed test cycle should be run with the battery connected between terminals 20 (+) and 19 (–), and again with the

battery replaced with a shorting jumper. The two integrated counts should differ by less than 0.1% of the computed integrator span, and the shorted input count should be between 1 and 4 counts total.

Upon completion, the jumpers and battery connections are disconnected at the rear of the Speedomax H indicator and the original connections restored. The input jumper and termination of the 16.66-ohm resistor should be reconnected to terminal 20. The Speedomax input cable should be also reinserted in the frequency meter output jack.

Integrator

The Royson Lectrocount II electronic integrator has three adjustable controls located internally on a printed-board chassis. The controls are accessible by removal of the rear cover of the instrument. When viewing the chassis from the rear, the "Span" adjustment is located near the right side of the chassis. The "Zero" control is located about 3 in. to the left of the SPAN pot, and the "Threshold" control is nearly in the center of the chassis.

Caution: The electronic integrator is temperature sensitive. After making an adjustment, always replace the rear cover and wait at least 1 min (for temperature equilibrium) before taking a count.

The integrator may be roughly calibrated using a 1000-ohm potentiometer or volume control connected to the input jack. Connect the ends of a 1000-ohm volume control to pins *A* and *B* of the signal input plug. The movable arm of the control is connected to pin *C*. A jumper across the pins of the "SHUNT" connector enables the front panel "COUNTER" switch to control the counter. To adjust the zero control, place the counter switch ON and rotate the volume control to the end, producing few, if any, counts. Adjust the ZERO control for a counting rate between 1 and 3 counts/min. Next, rotate the volume control shaft to the opposite extreme and adjust the "SPAN" control until about 2500 counts/min are obtained. The "SPAN" control is very sensitive; so its adjustment must be made in small increments. The "Sensitivity" control is adjusted at the factory.

The more precise method of calibration utilizes the ω^2 instrumentation. With the recorder output plug and test panel shunt plug inserted in the proper connectors at the integrator rear, the test panel selector switch is placed in zero speed position. Using the test timer, adjust the integrator "ZERO" control to yield between 1 and 4 counts in the timed interval of 101.5 sec. Be sure to replace the integrator rear cover after every adjustment. In a similar fashion, the SPAN adjustment is made, using the 50% of full scale speed position, until a total count of 1000 ± 5 is obtained. Verification of the count rate using the 90% test speed position (3225 ± 16) is suggested.

After the integrator controls have been adjusted and the rear cover replaced, wait 20 min and verify the test counting rates.

An accuracy of better than 99% will be achieved if the calibration is properly carried out and verified.

The final adjustment is the spacing between the speed pickup or proximity probe and the sprocket gear located on the rotor drive adapter assembly of the Spinco L centrifuge drive. The assembly is located between the drive unit and a speedometer cable which is connected to an external rotor speed indicator. The probe is screwed into a $\frac{1}{4}$–20 locknut all the way to the flats on the probe. The probe is then inserted into the tapped hole in the assembly until there is snug fit when a piece of matchbook cover is resting on the top of a sprocket gear tooth. The locknut is then tightened and the cardboard removed. This provides about 0.015 in. clearance between the probe tip and the gear teeth. A clearance of 0.005 to 0.015 in. is desirable. The gear should be slowly rotated to determine that none of the teeth strike the probe tip. Cable connections are then made between the probe, the detector located in the centrifuge cabinet, and the power supply located on the inside wall of the control cabinet. An oscilloscope, connected to the Bentley power supply output (pin *A* grounded and signal on pin *B*), will indicate the peak-to-peak detector output voltage. With the Spinco rotor rotating between 30,000 and 50,000 rpm, the probe drive is adjusted to obtain an output between 8 and 12 v peak to peak. The drive adjustment is located in the end of the D 152 distance detector. The 8- to 12-v signal is required to properly drive the frequency meter

when its "Sensitivity" control is set midway in its adjustment.

C. ω^2 INSTRUMENTATION OPERATION

Operational Calibration Checks

The B-IV control and ω^2 instrumentation panels must have power applied at least 20 min before calibration and operation. This will enable the electronic components to reach a temperature equilibrium, thereby minimizing drift from calibration.

The position of the various front panel controls should be checked before making a calibration verification test. The frequency meter "Sensitivity" control should be placed midway in its adjustment and the "Range" selector placed in the 1-kc position. The electronic integrator count register should be reset to zero and the "Count" switch placed in the ON position. Adjust the test panel "Input" switch to the desired test position. Wait 5 to 10 sec to permit the Speedomax indicator and the integrator circuit to become stabilized, and then press the "Start" button on the test panel. Observe the frequency meter deflection, the Speedomax speed indication, and, following the timed interval, the total accumulated count on the integrator panel. The target calibration values are tabulated below.

A compromise may have been necessary to obtain maximum accuracy at speeds normally used during centrifugation. However, total count deviation greater than twice the target value (e.g., greater than 1% deviation) indicates the need for recalibration by technically qualified personnel.

Upon completion of the calibration verification, the integrator "Counter" switch is placed in the OFF position and the test panel "Input" switch is placed in the centrifuge position. The "Counter" switch is used to start and stop the integrating circuit counter.

Test Speed (% full scale)	Frequency Meter (1 kc)	Speedomax Indication (1000 cpm)	Integrator Counts (101.5 sec)	Count Deviation (±0.5%)
			$\times 10^6$	
0	0	0	1–4	
10	0.6	6	40	1
50	3.0	30	1000	5
90	5.4	54	3225	16

VIII. Containment and Sterilization

A. DEVELOPMENT OF A CONTAINED LABORATORY

N. Cho

The problems of containment and sterilization of virus separation systems continue to be explored both as problems in themselves and as necessary adjuncts to the design and construction of centrifuges and other instrumental systems. Two general approaches have been taken to the problem of virus containment. The first is to decrease the possibility of contamination from experimental systems now in use, illustrated by the development of leak-proof centrifuge tubes to replace the thin metal capped tubes which have always been used previously. The second approach has been to develop complete containment systems in which all procedures normally carried out in a virology laboratory may be performed. During this report period, design work on a containment system for centrifuges and associated equipment for the National Institute of Allergy and Infectious Diseases was begun. Previous containment systems constructed during this program have been of hybrid design, with the sterile enclosure attached to the top of a zonal centrifuge, but with the centrifuge drive and associated seals open to the outside. Mating of complex systems such as centrifuges to glove boxes is expensive and rarely completely reliable. In the system now being designed, all equipment will be enclosed without modification in a large welded aluminum frame 28 ft long, 4 ft wide, and 7 ft 5 in. high covered with transparent acrylic sheeting. Space will be provided for three centrifuge systems: the A-XII, B-IV (or V and IX), and an unmodified preparative ultracentrifuge. A conveyor system inside the enclosure allows materials to be moved easily to any point. Rotors, glassware, and accessories will be passed into and out of the sealed area through a double-door autoclave equipped for gas or steam sterilization. Storage space for sterile supplies will be provided beneath stainless steel work surfaces. Refrigeration space will be provided for temporary storage. Glove ports are provided at several levels as needed for efficient operation. The entire system will be sealed until no Freon leakage can be detected.

Completely automatic interlocked systems for sterilization of the entire enclosure with ethylene oxide before and after use are provided. The correct amount of gas will be valved into the enclosure, after which the temperature and relative humidity will be adjusted to 130°F and 50%, respectively, and maintained at these values for the sterilization period. After sterilization the enclosure is degassed using air filtered through an absolute filter. During operation the temperature will be maintained at 70°F and the relative humidity at 20%. The low humidity is essential for optimum operation of optical equipment. Since a large amount of heat will be generated by the three centrifuges and by other equipment, including the end sterilizer, large cooling coils will be arranged to extend nearly the entire length of the enclosure.

A small amount of filtered air will be constantly supplied through an absolute filter during normal operation. Exhaust air is discharged to the atmosphere above the building through a high-temperature gas-fired incinerator maintained at a minimum temperature of 800°F.

Special attention has been paid to the effect of accidental opening of the enclosure during operation on the exhaust air incinerator. For the safety of operating personnel the cabinet is maintained at a negative pressure of $\frac{1}{2}$ in. of water; thus, any leakage will be inward. The exhaust air fan is sized such that negative pressure is maintained even when accidental removal of a glove occurs.

The excess air drawn in during such an incident is used as part of the inlet air of the incinerator. This requires that the incinerator respond very rapidly to changes in the volume of exhaust air. During normal operation the air flow from the enclosure to the incinerator is about 5 cfm, and the additional air required to burn the inlet gas is supplied by a separate combustion blower. If a large leak occurs, the amount of air supplied from the blower is decreased automatically and the excess exhaust air used in its place.

The complete unit will be used to evaluate the problem of designing a completely contained virus laboratory in which a variety of procedures may be carried out without danger to operating personnel.

B. SIMPLIFIED VIRUS ISOLATION SYSTEMS

N. G. Anderson N. Cho

Isopycnic banding appears to offer the greatest hope at present for a simple, rapid method for isolating virus and virus-like particles from source materials. If this technique is to come into general use for examining plasma, saliva, milk, plant, and fecal extracts from human pathogens, it appears that certain requirements should be met. The chief of these is the requirement for adequate containment. Since a choice must ultimately be made between absolute containment and convenience, we have endeavored to begin by eliminating the obvious sources of contamination with the aim of gradually approaching workable, complete containment for the system under consideration here.

Briefly, the system will consist of sterile disposable plastic high-speed centrifuge tubes containing a gradient solute in concentrated solution, and colored plastic density-indicator beads. Solutions suspected of containing virus particles are layered over the gradient solution, and the tubes are sealed and centrifuged in a conventional angle-head rotor at 24,000–30,000 rpm. After centrifugation the tubes are placed in a combination camera–band-recovery unit, where the bands are photographed by scattered light using a Polaroid camera, and the observed bands recovered using motor-driven disposable blunt needles and plastic syringes.

During the report period our efforts have been directed toward the development of the centrifuge tube, the density beads, and a prototype of the withdrawal assembly.

C. A LEAK-TIGHT, DISPOSABLE PLASTIC CENTRIFUGE TUBE

N. Cho

The metal closures for high-speed centrifugation have been used, with only slight modification, for the past 25 years. They probably constitute the single greatest source of contamination in a virological laboratory.

A series of polycarbonate centrifuge tubes were machined at the Oak Ridge Gaseous Diffusion Plant to determine whether the plastic tubes and closures could stand the centrifugal force to be used. No failures were observed; however, it was evident that machined tubes would be too expensive. Several alternate designs suitable for blow-molding were prepared at Oak Ridge, and, in collaboration with the Nalge Company, Rochester, New York, were fabricated from a new resin developed by the General Electric Company specifically for molding by this method. Two versions have now been made in numbers sufficient to allow extensive trials. They differ in the size of the opening at the top (Fig. VIII-C-1). The type designated Oak Ridge type 30 A has a $\frac{1}{4}$-in.-diam opening, while the Oak Ridge type 30 B has a $\frac{1}{2}$-in.-diam opening (Fig. VIII-C-2). The A type can hold 27 ml when spun without having the cap in place. By using this volume, or less, no fluid is allowed to press against the cap. Thus far, of the many hundred tubes tested, none have ruptured causing leakage out of the tube during centrifugation. The polypropylene caps are inexpensive and do not deform during centrifugation. The type B tubes contain 25 ml when filled to a level where no fluid will reach the cap during rotation. The tubes can be run only partly filled, and will not collapse even if run empty. Both the tube and the closure can be autoclaved.

If sufficient demand exists for these tubes, the production costs will probably be low enough to allow them to be used as disposable components for nonviral as well as viral isolations.

ORNL-DWG 64-11866

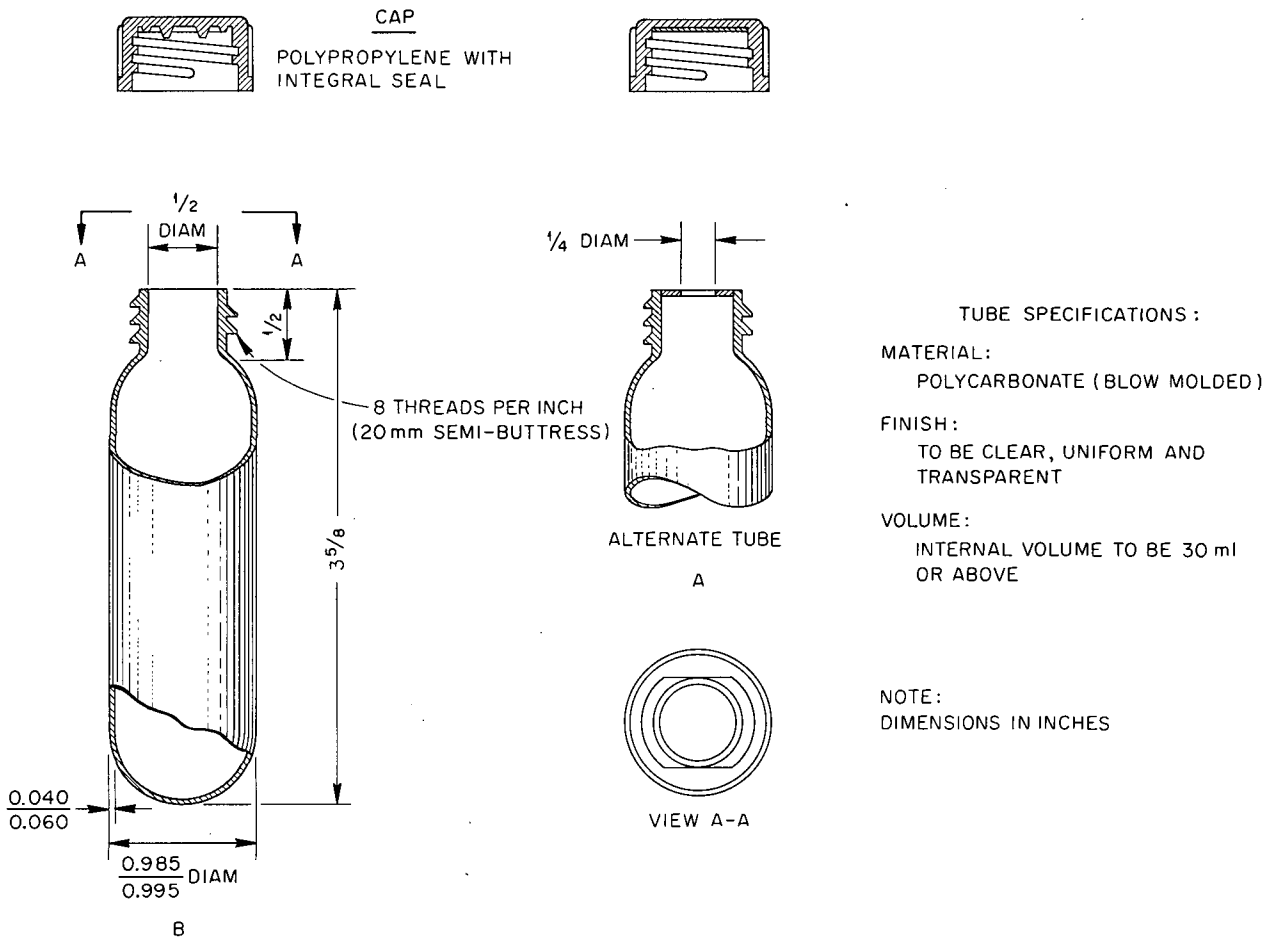

Fig. VIII-C-1. Plastic Centrifuge Tubes Developed for Virus Isolation. Tube and closure may be autoclaved.

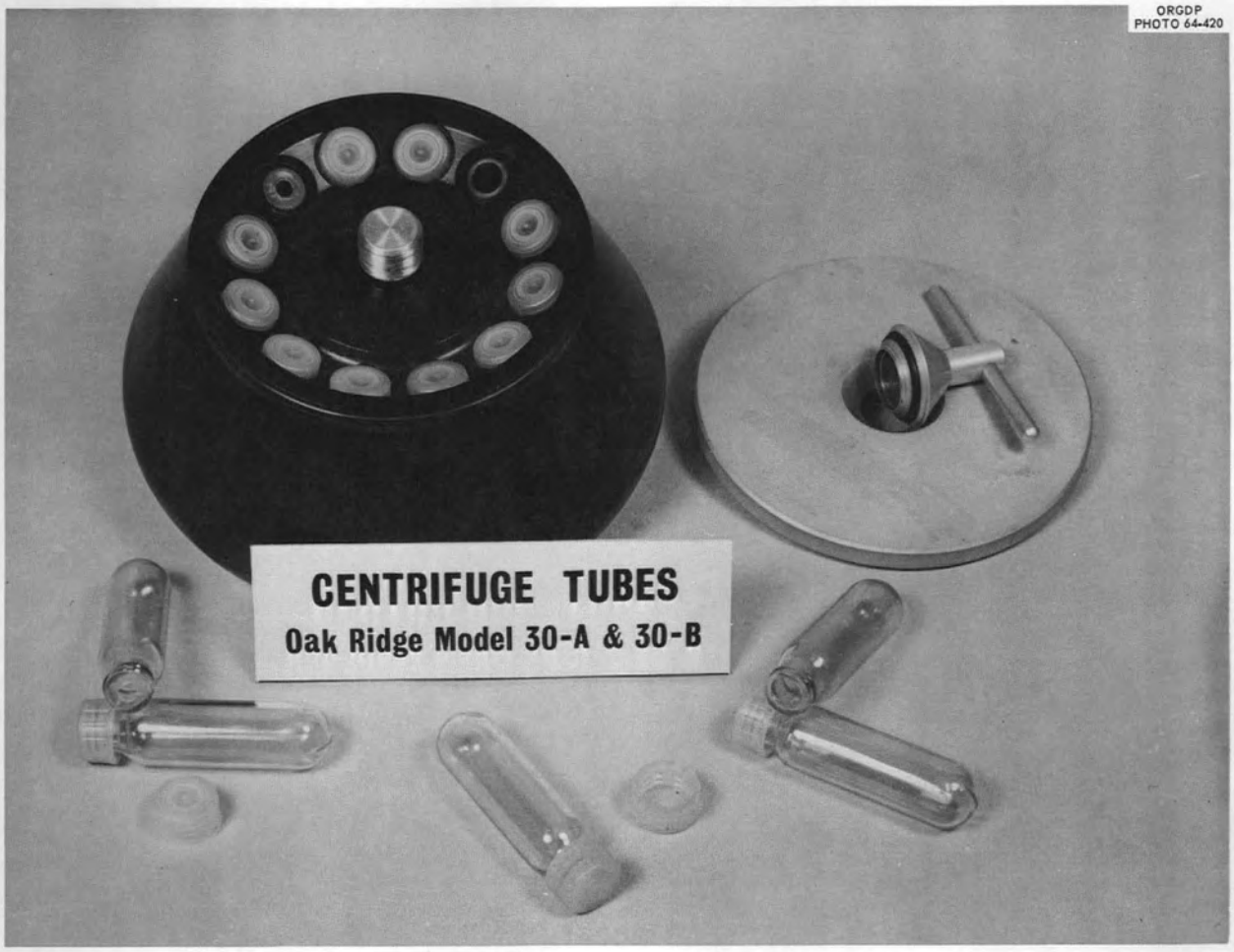

Fig. VIII-C-2. Disposable Leakproof Centrifuge Tubes.

IX. Ancillary Studies

A small fraction of this program is concerned with the exploration of new concepts or previously unexploited technologies. Studies are carried to the point of proof of principle, at which time a decision regarding arrangements for additional or separate support can be made.

A. A RAPID COUNTERCURRENT DISTRIBUTION SYSTEM

R. H. Stevens N. G. Anderson

The countercurrent distribution cells presently being developed are expected to accomplish the same general type of automatic separations attained by Craig;[1,2] however, significant reductions in the time per extraction step and the cost per stage are anticipated. These reductions will be possible through the use of power mixing to promote rapid equilibration, centrifugation to promote rapid phase separation, and a unique design which allows the instrument components to be fabricated by injection molding techniques. Each cell is constructed as a relatively flat hollow disk, containing the two liquid phases, which is rotated about its cylindrical axis on a programmed basis to obtain the desired sequence of operation. The inside of the cell is fitted with suitable barriers and channels to cause the phases to flow into separate compartments following equilibration, and each phase is then moved forward or backward to the adjoining cell. The cells will be stacked face-to-back on a common central shaft to build up a separative capacity of many stages. Because of the widely varying physical properties expected for the extraction solvents used in this work, two different cell designs are being developed and will be compared experimentally.

One design requires a more complicated barrier and grooving arrangement within each cell, but accomplishes liquid transfer between cells by gravity flow. The other, while simpler from a constructional standpoint, requires the use of low-pressure air to move the phases between cells. The latter may be especially helpful when operating with solvents that are prone to foam generation, since large numbers of bubbles could cause flow resistance in small interconnecting lines. Figure IX-A-1 is an internal view of the gravity-flow type cell; Fig. IX-A-2 is a view of the air-flow type cell. Figure IX-A-3 shows a series of three air-flow cells stacked into a separative cascade. Existing cells have been made of Lucite to observe phase separations inside the disk. Later models will likely be fabricated of polypropylene for solvent and reagent resistance.

In operation, the cell is initially rotated to locate the dispersing plate at the bottom. Two 20-ml (nominal) liquid phases are then admitted to the cell and agitated by a rapid rocking motion about the cylindrical axis of the cell. The small dispersing plate, perforated with 1-mm-diam holes, acts to break up the liquid into small droplets. Following solute equilibrium, the cell is spun to centrifugally force the heavier phase to the wall and accelerate the reestablishment of two homogeneous phases. The ability to centrifuge the cell is expected to be a major time-saving feature, since many extraction solvents readily disperse into the second phase and may require many

[1] L. C. Craig, "Extraction," *Symposium on Trace Analysis, New York Academy of Medicine*, pp. 102–25 (Nov. 2, 1955).

[2] L. C. Craig and T. P. King, *Federation Proc.* 17, pp. 1126–34 (December 1958).

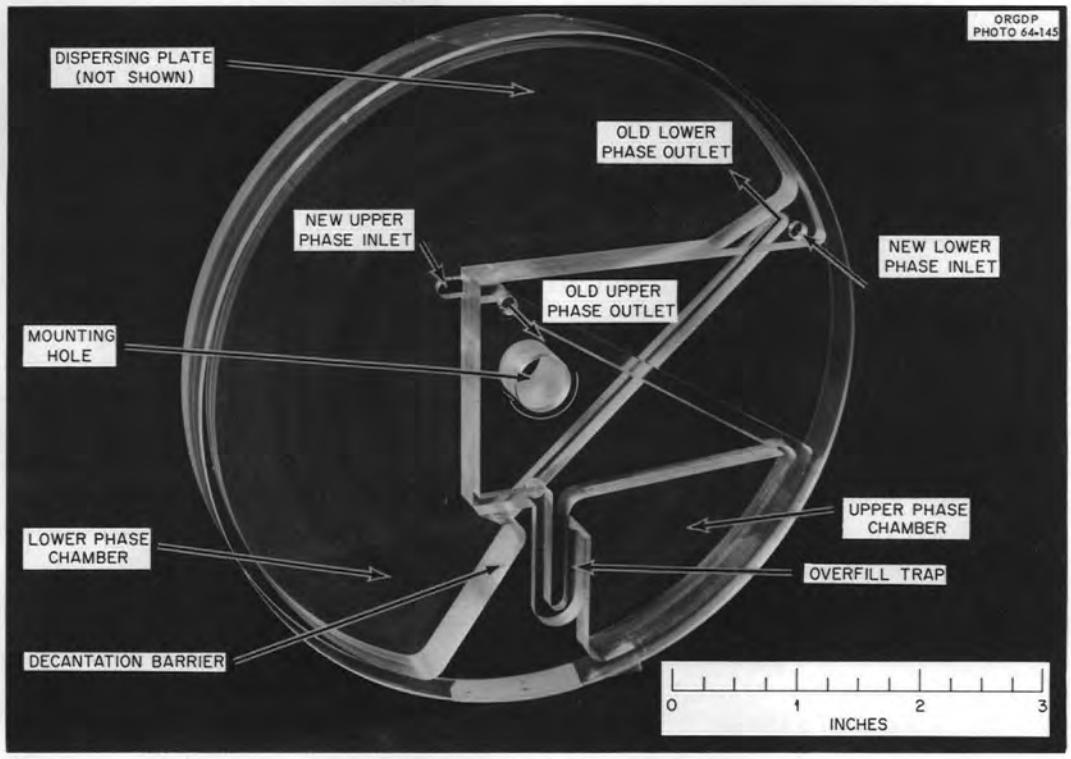

Fig. IX-A-1. Countercurrent Distribution Cell, Gravity Flow Type.

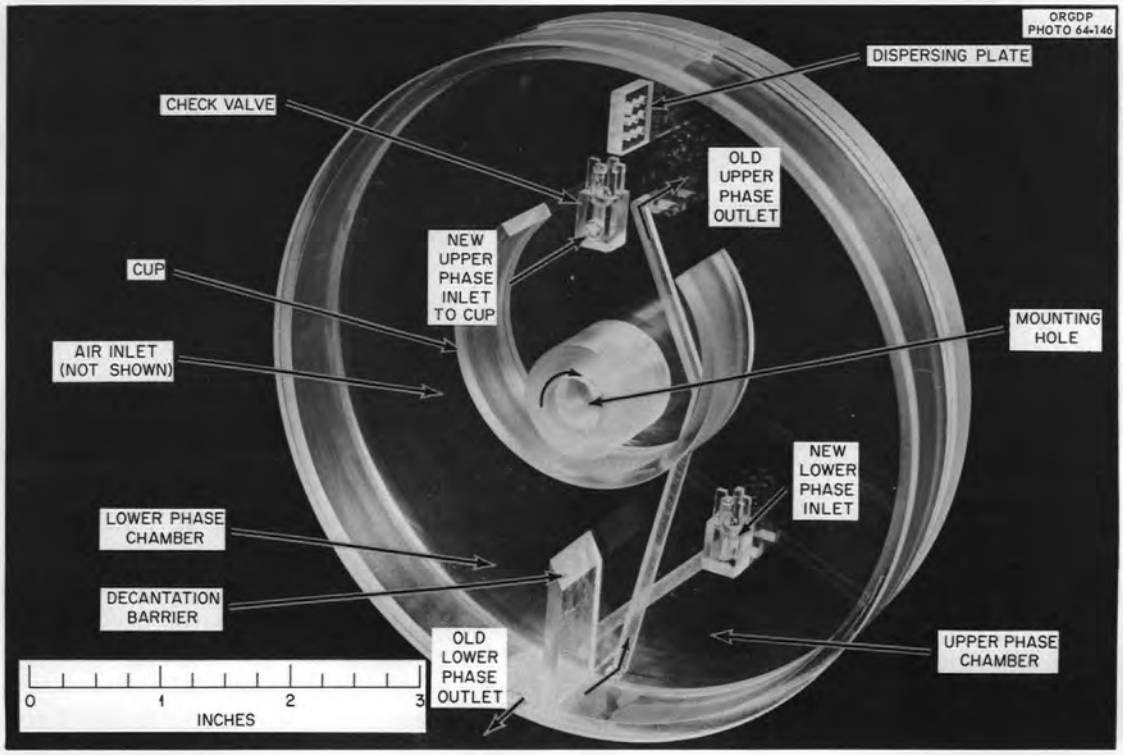

Fig. IX-A-2. Countercurrent Distribution Cell, Air-Flow Type.

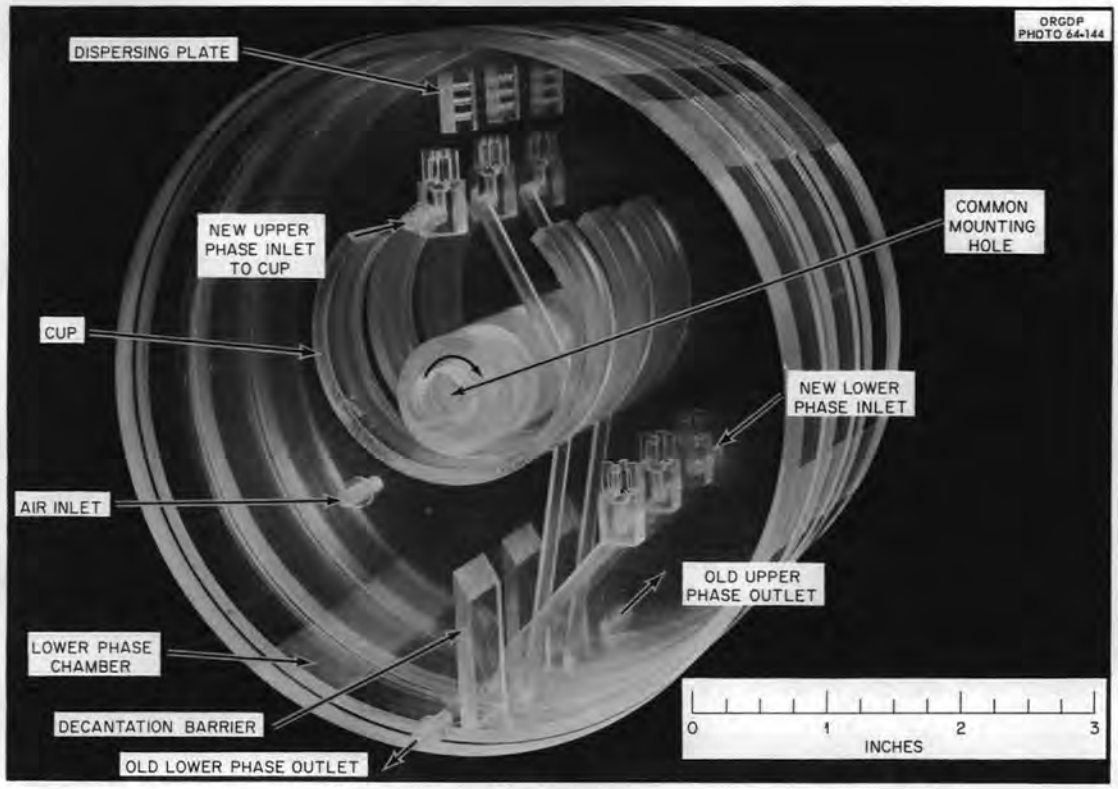

Fig. IX-A-3. Countercurrent Distribution Cell Cascade, Air-Flow Type. Three stages are shown.

minutes to separate under quiet conditions. Following centrifugation, the cell is rotated clockwise until the upper phase is decanted over the barrier (and flows into the right-hand compartment in the case of the gravity-flow cell). From this point, operation of each type cell is different. For the gravity-flow cell, the disk is rotated further in a clockwise direction to cause the lower phase to flow from the left-hand chamber, through the channel on the back of the rear cell face, and into the large open volume of the next cell downstream. After this transfer the cell is again rotated further to cause the upper phase to flow from the right-hand compartment, through the channel on the front of the front cell face, and into the open volume of the next cell upstream. Additional rotation then locates the dispersing plate at the bottom in preparation for the next agitation step. For the air-flow type cell, following the decantation of the upper phase over the barrier, the cell is rotated counterclockwise to place the barrier at the bottom. Air is then forced into the cell near the center of the near face; this seats the check valve and forces the upper (right-hand) phase to move through the back face, and into the cup of the next cell downstream via its upper check valve. The upper phase in each cell is progressively shifted by the air flow to the next downstream cell when the disks are cascaded. The air pressure is then applied to the opposite end of the cascade, or cell face, and the lower phase is forced to flow through the near face (through a channel not shown), and into the empty right-hand chamber of the next cell upstream via its lower check valve.

The rotational sequence for either type cell can be programmed for automatic operation. Several modes of phase shifting are also possible, for example, both phases shifted after an extraction step, alternate phases shifted after alternate extraction steps, or one phase stationary. The flow and phase-separation characteristics have been

determined thus far for single cells of each design. Parts for a minimum cascade of four cells of each type are ready for further testing.

B. CARBOHYDRATE ANALYZER: IMPROVED SYSTEM FOR COLOR DEVELOPMENT

J. G. Green N. G. Anderson

The general design and subsequent improvement of an automated carbohydrate analyzer have been reported previously. The most unsatisfactory element of the system has been the color development device, which employed the segmenting of the mixed reagent stream with air bubbles, the layering of the aqueous sample on the dense reagent segment, and the development of color in an air-cooled heat exchanger. A different system employing boundary-layer diffusion, which obviates the inherent disadvantages of the former system, is described here.

The boundary-layer diffuser, shown in Fig. IX-B-1, consists of a column of glass beads 3 mm in diameter supported in glass tubing which is 0.6 cm in diameter and 67 cm long. The effluent from the column and the phenol solution enter at the top of the column and mix during vertical passage down the upper portion of the device. Concentrated sulfuric acid is added to the stream at the 22-cm

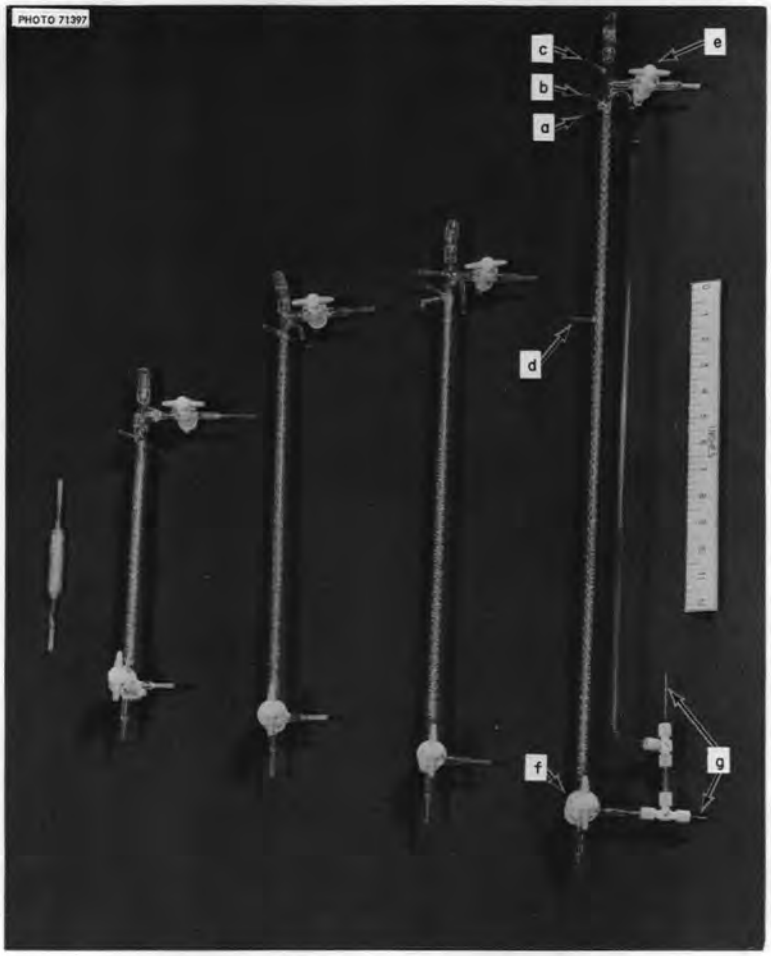

Fig. IX-B-1. Evolution of the Boundary-Layer Diffuser. The form of the BLD in use currently is at the right in the photograph. An intermediate form using manual gas bleed is not shown. Parts shown are (*a*) sample inlet, (*b*) phenol reagent inlet, (*c*) air inlet, (*d*) acid inlet, (*e*) bleed valve (metering stopcock), three-way stopcock, (*g*) electrodes in capillary sidearm.

length, and the mixed stream passes an additional 40 cm down the column and is pooled in the base of the diffuser. The 22-cm length allows ample mixing of the phenol and column effluent, and the 40-cm length, coupled with thermal agitation resulting from the addition of the acid, permits thorough mixing and degassing of the reagent stream.

To prevent bubble formation in the process line, gases liberated during passage of the stream through the BLD must be vented from the system. The level of the pool in the base of the diffuser is sensed by a thyratron-controlled, normally open relay system through platinum electrodes introduced into a capillary sidearm system through Teflon fittings. Opening of the relay circuit caused by depression of the pool level by accumulated gas opens a solenoid pinch valve, and the gas is bled slowly from the system through a needle valve. When the relay circuit is energized by elevation of the pool level to the upper electrode, the pinch valve is closed and gas release ceases.

The mixed stream is conducted from the diffuser to the flow cell of the colorimeter or, more satisfactorily, is routed through a coil of Teflon tubing ($\frac{1}{8}$-in. OD × 0.030-in. wall) which is immersed in an improvised boiling-water bath to prolong incubation and enhance color intensity. The introduction of the BLD has altered the optimum flow rates of reagents utilized in the system. Column eluant is metered directly at 1.1 ml/min, and concentrated sulfuric acid is metered at 2.65 ml/min. Chromatographic-grade liquefied phenol (approx 88%) may be metered directly into the system; however, the optimal flow rate of 0.040 ml/min is difficult to maintain reproducibly. Alternately, 5% phenol obtained by diluting the liquefied reagent allows a reproducible flow rate to be obtained at the optimum flow rate of 0.430 ml/min. In both cases, the molar absorbancy index of each processed sugar is dependent upon the rate of addition of the phenol reagent; therefore, that reagent must be delivered precisely and reproducibly.

The entire reagent dispersing and processing system can be purged by the admission of air to the top of the BLD and suitable manipulation of valves located at the base of the diffuser and at each pump.

Laminar flow and layering of the reagent and sample streams, which differ substantially in density, are mitigated by boundary-layer turbulence induced by the surfaces of the system. Adhesion of the fluids to solid surfaces, coupled with intermolecular cohesion, causes localized turbulence in the streams as they flow around the glass beads, and the mixing is further enhanced by convection currents established during the exothermic mixing of the streams after addition of the acid. The streams flow preferentially over the surface of the beads, and diffusion during passage of the mixed stream further reduces any irregular proportioning which might occur. A bead column of given volume has minimal void space per unit of surface area; therefore, the effect of mixing and diffusion on the resolution of the system is negligible, as demonstrated in Fig. IX-B-2, where a comparison of elution curves from the two systems is made.

In the bubble-segmented system, the aqueous sample layer was floated on the denser reagent stream; however, at acid concentrations above 88%, boiling occurred at the interface of the liquids. Varying back pressure from the intermittent boiling caused irregular flow from the phenol source, which disrupted the base line in the manner indicated by the arrow in Fig. IX-B-2*a*, and the use of diluted acid caused reduced glucose sensitivity in the colorimetric system. The characteristic irregular flow pattern is not reflected in the trace in Fig. IX-B-2*b*, and the use of concentrated acid yields maximal glucose sensitivity in the new system with a reduced reagent consumption.

In early trials of the system, microbubbles of gas were trapped in the three-way stopcock at the base of the diffuser, and the ultimate fusion of the bubbles resulted in their periodic passage into the stream with a concordant base-line disruption. This difficulty was overcome by decreasing the interior diameter of the column from 8 to 6 mm and increasing the length of time of exposure of the stream on the bead column by lengthening the column. Interestingly, increasing the length of the column from 10.5 to 34 cm did not materially reduce the resolution of eluted peaks, as shown in Fig. IX-B-3. However, increasing the diameter of the bead column from the initially selected 7-mm inside diameter to 10 mm markedly reduced the mixing efficiency of the system. Resolution in

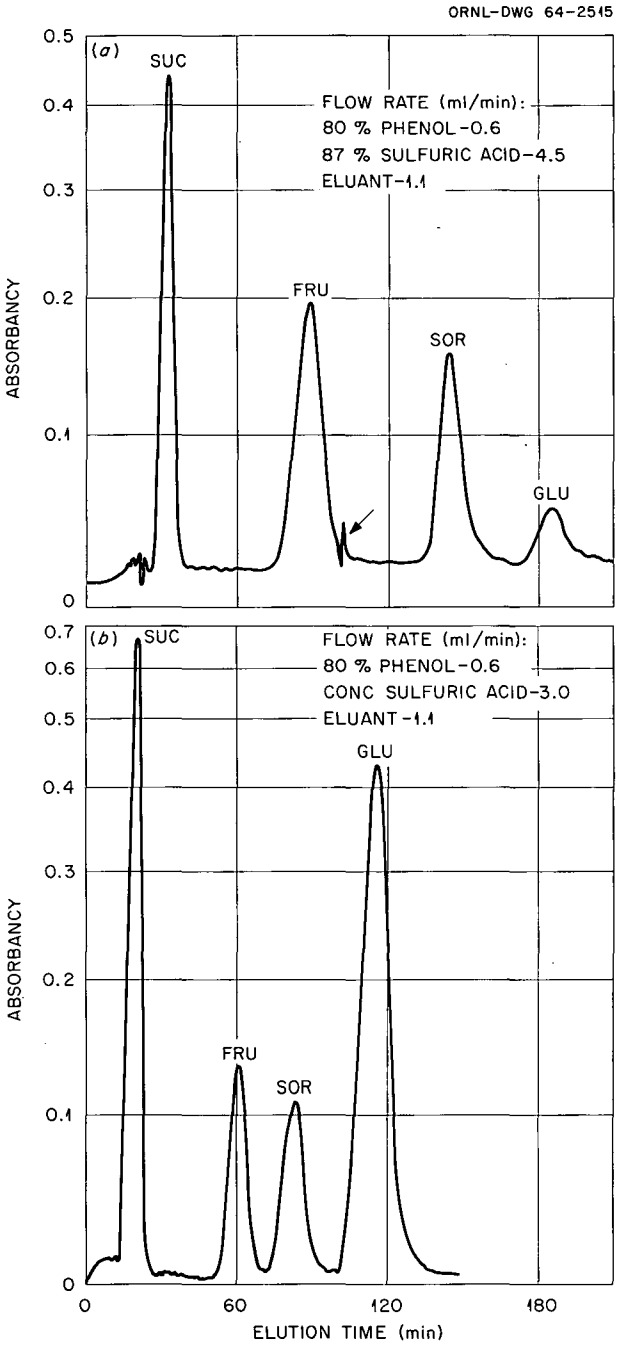

Fig. IX-B-2. Comparison of Elution Times for Two Systems. (*a*) Separation of 2.5 micromoles each of sucrose, fructose, and sorbose and 7.5 micromoles of glucose with initial color-developing system. Arrow denotes effect of interfacial boiling phenomenon. (*b*) Separation of 2 micromoles each of sucrose, fructose, and sorbose and 6 micromoles of glucose using boundary-layer diffuser color-developing system. Note superior sucrose and glucose sensitivity, reduced reagent consumption, and absence of interfacial boiling effect.

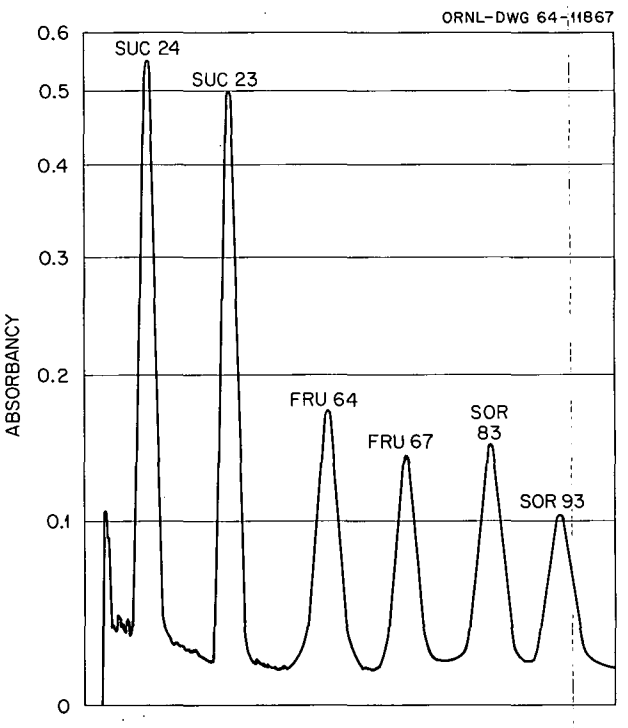

Fig. IX-B-3. Composite Curve Illustrating the Effect of Bead Column Length in the Boundary-Layer Diffuser. In each pair of curves, the one on the left was developed on a 0.7 × 14 cm column and the one on the right on a 0.6 × 34 cm column. The sugars are sucrose, fructose, and sorbose, and the numbers denote elution volume to maximum peak height. Variations in peak form are attributable to concentration and to differences in retention volumes rather than column height.

the system appears to be governed more by the pool volume than by the column length, and the presence of beads in the pooling portion of the column reduces the pool volume to a minimum.

The development of the boundary layer diffuser has solved the principal problems in processing the column effluent, and the concept may be applicable to other stream processing applications such as continuous-flow hydrolysis or digestion. Although the analyzer is suitable for routine use in its present form, studies continue to refine the analytical system and to increase its applicability.

C. CAPILLARY COLUMN CHROMATOGRAPHY: PRELIMINARY STUDIES ON NUCLEOTIDE SEPARATIONS

J. G. Green C. E. Nunley
N. G. Anderson

Decreasing bead size of an ion exchange resin improves column resolution markedly, permitting reduction of the column length and elution time in a system. However, the pressure required to maintain a desired flow rate is increased, and the increase is only partially compensated by the reduction in column length. Although decreasing the bore of a column does not materially affect the resolving capability, the flow rate of the eluting buffer may be decreased and eluted bands appear in minimal volumes of eluate. Again, decreasing the column bore causes an increase in the pressure required to maintain a desired cross-sectional flow rate. An experimental system, discussed here, has been devised to evaluate the performance of capillary columns and the behavior of fine resins at high pressures.

Since pressures exceeding the capabilities of glass columns were expected, the column was fabricated from 316 stainless steel. The column, a steel tube $\frac{1}{8}$-in. ID by $\frac{3}{8}$-in. OD by 30 in. long, supports the resin on a sintered stainless steel disk of 5-μ porosity and is supported and jacketed through use of heat-exchanger fittings. Ready access to the top of the column without disconnecting the line from the pump is provided, and the eluate is taken from the bottom of the column assembly through stainless hypodermic tubing and AWG No. 22 Teflon tubing. The resin is introduced into the column as a 30% slurry and packed hydraulically in increments. Samples in a volume of 100 μl or less are absorbed on a small cotton pledget which is tamped in the column on the surface of the resin, and appear to transfer readily to the resin at the initiation of elution.

The eluting buffer is delivered to the column by a Whitey laboratory feed pump with a rated capacity of 0 to 9 ml/min and an operating pressure of 3500 psi, although delivery rates are reduced at higher pressures. In the preliminary studies, the pump has been adjusted to deliver 1.0 ml/min at 3200 psi. The spectrophotometric monitoring system has been described previously.[3]

Resins with a bead diameter of 5 μ or less are not readily obtainable; therefore, the anion exchange resin employed in this study was hydraulically fractionated from a specially formulated –600 mesh lot obtained from a commercial supplier. Colloidal particles were removed by multiple settling, and the residual particles (mean diameter, 6 μ) were placed on a filter-paper disk supported on a sintered glass plate in a large-bore glass column which could be pressurized to encourage liquid flow through the settled resin. The resin in chloride form was washed successively with distilled water, anhydrous methanol, 6 *N* sulfuric acid, 1 *N* hydrochloric acid, 1 *N* sodium hydroxide, and 3 *M* sodium acetate–acetic acid buffer at pH 4.4. Between reagent washes, the resin was rinsed with large amounts of distilled water.

Initial studies have been conducted with a simulated RNA hydrolysate containing the commonly occurring 2′ and 3′ nucleotide monophosphates at 10 m*M* concentration, and a typical sample contains 1 micromole of each nucleotide in 100 μl of buffer. Best results have been obtained with acetate gradients progressing from 0.5 to 1.5 *M* at pH 4.1 to a total volume of 350 ml. Before entry into the system the buffer is freed of excess dissolved gas by prewarming in a jacketed gradient cylinder to the column temperature of 45°C.

A typical chromatogram obtained with the experimental system is shown in Fig. IX-C-1. Separation of the nucleotides is acceptable and may be improved with further study. A sample is eluted in less than 6 hr, rather than 13 hr required in a system described previously,[4] and a band elutes in 12 to 20 ml of buffer rather than 48 to 100 ml required for the older system.

Preliminary investigation indicates that chromatography with very fine resins, even colloidal forms, appears to be practical and offers advantages in miniaturization, volume and sample reductions, time saving, and resolution over previously adopted systems. Further exploration of these advantages may require systems with capabilities to 10,000 psi and refined monitoring procedures.

---

[3]N. G. Anderson, *Anal. Biochem.* **4**, 269–83 (1962).

[4]N. G. Anderson *et al.*, *Anal. Biochem.* **6**, 153–69 (1963).

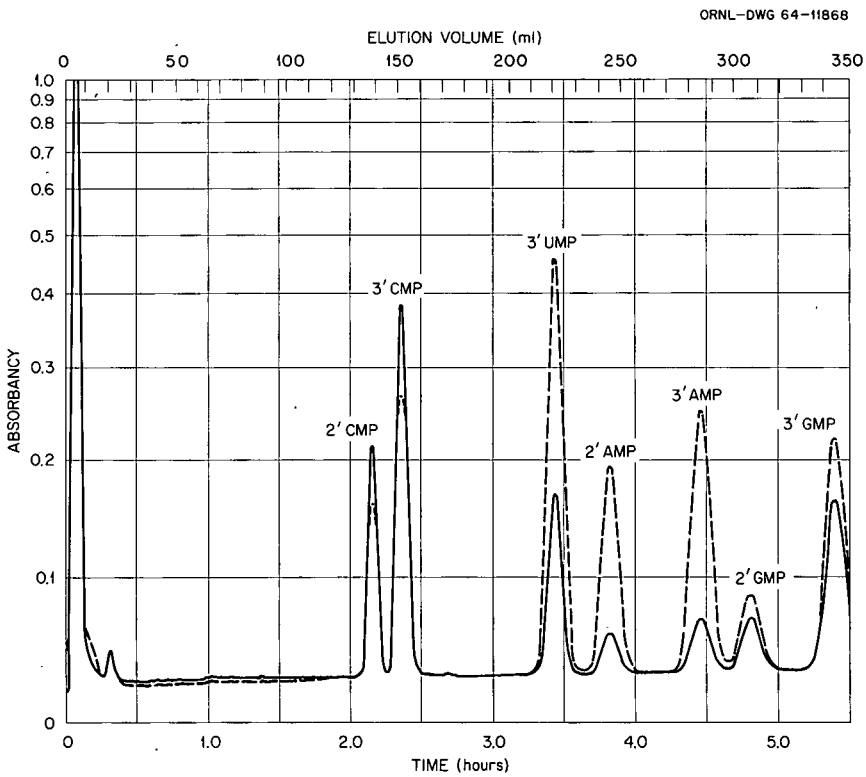

Fig. IX-C-1. Elution of a Simulated RNA Alkaline Hydrolysis by a High-Pressure System. Similar separations require 12 hr in a conventional low-pressure system, and 3-hr elution times are feasible with the present system.

D. FLAME IONIZATION ANALYZER FOR DETERMINING CARBON IN LIQUID STREAMS OR SOLID SAMPLES

R. H. Stevens

The determination of the minimum detectable weight of carbon and the sensitivity of the flame ionization analyzer used in the last report period[5] was complicated by two effects: precombustion evaporation of the sample from the wire when proximal to the flame, and apparent surface ionization to provide positive ions of other elements present on the wire when heated in the flame. These two effects are still under investigation, but some progress can be reported.

The evaporative loss of sample occurs because of the high temperature attained by the wire immediately outside of the flame envelope through thermal conduction within the wire itself. Dry samples conveyed by wire movement into the proximity of the flame are thus subjected to wire temperatures from near to greatly in excess of their boiling points. For this reason, a partial and often complete loss of sample has been experienced, depending on the initial sample weight, the temperature of the wire in the flame, and the rate of wire movement into the flame. Samples containing water of hydration, or individual cells having a high water content, have frequently shown a greater sensitivity, presumably because the evaporation of the organic material was slowed during the period of water loss from the sample.

To prevent this effect, a 1-mm-ID × 0.13-mm-wall platinum-rhodium tube was placed over the wire to contain the evaporate until the sample reached

[5]R. H. Stevens, *Joint NIH-AEC Zonal Centrifuge Development Program Semiann. Rept. July 1–Dec. 31, 1963*, ORNL-3656, p. 78.

the flame. The end of the 2.6-mm-long tube penetrated the flame envelope approximately 2 mm. Although the sensitivity was increased somewhat by this modification, a nitrogen gas flow was introduced into the tube to convey the sample vapor into the flame and prevent loss by back flow out of the other end of the tube. This addition resulted in a sensitivity increase to 0.003 coulomb per gram of carbon, a value equal to that obtained when using a known weight gaseous sample introduced through the jet. The latter arrangement precludes any sample loss and gives the highest possible sensitivity with a given ionization chamber configuration. On the basis of this work, a new jet design is being fabricated. This design incorporates a coaxial assembly of the tube and the hydrogen jet, the latter being oriented to permit passage of the horizontal wire along the common tube and jet axis.

The second effect, that of the difference in magnitude between the positively and negatively charged ionization currents produced from the same sample, is being studied to determine the specificity of either current for carbon. The negative current appears to be specific for carbon when strictly C-H compounds are studied. The positive current, being about 100 times greater in magnitude, presumably originates from surface ionization of other elements on the hot wire. A gas-phase ion-pair formation mechanism appears unlikely for about 99% of the positive current because of the lack of the electron collection that would be observed if gas-phase pair formation occurred. The new jet design will permit a more accurate evaluation of specificity by eliminating sample loss prior to combustion.

Several tests were made during this report period, both with and without the tube over the wire, to demonstrate additional analyzer applications. In one case, the wire was passed through drops of liquid containing different concentrations of bovine serum albumin (2 and 5% w/w) dissolved in up to 0.5 *M* $(NH_4)H_2PO_4$ buffer solution. This experiment, run *prior* to installation of the tube over the wire, indicated that semiquantitative pickup of solute was possible using this "wire-through-drop" technique. Signal ratios of 3.5 and 1.8 were observed between the two solutions. These values were surprisingly close to the 2.5 true value considering the large known variability in sample reaching the flame when the tubing is not employed over the wire. These results suggest that the instrument could be used as a continuous carbon monitor for column effluents.

A second experiment was made to evaluate the "wire-through-drop" technique for cell counting and sizing applications. A drop of culture solution containing the protozoan *Tetrahymena pyriformis* was placed around the wire in the same manner as described above. Individual cells were dragged out of the drop by the wire and were observed on the chart record as well-defined, measurable peaks (Fig. IX-D-1). This test, performed with a nitrogen-purged tube over the wire, demonstrates the approximate present lower limit of detectability of the equipment. Using the sensitivity values observed for "no sample loss" conditions, the carbon weight range for the several cells analyzed was calculated to be 1 to 3×10^{-8} g/cell.

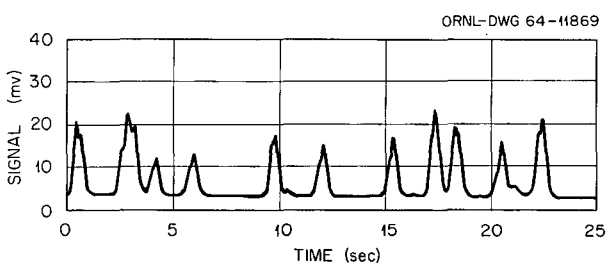

Fig. IX-D-1. Flame Ionization Analyzer Recording of Individual *Tetrahymena* Cells Obtained by Passing the Sample Transport Wire Through a Drop of Culture Solution. Average carbon weight was calculated to be 1.5×10^{-8} g/cell.

INTERNAL DISTRIBUTION

1. S. I. Auerbach
2. R. Baldock
3. R. E. Biggers
4. A. L. Boch
5. D. S. Billington
6. E. P. Blizard
7. C. J. Borkowski
8. G. E. Boyd
9–10. Clark E. Center (ORGDP)
11–12. D. D. Cowen
13. C. J. Collins
14. F. L. Culler
15. P. B. Dunaway
16. J. L. Fowler
17. J. H Frye, Jr.
18. R. F. Hibbs (Y-12)
19. A. S. Householder
20. J. S. Johnson
21. R. W. Johnson
22. W. H. Jordan
23. K. A. Kraus
24. M. T. Kelley
25. J. A. Lane
26–27. C. E. Larson
28. T. A. Lincoln
29. S. C. Lind
30. R. S. Livingston
31. K. Z. Morgan
32. D. J. Nelson
33. M. L. Nelson
34. J. S. Olson
35–36. R. B. Parker
37. M. E. Ramsey
38. R. M. Rush
39. M. J. Skinner
40. E. H. Taylor
41. A. M. Weinberg
42. G. C. Williams
43. H. I. Adler
44–63. N. G. Anderson
64. W. A. Arnold
65. R. H. Baum
66. M. A Bender
67. F. J. Bollum
68. S. F. Carson
69. E. H. Y. Chu
70. G. B. Cline
71. W. E Cohn
72. C. C Congdon
73. F. J. de Serres
74. D. G. Doherty
75. W. D. Fisher
76–78. C. J. Whitmire, Jr.
79. A. H. Haber
80. A. Hollaender
81. S. Karasaki
82. M. A. Kastenbaum
83. R. F. Kimball
84. S. P. Leibo
85. D. L. Lindsley, Jr.
86. T. Makinodan
87. P. Mazur
88. G. D. Novelli
89. T. T. Odell, Jr.
90. G. M. Padilla
91. A. P. Pfuderer
92. M. L. Randolph
93. W. L. Russell
94. R. B. Setlow
95. G. E. Stapleton
96. A. C. Upton
97. E. Volkin
98. R. C. von Borstel
99. S. Wolff
100. T. Yamada
101. E. F. Babelay
102. E. J. Barber
103. H. P. Barringer
104. J. C. Barton
105. A. S. Berman
106. H. A. Bernhardt
107. Barbara S. Bishop
108. H. D. Culpepper
109. J. T. Dalton
110–124. E. C. Evans
125. J. Farquharson
126. R. L. Farrar, Jr.
127. W. W. Harris
128–130. W. L. Harwell
131. E. T. Henson
132. A. P. Huber
133. J. L. Liverman
134. Nakwan Cho
135. J. G. Green

136. H. G. MacPherson
137. G. R. Jamieson
138. E. C. Johnson
139. T. J. Lewis
140. L. L. McCauley
141. C. E. Nunley
142. P. R. Vanstrum
143. D. A. Waters
144. C. W. Weber
145. S. J. Wheatley
146. W. J. Wilcox, Jr.
147–148. Biology Library
149–151. Central Research Library
152. Reactor Division Library
153–154. ORNL – Y-12 Technical Library Document Reference Section
155–195. Laboratory Records Department
196. Laboratory Records, ORNL, R.C.
197. Laboratory Shift Supervisor

EXTERNAL DISTRIBUTION

198. D. J. Davis, NIAID (Director), Bethesda, Maryland
199. R. W. McNamee, Union Carbide Corporation, New York
200. G. A. Andrews, ORINS
201. C. Baker, National Cancer Institute, Bethesda, Maryland
202. F. Baronowski, AEC Production Division, Washington, D.C.
203. N. F. Barr, Atomic Energy Commission, Washington, D.C.
204. N. Berlin, National Cancer Institute, Bethesda, Maryland
205. H. E. Bond, U.S. Naval Radiological Defense Laboratory, San Francisco, California
206. Myron Brakke, U.S. Department of Agriculture, Agriculture Research Service, Plant Physiol. Department, University of Nebraska, Lincoln 3, Nebraska
207. H. D. Bruner, Atomic Energy Commission, Washington, D.C.
208. W. R. Bryan, National Cancer Institute, Bethesda, Maryland
209. J. C. Bugher, Puerto Rico Nuclear Center, Rio Piedras, P.R.
210. W. W. Burr, Jr., Atomic Energy Commission, Washington, D.C.
211. R. M. Chanock, National Institute of Allergy and Infectious Diseases, Bethesda, Maryland
212. R. A. Charpie, Union Carbide Corporation, New York
213. M. A. Churchill, Chief, Stream Sanitation Staff, Edney Bldg., TVA, Chattanooga, Tennessee
214. W. D. Claus, Atomic Energy Commission, Washington, D.C.
215. Helen Coates, National Institute of Allergy and Infectious Diseases, Bethesda, Maryland
216. B. T. Cole, Department of Zoology, University of South Carolina, Columbia, S.C.
217. E. Dapper, U.S. Army Chemical Corps, Fort Detrick, Maryland
218. C. M. Davidson, Environmental Hygiene Branch, Edney Bldg., TVA, Chattanooga, Tennessee
219. W. W. Davis, Eli Lilly Co., Indianapolis, Indiana
220. O. M. Derryberry, Director of Health and Safety, Edney Bldg., TVA, Chattanooga, Tennessee
221. Harold S. Diehl, Sr., Vice President for Research in Medical Affairs, American Cancer Society, 521 W. 57th St., New York 19, New York
222. C. L. Dunham, Atomic Energy Commission, Washington, D.C.
223. K. M. Endicott, National Cancer Institute, Washington, D.C.
224. S. G. English, Assistant General Manager for Research and Development, AEC, Washington, D.C.
225. J. L. Fahey, National Cancer Institute, Bethesda, Maryland
226. E. Frei, National Cancer Institute, Bethesda, Maryland
227. F. E. Gartrell, Assistant Director of Health and Safety, Edney Bldg., TVA, Chattanooga, Tennessee
228. H. Bentley Glass, Johns Hopkins University, Baltimore, Maryland
229. Donald A. Glaser, Virus Lab., U. of Calif., Berkeley 5, Calif.
230. H. N. Glassman, U.S. Army Chemical Corps, Fort Detrick, Maryland
231. E. Grabowski, AEC Production Division, Washington, D.C.
232. S. T. Grey, Food and Drug Administration, Washington, D.C.

233. N. S. Hall, University of Tennessee, Knoxville
234. John Harris, AEC Public Relations Division, ORO
235. Fred J. Hodges, University of Michigan, Medical Center, Ann Arbor
236. E. C. Horn, Department of Zoology, Duke University, Durham, N.C.
237. J. G. Horsfall, Connecticut Agricultural Experimental Station, New Haven
238. R. D. Housewright, U.S. Army Chemical Corps, Fort Detrick, Maryland
239. R. J. Huebner, National Cancer Institute, Bethesda, Maryland
240. J. S. Kirby-Smith, Atomic Energy Commission, Washington, D.C.
241. R. M. Kniseley, ORINS Medical Division
242. K. W. Kohn, National Cancer Institute, Bethesda, Maryland
243. P. Kotin, National Cancer Institute, Bethesda, Maryland
244. E. L. Kuff, National Cancer Institute, Bethesda, Maryland
245. W. T. Lammers, Davidson College, Davidson, N.C.
246. A. D. Langmuir, Chief, Epidemiology Branch, Communicable Disease Center, Atlanta, Georgia
247. R. E. Learmouth, National Cancer Institute, Bethesda, Maryland
248. R. F. Loeb, College of Physicians and Surgeons, Columbia University, New York
249. W. H. Magruder, National Cancer Institute, Bethesda, Maryland
250. W. E. McMahon, Atomic Energy Commission, ORO
251. R. G. Meader, National Cancer Institute, Bethesda, Maryland
252. J. L. Melnick, Department of Virology and Epidemiology, Baylor University, College of Medicine, Houston, Texas
253. G. R. Mider, National Cancer Institute, Bethesda, Maryland
254. Carl V. Moore, Washington University, St. Louis, Missouri
255. P. T. Mora, National Cancer Institute, Bethesda, Maryland
256. J. E. Moynahan, National Institutes of Health, Bethesda, Maryland
257. M. A. Mufson, National Institute of Allergy and Infectious Diseases, Bethesda, Maryland
258. W. G. Pollard, ORINS
259. C. A. Price, Department of Plant Physiol., Rutgers·The State University, New Brunswick, N.J.
260. R. Quimby, National Aeronautics and Space Administration, Washington, D.C.
261. H. M. Roth, Research and Development Division, AEC, ORO
262. W. P. Rowe, National Institute of Allergy and Infectious Diseases, Bethesda, Maryland
263. P. S. Sarma, National Institute of Allergy and Infectious Diseases, Bethesda, Maryland
264. John Schacter, Union Carbide Corporation, New York
265. D. G. Sharp, University of North Carolina, Department of Biophysics, Chapel Hill
266. Byron T. Shaw, Administrator, Agricultural Research Service, U.S. Department of Agriculture, Washington, D.C.
267. C. S. Shoup, Atomic Energy Commission, Oak Ridge
268. R. G. Smith, Food and Drug Administration, Washington, D.C.
269. H. A. Sober, National Cancer Institute, Bethesda, Maryland
270. Sol Spiegleman, Department of Microbiology, University of Illinois, Urbana
271. W. M. Stanley, Virus Laboratory, University of California, Berkeley
272. S. R. Tipton, Department of Zoology, University of Tennessee, Knoxville
273. John Totter, Atomic Energy Commission, Washington, D.C.
274. Rodes Trautman, Plum Island Lab., USDA, Greenport, L.I., New York
275. Shields Warren, New England Deaconess Hospital, Boston, Massachusetts
276. A. G. Wedum, U.S. Army Chemical Corps, Fort Detrick, Maryland
277. J. White, National Cancer Institute, Bethesda, Maryland
278. H. G. Wood, Western Reserve University, Cleveland, Ohio
279. M. Zelle, Argonne National Laboratory, Argonne, Illinois
280. R. E. Stevenson, National Cancer Institute, Bethesda, Maryland
281. A. B. Sabin, Children's Hospital Research Foundation, Cincinnati, Ohio

282. C. E. Carter, Western Reserve University, Cleveland, Ohio
283. E. R. Stadtman, National Heart Institute, Bethesda, Maryland
284–288. C. G. Zubrod, National Cancer Institute, Bethesda, Maryland
289. Atomic Energy Commission, Washington, D.C.
290. General Electric Company, Richland, Washington
291. New York Operations Office
292. AEC Patent Branch, Washington, D.C.
293–297. Division of Technical Information Extension, Oak Ridge
298. UCLA Medical Research Laboratory
299. Erwin Chargoff, Columbia University, New York, N.Y.
300. R. D. Hotchkiss, The Rockefeller Institute, New York
301. Curt Stern, University of California, Berkeley
302. M. M. Wintrobe, University of Utah, Salt Lake City
303. Arne Tiselius, University of Uppsala, Uppsala, Sweden
304. Peter Alexander, Chester Beatty Cancer Institute, London, England
305. Wayne Rundles, Medical School, Duke University
306. J. A. Swartout, Asst. Gen. Mgr. for Reactors, USAEC, Washington, D.C.
307. Biomedical Library, University of California, Center for the Health Sciences, Los Angeles, California